LLB MACRO-SPIN MODELLING OF NANOGRANULAR $L1_0$ FePt HIGH ANISOTROPY THIN FILMS

LEWIS ATKINSON

A Thesis submitted for the degree of Master of Science (by Research)

University of York

PHYSICS

JANUARY 2012

Abstract

New recording media and recording methods are required if magnetic data storage is to continue the historic growth seen in the areal density, beyond the level currently imposed by the superparamagnetic limit. High anisotropy nano-granular $L1_o$ FePt thin films are currently being studied as a proposed material capable of continuing the exponential growth in areal density. FePt is so successful at maintaining a permanent magnetisation, that no applicable magnetic field is capable of reversing the magnetisation, as in the recording process. Heat assisted magnetic recording is a proposed method of lowering the anisotropy, of the high anisotropy recording media, to a level that can be recorded in. In this thesis a nano-granular high anisotropy FePt thin film is modelled using the newly developed Landau-Lifshitz-Bloch equation (to model the dynamic motion if the magnetisation) combined with a voronoi construction. The HAMR process is described over a range of maximum temperatures and modelled thin films of increasing anisotropy. It is shown that a 12000Oe applied field and a maximum temperature of T_c are required to reverse the magnetisation to the desired level. The model is used to demonstrate the lowering of the anisotropy field at elevated temperatures, allowing relatively low applied fields to set the magnetisation. The LLB equation also recovers the newly discovered fast acting linear reversal mode, at temperatures close to the Curie point.

Table of Contents

List of Figures

1. Aknowledgements

I would like to take this opportunity to that all persons involved in the implementation of this project. Firstly I would like to thank project supervisor Roy Chantrell. It has been an honor and pleasure to consider myself as a part of his group research good, and look forward to continued success. I'd also like to give a special thanks to Richard Evans for his tireless help and devotion to the project. I'd also like to thanks Seagate Technologies for the funding that made the research possible. Again a special thanks to Roy and Richard for the LLB thin film program, which made the research possible.

2. Declaration

I declare that this is my own original work.

3. Introduction

3.1 Introduction

Magnetic data storage was first proposed over 100 years ago by Oberlin Smith in 1878 and was then implemented by Vladimir Poulsen in around 1900, although the technology didn't come into general use until the 1950's. The technology has existed in many forms over its lifetime and today the primary storage media are hard disks. Hard disks are circular disk comprised of layers of both magnetic and non magnetic materials. The bottom substrate layer is usually made of non magnetic; aluminum, glass or ceramic so not to interfere with the magnetic properties of the recording layer. Layers of non magnetic metals are deposited on the substrate to optimise the atomic structure (as a result the magnetic properties) and size of the magnetic nano particles within the granular recording layer. In current technologies data is stored digitally by setting the non volatile magnetisation of an area on the hard disk, called a bit, to the desired orientation. A bit is comprised of a number of aligned uniaxial magnetic nano particles (grains) that retain the magnetic properties to maintain the information for read back at a later time [18].

The increase in magnetic storage (areal) density over the past 60 years has been truly remarkable and is comparable with the much quoted increase in transistor device density, Moore's Law, figure 3.1 [18]. The increase in areal density has in the main resulted from an adherence to geometric scaling, as the characteristic dimensions of the device have been reduced over successive time intervals. Also the methods used for storage have changed over the lifetime of the technology resulting in increased areal density. In around 2005 the orientation of the magnetic particles used for storage was altered from longitudinal (the magnetisation laying in the plane of the storage media) to perpendicular (the magnetisation laying perpendicular to the storage media). This increased the grain density, making smaller bits possible. Currently information is recorded on a length scale of nano meters, (200 -250nm in radial diameter for the recorded bit and 10nm for the component grains). At such length scales physical boundaries are coming into play which affect the thermal stability of the nano particles, the writability of the data on the storage media and the signal to noise ratio (SNR) on data read back.

SNR is effected by a number of factors; the bit shape, the number of grains per bit and the interference from neighboring bits and tracks, but a good statistical

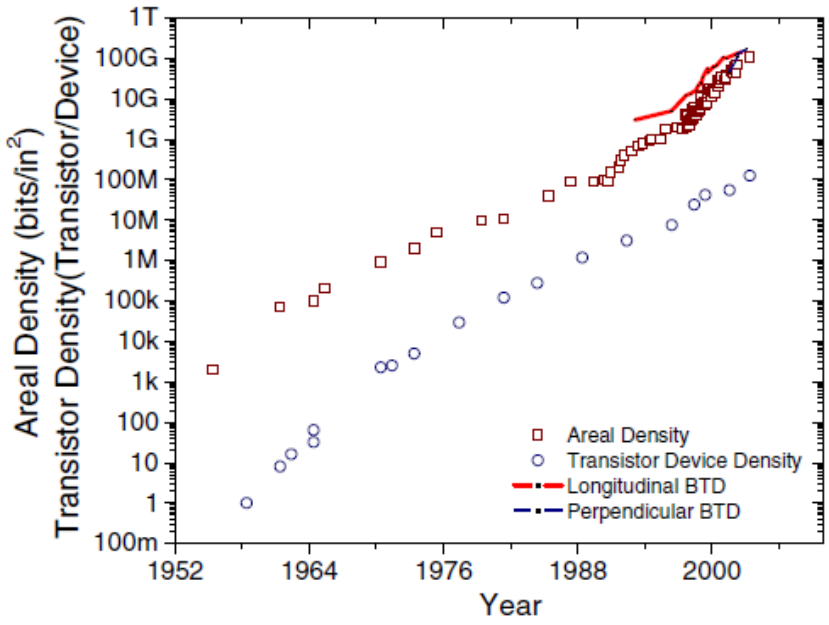

Figure. 3.1: The increase in areal density between the late 1950's and early 21st Century is comparable with the much quoted increase in transistor density.

estimate is that the SNR scales as $N^{\frac{2}{3}}$ to N^1, where N is the number of grains per bit. Therefore smaller bits require smaller grains to maintain the signal to noise ratio and as a result the grains size dictates the areal density of the disk. The grains in current hard disk are approximately 8 - 10nm in diameter. On these scales the thermal stability of the magnetisation must be considered when designing new recording media[18, 29, 28, 24].

The Arrhenius-Néel relaxation time (τ_n) approximates the time between thermally activated flips of the magnetisation. The relaxation time is governed by the particle volume (V), the temperature (T) and the magnetocrystalline anisotropy (K_v), set out in equation 3.1, where k_B is the Boltzmann constant. The Arrhenius-Néel equation shows that small decreases in the volume can result in dramatic decreases in the relaxation time. At temperatures sufficiently below T_c the magnetisation of nano particles are seen to flip orientation from one energy minimum to another, due to the associated thermal energy alone, which would result in the loss of stored data. An obvious requirement of data storage is a long storage lifetime, which has resulted in the criteria set out in equation 3.2 [20, 3, 17].

$$\tau_n = \tau_o \exp\left(\frac{K_v V}{k_B T}\right). \tag{3.1}$$

$$n_o = \frac{K_v V}{K_b T} > 60 \tag{3.2}$$

The historic solution to maintaining n_o has been to use materials with a larger bulk magnetocrystalline anisotropy constant K_v, which are thermally stable at a smaller volume, V. Therein lies a problem, the maximum output field of the inductive read/write head is held by the material limit of the highest saturation magnetisation found in magnetic solids, M_s ~2000 emu/cc which gives a write head field of about 12000Oe [22]. The write field necessary to achieve recording scales roughly with the anisotropy field $H_K = 2K_v/M_s$. Therefore K_v cannot be scaled up to the desired level to maintain n_o, as the output field of the inductive write head must scale with the recording materials mean switching field which scales with K_v. Therefore the maximum value of K_v is limited by the capability of write head technologies.

These factor all contribute to what is called the 'magnetic recording trilemma'. The increase in areal density requires smaller bits, therefore smaller grains are needed to maintain the SNR. The smaller grains require larger K_v to maintain the information lifetime which raises the switching field to a level beyond the physics of write head technologies. These physical limits mean that at some point in the near future the increase in areal density will halt, unless a new method for storage can be found.

Fortunately the magnetic properties governing the recording process are not fixed and are temperature dependant. The magnetocrstalline anisotropy of a ferromagnetic material drops towards zero as the materials temperature approaches the Curie point (T_c) and has been well understood since Callen-Callen theory was developed [12]. This gives an approximate scaling law for $K(T)$ as $K(T)/K(T=0)=(M_s(T)/M_s(T=0))^n$, where the exponent n is typically 3 for uniaxial anisotropy and 10 for cubic anisotropy. Therefore n_o can be varied from a condition of media stability at ambient temperature, to approximately zero at temperatures approaching T_c. This being true, the temperature of the storage material could be raised locally and momentarily, solving the problems of writability and media stability at the same time. This would allow for increasingly smaller grains to be used in the storage media, helping to increase the areal density.

Heat assisted magnetic recording (HAMR) is one approach exploiting the temperature dependance of K_v. HAMR uses a laser to locally and momentarily heat the storage material which lowers the anisotropy field, theoretically allowing a relatively smaller applied field to set the magnetiastion to the

preferred direction. The $L1_o$ ordered FePt granular thin film is one of the most promising candidates for HAMR media due to its high bulk perpendicular magnetocrystallne anisotropy constant $K_v = 9.2 \times 10^7$ ergs/cc [26].

The magnetisation reversal process in standard magnetic recording is complex and involves many contributing fields and factors. In addition to the anisotropy field the grains sit in a dynamic field generated by the neighboring grains within the thin film (the dipole and exchange fields)[2]. Understanding these fields and the way they interact to affect the reversal process is essential when designing new recording media. The HAMR process is more complex and contains many additional temperature dependant factors. Raising the temperature of the system doesn't simply reduce the anisotropy for a period allowing a relatively smaller applied field to reverse the magnetisation to the desired direction. The maximum system temperature affects a number of the system parameters including the magnetisation ($\mathbf{M}$(T)), the anisotropy energy (K_v(T)V), the anisotropy field (H_K(T) = K_v(T)/M_s), the thermal energy (k_BT), the inter granular exchange field and the cooling rate. All these factors contribute to the reversal process and the thermal effects must be understood if HAMR is to be a viable successor to standard magnetic data recording.

In recent years computational micromagnetics has become an essential tool in understanding the behavior of magnetic materials on the sub-micrometer scale. The Landau-Lifshitz-Gilbert (LLG) equation has been implemented to model the magnetisation dynamics of single domain magnetic particles with great success. The LLG equation treats the magnetisation of the single domain particle as a single spin, representing the sum of the atomic spins. It is apparent that the LLG equations predictive power is limited at temperatures approaching T_c as is doesn't include any thermal relaxation effects. These restrictions impair the predictive power of the LLG equation in higher temperatures regimes and is therefore not applicable in the modeling of HAMR. The recently proposed stochastic form of the Landau-Lifshitz-Bloch (LLB) equation includes longitudinal magnetisation fluctuations. As a result the LLB equation is capable of modeling the magnetisation on the sub-pico second timescale and at temperature up to and above the Curie point [9, 5].

The granular thin films used in hard disk recording are complicated structures containing an ensemble of individual single domain magnets and accurately modeling this structure, including granular interactions, is essential for the LLB to produce accurate results. A voronoi construction is used to model the granular structure of the thin film, including a realistic grain size dispersion and irregular

grain shape. The voronoi construction is also used to determine the required properties of the thin film to model the granular interactions.

The following work briefly describes the physics governing magnetic data storage and the superparamagnetic limit (the physical limit currently threatening the continuation of the technology). The physical principles behind heat assisted magnetic recording are outlined using a simplistic Stoner-Wohlfarth energy model. The Landau-Lishitz-Bloch model with voronoi construction is introduced as a new method of describing the time evolution of both the magnetisation of the individual grains with in the thin film and also the system as a whole. The LLB model is implemented as a powerful method to investigate the magnetic properties of the component nano particles and there subsequent interaction in the HAMR process. Note all units are given in cgs, with the applied field quoted in Oe.

4. Theory

The physical properties governing HAMR media are briefly discussed to outline some of the principles and ideas governing magnetisation reversal in the proposed technology. The recording layer (RL) in hard disk media is comprised of single domain uniaxial magnetic nano particles (grains), with the easy axis aligned perpendicular to the recording media surface. Figures 4.1 and 4.5 show a simplified grain in isolation and in the RL. The magnetic properties of the constituent grains in the RL have made the increase in areal density possible. The anisotropy of the grains has been raised (the anisotropy is raised by using a different material with a higher K_v) over successive size reductions to hold off the superparamagnetic limit and retain SNR. The scaling process will soon require the anisotropy to a have values which preclude the writing of information, which would halt the historic increase in the areal density unless technologies like HAMR are made workable. Here the HAMR process is described using the Stoner-Wohlfarth (S-W) model, describing the reversal process in terms of energy barriers and changing energy profiles. This simplistic approach neatly shows the principles and physics that govern the process, although it is very limited in its predictive power. Note the terms magnetisation, grain, spin and **m** are used interchangeably when referring to the magnetisation of an individual grain. When referring to the magnetisation of the thin film magnetisation and **M** are used. Where magnetisation is used it is made clear whether the individual grain or thin film is being referred to.

4.1 Magnetic Nano Particles in Isolation

The properties of the grains used in the RL have made magnetic recording possible. Magnetism arises in ferromagnetic materials as the crystal structure of the material causes the magnetic dipole moment of the atoms to align, giving rise to a permanent magnetisation, **m**. For magnetic nano-particles (grains) below a critical size it is energetically favorable to maintain only a single domain, first predicted by Frenkel and Dorfman [7]. Figure 4.1 shows a simplified single domain magnetic nano particle with uniaxial anisotropy. This configuration allows a two state system (up $\uparrow$ and $\downarrow$ down) capable of storing binary data. The uniaxial anisotropy arises from the magnetocrystalline anisotropy and the small particle volume. The strong anisotropy of $L1_o$ transition metals like FePt arises from the spin orbit coupling of the Pt atom and the hybridisation of the d-band

between the Fe and Pt atoms. This effect gives rise to a single easy axis and a hard plane for the magnetisation. The hard plane arises as the magnetic properties are rotationally similar around the easy axis. When K_v is sufficiently large the nano particle will maintain a fixed magnetisation for a long period (fixed in the sense the orientation of the magnetisation doesn't change, at ambient temperature the magnetisation of the grains precess and oscillate making a relatively small angle with the easy axis). To deflect **m** away from the easy axis requires a certain amount of energy defined as the anisotropy energy, given by equation 4.1 for a uniaxial particle. It can be seen from equation 4.1 that there are two energy minimum for the magnetisation at θ= 0°, 180°, enabling the two state system where each state is equally preferable. The anisotropy energy gives rise to the anisotropy field, equation 4.2 [8, 4, 15].

$$E(\theta) = K_v V \sin^2(\theta) \tag{4.1}$$

$$H_k(T) = \frac{2K_v(T)}{m_s(T)} \tag{4.2}$$

As mentioned above the magnetic properties of materials are different when the characteristic dimension approach the nano scale. In equilibrium conditions the build up of affective magnetic charge on the surface of the material will work to oppose the magnetisation that created it and can contribute an effective shape anisotropy. If the magnetocrystalline anisotropy of the nano particle is sufficiently small and the shape is non-spherical, shape anisotropy can can become the limiting anisotropy. Here we are considering systems with large magnetocrystalline anisotropy and regular shape, so shape anisotropy is not included in the model.

The stability of the magnetisation is governed by the particle volume (V), temperature (T), and the magnetocrystalline anisotropy constant (K_v). This is characterised by the Arrhenius-Néel law:

$$\tau_n = \tau_o \exp\left(\frac{K_v V}{k_B T}\right). \tag{4.3}$$

Here τ_o is the attempt time, estimated to be between T1=10^{-9} and T2=10^{-10} seconds, and k_B is the Boltzmann constant.

Relatively low particle volume and low K_v and/or elevated temperature can cause the magnetisation to flip from one stable position to the other. Thermally

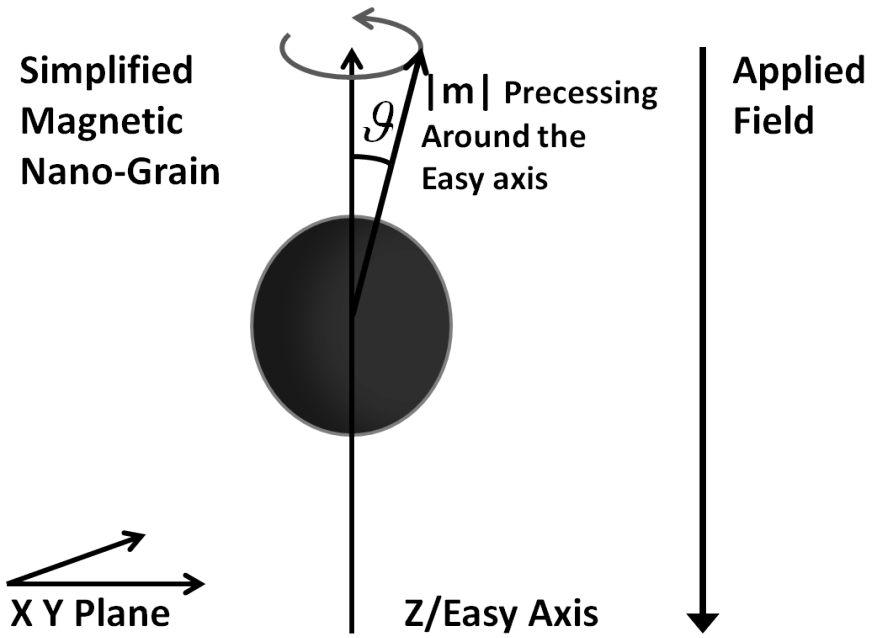

Figure. 4.1: A simplified picture of a magnetic nano particle with uniaxial anisotropy. The applied field direction is anti parallel with easy axis of the nano particle. The magnetisation is shown precessing around the easy axis.

activated switching is seen in nano and even micro scale magnetic particles at temperatures far below T_c. The relaxation time (τ_n) is exponentially linked to K_v as, $\tau_n \propto \exp(K_v)$. Increasing K_v from 0.9×10^7ergs/cc to 1.2×10^7 ergs/cc increases the relaxation time by 7 orders of magnitude, from 2×10^{11}s to 2×10^{18}s, figure 4.2 shows the exponential nature between τ_n and K_v. τ_n has a more complex relationship with the grain size, following the relationship $\tau_n \propto \exp(d^3)$, where d is the characteristic diameter of the grains. Therefore the grain size has a more critical relationship with the relaxation time and τ_n reduces rapidly when the grains drop below a critical volume. The grains are assumed to cubic, where a 6nm grains size is equal to 2.16×10^{-19}cm^3. With a 6nm grain and K_v equal to 1.15×10^7ergs/cc, the relaxation time is approximated to 1.14×10^{17}s or about 90 billion years. Reducing the grain dimensions to 4nm reduces τ_n to less than 1/10 of a second, figure 4.2. This shows the critical nature of superparamagnetism and how it can seriously alter the storage lifetime of recording media. Granular thin films do contain dispersions of grain size and anisotropy, leading to potentially large dispersion of relaxation times.

Superparamagnetism is well understood and occurs in ferromagnetic nano particles that sustain a single domain, at temperatures much lower than T_c. The magnetisation of ferromagnetic nano particles can flip due to the thermal energy

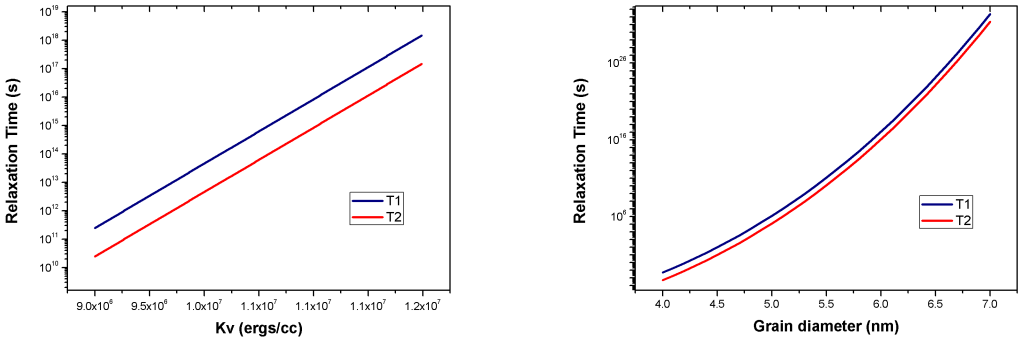

Figure. 4.2: On the left hand side: The anisotropy dependence on the relaxation time, τ_n, calculated for 6nm cubic grains at 300K. The relaxation time increases exponentially with increasing anisotropy. On the right hand side: The grain size dependence on the relaxation time, τ_n. The dimension given is 1 side of the cubic grain. The anisotropy was held at 1.15×10^7ergs/cc and the system temperature was 300K. T1 and T2 represent the different attempt times, τ_o, T1=10^{-9} and T2=10^{-10}.

associated with nano particle. If the time taken to measure the magnetisation of the nano particles is larger than the relaxation time then the particles are said to be superparamagnetic, as the magnetisation of and ensemble of the nano particle will be read as zero in the absence of an applied field.

4.2 Temperature Dependance of the Magnetisation

The spontaneous magnetisation and anisotropy energy of ferromagnetic materials are temperature dependent. The magnetisation is seen to reduces from a maximum of m(0) = $(m(0)/m_s^0)$ = 1 at 0K, to approximately zero at the Curie point, roughly following the relationship m(T) = m(0)$((T_c\text{-}T)/T_c)^{0.365}$, seen in figure 4.3. At 0.0K and with a perfect crystallographic structure the spin for each atom is perfectly aligned and the magnetisation is therefore at a maximum. As the temperature is raised the thermally activated motion of the individual atomic spins causes the alignment to be lost and the overall magnetisation of the material reduces. Above T_c the atomic spins are in a disordered state and the material no longer maintains a magnetisation. The Curie point is materials dependant and is approximately 750K for Bulk FePt, although as the material dimensions approach the nano scale T_c has been observed at the lower temperature of 660K [23, 14, 25].

The temperature dependence of the anisotropy energy of pure ferromagnetic materials has been well understood since the development of the $l(l+1)/2$ power law of Callen-Callen (C-C) theory, although not all ferromagnetic materials show C-C dependance and the $l(l+1)/2$ power law is only valid at temperatures far

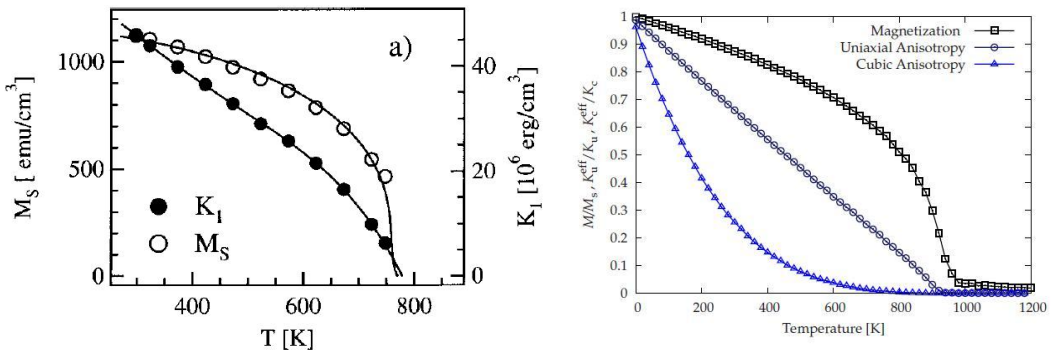

Figure. 4.3: On the left hand side: Experimental data from Thiele et al, showing the temperature dependence of the magnetisation and the subsequent relationship with K_v. The hollow circle line indicates the magnetisation and the black circle line indicates the anisotropy dependence. On the right hand side: The same information calculated with the constrained Monte Carlo method by Evans et al [23, 14, 25].

below T_c. The strong anisotropy energy of FePt arise due to the crystallographic structure and as a result has a more complicated temperature dependence that does not conform to C-C theory. Figure 4.3 shows the temperature dependant; magnetisation and anisotropy energy, observed experimentally by Thiele etal and recovered using the constrained Monte Carlo method by Evans etal. The temperature dependance of the anisotropy is found to be $K_v(T)=K_v^0 m(T)^{2.1}$ in both cases[23, 14, 25]. HAMR plans to exploit the temperature dependant nature of the anisotropy, allowing data recording in a lower anisotropy regime.

4.3 Magnetisation Reversal

The only way to maintain a fixed magnetisation for the desired time scale (when reducing the grain size) is to increase K_v. As already mentioned this encounters other physical limits which standard magnetic recording can not overcome. An increase in the anisotropy energy has a consequent rise in the anisotropy field, equation 4.2, which increases the coercivity of the media requiring a larger applied field to reverse the magnetisation.

The Stoner-Wohlfarh model (S-W) describes the magnetisation switching of single domain particles, where the easy axis is aligned with the symmetry axis of the particle. The S-W model assumes a constant magnetisation throughout rotation, essentially assuming a large atomic exchange interaction. Consequently the energy barrier for reversal is entirely due to the anisotropy energy and the effect of the applied field (Zeeman energy). For the simple uniaxial case the S-W model gives the energy of the particle as, $E(\theta, \phi)$.

$$E(\theta,\phi) = K_v V \left[\sin^2(\theta) - 2H_{eff}\cos(\phi-\theta)\right] \tag{4.4}$$

Where the first term is the anisotropy energy as function of θ (where θ is the angle between the magnetisation and the easy axis) and the second term is the zeeman energy as a function of θ and ϕ (where ϕ is the angle between the applied field and the easy axis and can be considered as zero as the easy axis and applied field coincide). K_vV is the anisotropy energy, H_{eff}=H/H_k, H is the applied field, H_k=2K_v/m_s is the anisotropy field and m_s is the saturation magnetisation. For the purpose of the this description ϕ can be ignored as the applied field lies anti-parallel with easy axis.

The height of the energy barrier for reversal and therefore the magnitude of the H-field required to overcome that barrier is dictated by K_vV (where K_v = 1.15×10^7 ergs/cc and V = 2.16×10^{-19}cm^3). The zero H-field case in figure 4.4 gives the height of the energy barrier to be 2.48×10^{-12}ergs which is equal to K_vV in this case, as $\sin^2(\pi/2)$=1. The ratio of H and H_k changes the energy profile of the system. Where H_{eff}=0 (no applied field case) only the anisotropy energy remains and there are 2 energy minima seen at θ = 0° and 180°, figure 4.4. In the case $\phi = 0$, increasing H so that $0 < H_{eff} < 1$ changes the shape of the energy wells so that a stable position exists at θ = 180° and a metastable state occurs at θ = 0°. Further increasing H to where H_{eff}=1 removes the double well entirely and an energy minima exists only at θ = 180°. Further increasing H increases the height of the energy well. Therefore reversing the magnetisation of the grains can be thought of as managing the ratio of H with H_k, increasing H until the energy profile dictates the transition of the magnetisation from the initial, now energetically unstable position, to the opposite now energetically stable position.

This simplistic energy barrier model can also be applied to HAMR. In the above analysis the ratio of H_{eff} is altered by increasing the numerator, ie the applied field. The ratio can also be altered by reducing the denominator by raising the temperature of the material. This does not have an entirely similar effect to raising the applied field, as reducing H_k will also reduce K_v by a similar amount and increase the thermal energy of the particles. The reversal process is, in addition, aided by thermal activation over the energy barriers.

Figure 4.4 also shows the effect on the energy profile when rasing the temperature of the grains. The applied field is held at $H_k/2$ and the anisotropy field and anisotropy energy are reduced to simulated the temperature rise. As the temperature of the grains is raised the magnitude of the energy barrier, when switching from 0° to 180°, is lowered and above 600K the energy barrier for

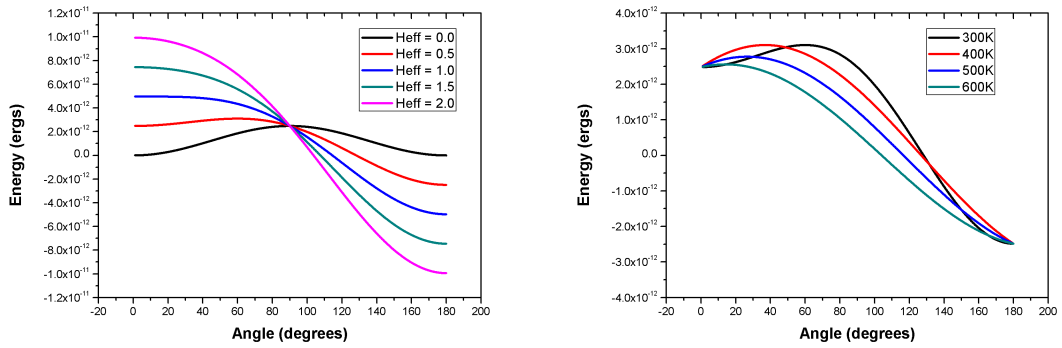

Figure. 4.4: On the left hand side: The energy barrier for reversal calculated using equation 4.4. H_{eff} is altered to simulate the effect of an applied field. Increasing the applied field raises the zeeman energy, altering the energy profile of the system, casing magnetisation reversal. On the right hand side: A similar energy diagram, where this time the energy profile is altered by raising the temperature and an applied field is held at $H_k/2$.

reversal is removed entirely. This means the the transition of the magnetisation from 0° to 180° will now occur with an applied field equal to $H_k/2$. This simply describes the HAMR process although not all factors have been included, as the increase in the energy of the grains, due to the increased thermal energy (k_BT) has not been accounted for. The S-W description is only used to indicated the physical process that HAMR will exploit.

4.4 Granular interactions within the thin film

In an ensemble of magnetic grains there are further fields acting on **m** and contributing to the dynamical motion. The thin film environment has all of the individual grains set in a two dimensional plane, with the easy axis of each grain aligned perpendicular to the plane of the thin film. This format has a specific field arrangement which brings additional challenges to simulating the recording process. A simplified diagram of a section of a granular thin film is shown in figure 4.5. Not all of the grains are showing the magnetisation and easy axis, and the grey scale is to indicate the field interactions for later discussion. The image is only a simplified image of a granular thin film to highlight the format and interactions. The grains in an actual thin film are not spherical, their shape is dictated by the boundaries they make with neighboring grains. In the model used here the grains are created using a Voronoi construction to be described later.

The demagnetisation field arises as the magnetisation (**m**) of each grain sits in a field generated by the magnetisation of the neighboring grains, figure 4.5.

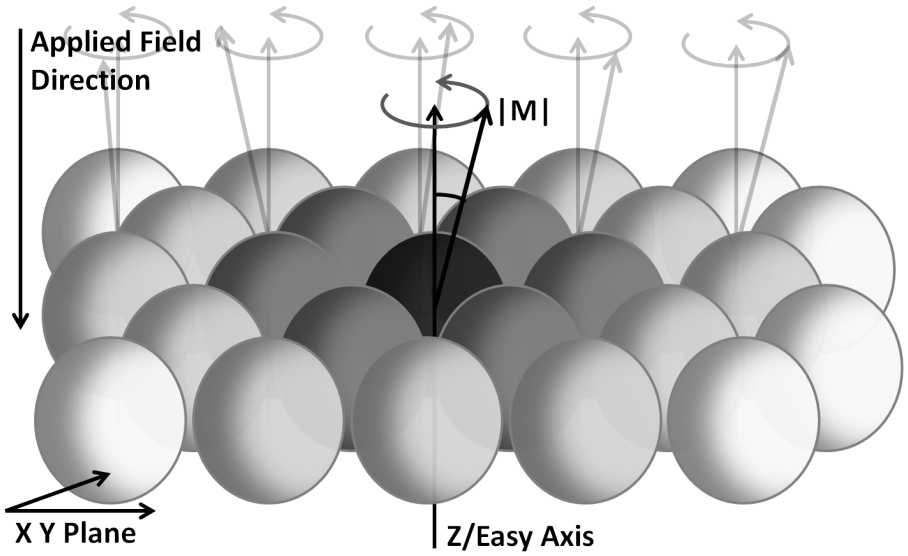

Figure. 4.5: Diagram of a single domain magnetic particle in the thin film environment. The black grain at the center is interacting, via the exchange field, with the neighboring dark grey grains. The black grain also interacts, via the dipole field, with the all the grains within a set radius from the black the grains, with diminishing effect.

For a thin film with perpendicularly orientated grains (where the magnetisation of the grains are roughly aligned) the demagnetisation field is equal to H_D=-$4\pi\mathbf{M}$, where **M** is the magnetisation of the whole system. Therefore H_D works to reverse the magnetisation the grains. Locally H_D is dependant on the orientation of the neighboring grains. For systems where H_D is of the same order as K_v the stability of **m** is effected by the dipole interaction between neighboring spins and can cause magnetisation switching in an otherwise thermally stable system. As a result, media with perpendicular magnetisation must satisfy the criterion $2\pi M_s^2 < K_v$. Given the dynamic changes in the magnetisation configuration, the dipole field is also dynamic and its effect is entirely dependant on the relative orientation of the neighbouring grains. The dipole field felt by the black grain at the center of the image in figure 4.5 is generated by the magnetisation of the nearby grains; and the effect diminishing with distance from the central grain [1, 6, 16].

The exchange field arises from an interaction between neighboring atoms, and is at a minimum when the angle between neighboring spin magnetic moments is zero, therefore causing the atomic spins to line up parallel. As the exchange energy is only dependant on the angle between neighboring atoms, there is no contribution to the anisotropy. As the exchange field arises from an interaction between neighboring atoms and is therefore short ranged, there must also be another mechanism for the interaction as there is an exchange

coupling between neighboring grains within a thin film which are separated by much further than the inter-atomic distance. Exchange coupling over this distance can occur via the Ruderma-Kittel-Kasuya-Yoshida (RKKY) interaction, where the exchange coupling comes via an intermediate conductive material in the boundary layer between the grains. Exchange coupling acts much like the inter-atomic exchange field and causes the magnetisation of the grains to align and precess together. Therefore the black grain in figure 4.5 has an exchange interaction with neighboring grains, coloured in the darkest grey.

Therefore the total field H_{tot} acting on the individual grains, when including an applied field, is equal to the sum of all the local field contributions, (each of which will be described in detail in the following section).

$$\begin{aligned} \underline{H}_{tot} = \underline{H}_{applied} + \underline{H}_{anisotropy} \\ + \underline{H}_{exchange} + \underline{H}_{Dip} \end{aligned} \tag{4.5}$$

The magnetisation reversal process in the thin film environment is a complex and contains many contributing factors. The magnetisation of each grain sits in a dynamic field which is altered by the motion and strength on the contributing grains. The temperature dependant properties contain further levels of complexity which puts further strain on our ability to accurately predict the outcome, when altering system parameters. The LLB model with voronoi construction takes in to consideration all the above principles to enable an accurate representation of a high anisotropy FePt granular thin film. Therefore the model is capable of an accurate analysis of the magnetisation reversal process undergoing HAMR style heating and cooling.

5. The LLB Thin Film Model with Voronoi Construction

Computational micromagnetics is a powerful tool when modelling the magnetisa tion of 'single domain nano particles' or 'discrete nano magnetic domains'. Micromagnetics is implemented to model relatively large systems as first principle and atomistic spin models are computationally more expensive and can therefore only be implemented for translationally invariant systems or small groups of atoms [19]. Historically micromagnetic models have treated the magnetisation as a constant vector, where the dynamic motion is described by the Landau-Lifshitz-Gilbert (LLG) equation. The LLG approach is very successful at describing the zero Kelvin dynamics, but is restricted in its accuracy at higher temperatures approaching T_c, as the LLG motion dynamics assume a constant magnetisation of 1. It has been shown that the LLG stochastic approach largely over estimates the Curie point of materials. Therefore the LLG equation is not suitable for modeling the magnetisation in the higher temperature regimes needed for HAMR. The Landau-Lifshitz-Bloch (LLB) equation (derived by Garanin [9]) has been shown to be a realistic alternative to the LLG for micromagnetic simulation at high temperatures up to and above T_c.

On its own the LLB equation is only capable of idealistic solutions. To enable a realistic approach for HAMR simulations a voronoi construction is implemented to model the structure of the thin film, including the granular interactions. The voronoi construction generates a realistic structure that, when coupled with LLB equation, is capable of simulating the magnetisation dynamics of the thin film.

Here the LLB equation is introduced including a description of the benefits that the LLB brings to micromagnetics. Also a brief description of the voronoi construction is given including how the granular interactions are considered.

The thin film model used in this study, including the LLB dynamics and the voronoi construction, was developed at York and modified by the author as appropriate to carry out the calculations described later. The original coding and parameter calculations for the model were performed by R.W.Chantell and R.F.L.Evans, coding in Fortran. The parameters used within the model such as the equilibrium magnetisation (m_e) and parallel and perpendicular susceptibility ($\chi_\parallel$ and $\chi_\perp$) were calculated using the mean field approximation.

5.1 LLB Equation of Motion

The Landau-Lifshitz-Bloch (LLB) equation (5.1) was derived by Garanin within the meanfield approximation from the classical Fokker-Planck equation for atomistic spins interacting with a heat bath. The LLB equation describes the precessional motion of the magnetisation of single domain uniaxial magnetic particles at temperatures up to and over the Curie point. The LLB treats the magnetisation of the single domain particle as a single macro-spin (similar to the LLG equation) including a longitudinal damping parameter to simulate the reduction in **m** associated with raised temperature. The magnetisation is treated as a dynamic temperature dependant variable in the LLB equation and therefore better describes the magnetisation dynamics at temperatures approaching T_c, T $\gtrsim 3T_c/4$ [19]. Initial investigations (by Kazantseva et al and Chubykalo-Fesenko etal) have shown the LLB equation is in agreement with atomistic calculations relating to linear domain wall type and relaxation time [19, 21, 10, 11].

The LLB equation can be written in the following form:

$$\begin{aligned}\dot{\mathbf{m}}_i = \gamma[\mathbf{m}_i \times \mathbf{H}^i_{eff}] + \frac{|\gamma|\alpha_{\parallel}}{m_i^2}(\mathbf{m}_i \cdot \mathbf{H}^i_{eff})\mathbf{m}_i \\ -\frac{|\gamma|\alpha_{\perp}}{m_i^2}[\mathbf{m}_i \times [\mathbf{m}_i \times (\mathbf{H}^i_{eff} + \eta^i_{\perp})]] + \eta_{\parallel}\end{aligned} \tag{5.1}$$

Where $\mathbf{m}_i$ is the magnetisation of the i^{th} grain and $\mathbf{H}^i_{eff}$ is the effective applied field experienced by $\mathbf{m}_i$. The effective field, $\mathbf{H}^i_{eff}$, acting on $\mathbf{m}_i$ is equal to the vector sum of the applied field **H**, the anisotropy field $\mathbf{H}_A$ and a temperature dependant term. Note the temperature dependant term is different below and above T_c.

$$\mathbf{H}^i_{eff} = \mathbf{H} + \mathbf{H}^i_A + \begin{cases} +\frac{1}{\tilde{\chi}_{\parallel}}\left(1 - \frac{m_i^2}{m_e^2}\right)\mathbf{m}_i & T \lesssim T_c \\ -\frac{1}{\tilde{\chi}_{\parallel}}\left(1 + \frac{3}{5}\frac{T_c}{T - T_c}m_i^2\right)\mathbf{m}_i & T \gtrsim T_c \end{cases} \tag{5.2}$$

$$\mathbf{H}^i_A = -\frac{(m^i_x e_x + m^i_y e_y)}{\chi_{\perp}} \tag{5.3}$$

Where m_e is the zero field equilibration magnetisation and $\tilde{\chi}_{\parallel}/_{\perp}=(\mathrm{d}m/\mathrm{d}\mathbf{H})_{H\to 0}$ is the parallel and longitudinal susceptibility. λ (set to 0.1 in the model) is a general damping term describing the coupling of the atomic spins to the heat bath and γ is the gyromagnetic ratio. $\alpha_{\parallel}$ is the longitudinal damping parameter and $\alpha_{\perp}$ is the transverse damping parameter.

$$\alpha_{\parallel} = \lambda \frac{2T}{3Tc} \tag{5.4}$$

$$\alpha_{\perp} = \lambda (1 - \frac{T}{3Tc}) \tag{5.5}$$

Equation 5.5 is only true below or equal to Tc (T $\leq$ Tc). Above Tc equation the equivalent expressions are

$$\alpha_{\parallel} = \alpha_{\perp} = \lambda \frac{2T}{3Tc} \tag{5.6}$$

In order to introduce finite temperature effects we introduce perpendicular and transverse noise parameters with the following properties.

$$\begin{aligned}
\langle \eta_i^{\mu} \rangle &= 0, \\
\langle \eta_i^{\perp}(0)\eta_j^{\perp}(t) \rangle &= \frac{2k_{\mathrm{B}}T(\alpha_{\perp} - \alpha_{||})}{|\gamma| M_{\mathrm{s}}^0 V \alpha_{\perp}^2}\delta_{ij}\delta(t), \\
\langle \eta_i^{||}(0)\eta_j^{||}(t) \rangle &= \frac{2|\gamma|k_{\mathrm{B}}T\alpha_{||}}{M_{\mathrm{s}}^0 V}\delta_{ij}\delta(t), \\
\langle \eta_i^{||}\eta_j^{\perp} \rangle &= 0
\end{aligned} \tag{5.7}$$

Where μ, ν = $\parallel$, $\perp$ and i,j represent the x,y,z components and V is the particle volume.

The LLB equation is set out in three parts. The first term describes the procession of the magnetic moment, the second term describes the damping of the magnitude of the magnetisation (the damping of the magnetisation is where the LLB differs from the LLG) and the third term describes the damping of the processional motion of the magnetic moment.

The LLB equation is solved using a Heun scheme with an initiating Euler step.

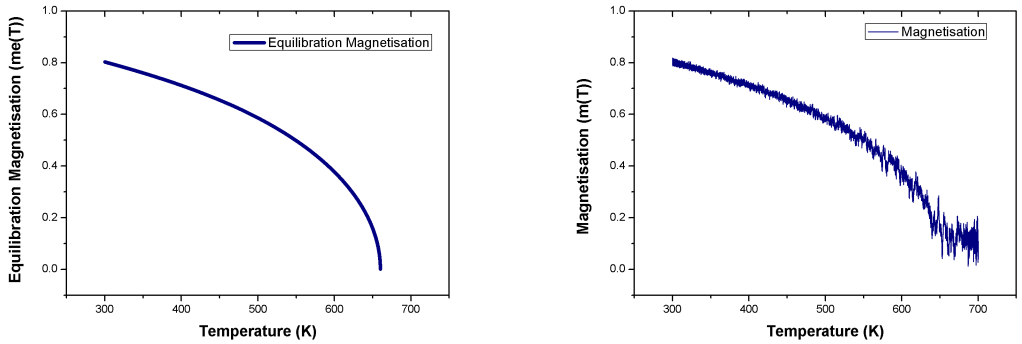

Figure. 5.1: The left hand side: The equilibrium magnetisation (m_e) calculated for the LLB model within the mean field approximation with a Curie point of 660K, for further calculation within the model. The left right side: The spontaneous magnetisation (m) for a single grain, calculated by the LLB model.

Figure 5.1 shows the temperature dependant equilibrium magnetisation (m_e) calculated for the model for use in the motion calculations and the temperature dependant spontaneous magnetisation (m), calulated by the LLB model, is also shown for comparison with m_e. Both m_e and m were calculated by setting the temperature to 700K at the start of the simulation and allowing the system to equilibrate. After sufficient time the system was cooled from 700K to 300K over a 10ns simulation time. The temperature dependence of the spontaneous magnetisation is more noisy than that of m_e. This is caused by the stochastic nature of the LLB equation. The spontaneous magnetisation is a result of many interacting temperature dependant factors which gives rise to a dynamic magnetisation.

5.2 Thin Film Dynamics

A voronoi construction is used to model the microstructure of the thin film and calculate the exchange field and dipole field acting on each grain. The voronoi construction produces a realistic picture of the thin film by randomly distributing points in 2 dimensional space and then plotting bisecting lines between the points to create grain boundaries. An image of the thin film produced by the voronoi construction is shown in figure 5.2. The model produces any required configuration. for this study it was used to generate 6nm, three dimensional grains with an average volume of 2.16×10^{-19}cc in an 80 $\times$ 80 $\times$ 1 format. The simulated thin film includes microstructural disorder and a realistic grain size dispersion. The voronoi model also determines the volume of each grain and the contact area each grain makes with its neighbours, enabling the calculation of

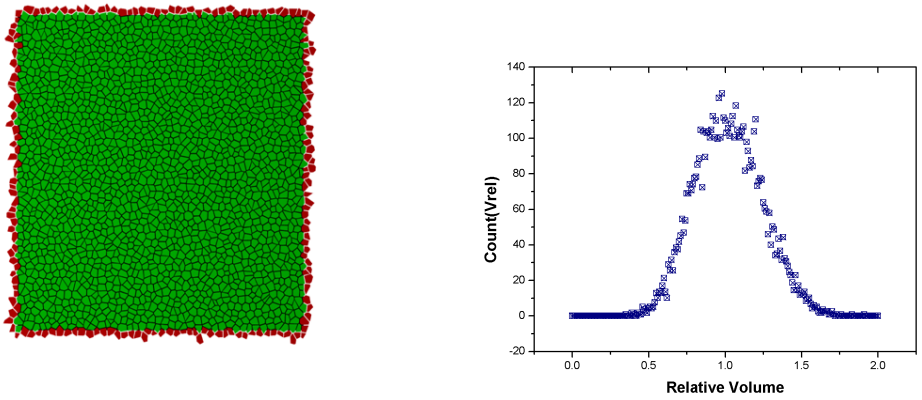

Figure. 5.2: The left hand side: A plan view of the granular thin film produced by the voronoi construction. The modeled thin film shows microstructural disorder and grain size dispersion. The thin film contains approximately 80 $\times$ 80 6nm grains. The right hand side: The relative volume spread for the grains in the thin film produced by the voronoi construction. A relative volume of 1.0 is equal to 2.16×10^{-19}cc.

the granular interactions. The magnetic grains within the thin film have a volume dispersion that approximates a Gaussian distibution, such that the smallest grains are 1/3 the size of the largest, figure 5.2. The spread in the volume means there will also be a spread in the anisotropy energy of the grains. This means the relaxation time and switching fields of the grains will also have a range which will effect the magnetisation reversal dynamics of the thin film.

As mentioned above the voronoi construction also calculates the exchange and dipole fields acting on the grains. The exchange field ($H_{exchange}$) felt by grain i is a function of the relative exchange strength, f_{ij}, which is proportional to the contact area between grain i and its neighbouring grains j, and the exchange parameter, H_{exc}, which is the average exchange field per grain when the system is at saturation. The mathematical expression for this is in equation 5.8. It should be noted that the exchange field ($H_{exchange}$) is not equal to the exchange constant (H_{exc}) and is a function of $\mathbf{m}_i$, $\mathbf{m}_j$ and f_{ij} and is therefore temperature dependant, as $\mathbf{m}$ is temperature dependant. Also it should be noted that H_{exc} is the figure quoted for the exchange field in the results section of the thesis.

The dipole field experienced by grain i is due to the dipole interaction with neighboring grains j. The partial contribution to the dipole field from grain j diminishes with increasing distance from i, until it has no contribution. Again the mathematical expression for this can be seen in equation 5.8.

Therefore the total field acting on the magnetisation of an individual

magnetisation, when including the anisotropy field and the interaction fields, is equal to:

$$\begin{aligned}\mathbf{H}_{eff} = \mathbf{H} &+ \underbrace{\sum_{ij} \frac{\mu_j}{r_{ij}^3}(3(\hat{r}_{ij}\cdot\hat{\mu}_j)\hat{r}_{ij} - \hat{\mu}_j)}_{dipole field} \\ &+ \underbrace{\sum_{ij} \mathbf{H}_{exc} f_{ij}(\hat{x}\hat{m}_x^i + \hat{y}\hat{m}_y^i + \hat{z}\hat{m}_z^i)}_{exchange field} \\ &- \underbrace{\frac{(m_x^i e_x + m_y^i e_y)}{\chi_\perp}}_{anisotropy field}\end{aligned} \tag{5.8}$$

Where **H** is the external applied field, which is equal at all points across the thin film. Also as a further point the temperature of the thin film is also equal at all points.

5.3 Dynamic Magnetisation at Elevated Temperature

At a given temperature the grains that make up the thin film have a dispersion in the magnetisation length. The spread for the magnetisation length was calculated using an ensemble of non interacting hexagonal 6nm grains at 650K. The magnetisation length was captured at each time step (over a 1.0ns simulation) and the spread in the magnetisation length determined. Figure 5.3 compares the analytic solution (obtained using equation 5.9) to the result determined with the LLB model. The two result are in close agreement, therefore the LLB model gives a realistic dispersion for the magnetisation length at a given temperature.

At lower temperatures the magnetisation length is well defined and the spread for the length of m is much less, figure 5.3 (the peak of each curve was set to 1.0 to highlight the increase in m(T) and the reduction in the spread of m(T). Had the data been represented as a probability as in the 650K example the peaks would have been at different heights, making the data more difficult to read). At higher temperature the individual magnetisation that make up the thin film are in a disordered state.

At high temperature the atomic spins that make up the magnetisation are in a disordered state and the degree of their alignment varies from instant to instant.

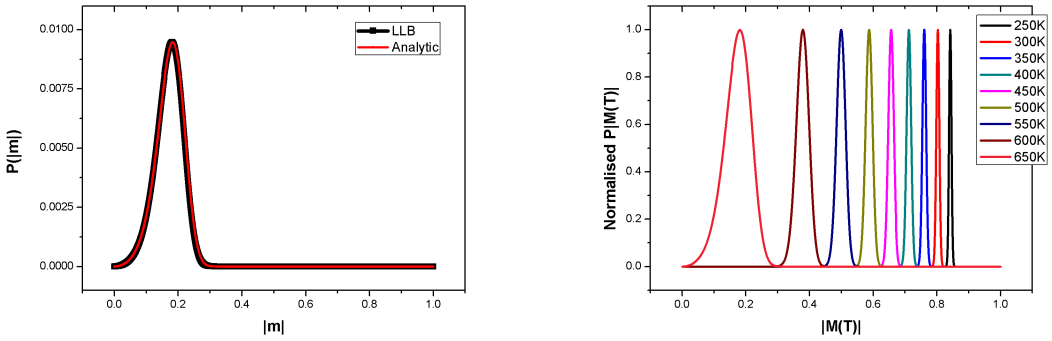

Figure. 5.3: The left hand side: The spread of |m| at 650K calculated with the LLB model is compared with the analytic solution, calculated with equation 5.9. The right hand side: The relative volume spread for the grains in the thin film produced by the voronoi construction. A relative volume of 1.0 is equal to 2.16×10^{-19}cc.

This effects the nature of the magnetisation causing it to vary in magnitude from moment to moment.

5.4 Analytic Calculation for the Spread of m at Elevated Temperature

The following sets out the basis for calculating the the spread of the magnetisation length at elevated temperatures above zero Kelvin. Where F(x) gives the analytic solution for the volume spread and f(m) is the free energy of the magnetic grain. All the other parameters where taken directly from the thin film model, which are fitted function to the results calculated within the mean field approximation.

$$F(x) \propto m^2 \exp\left(\frac{-f(m)}{k_B T}\right)$$
$$f(m) = \frac{m_s V (m^2 - m_e^2)^2}{8\chi_{\parallel}(T) m_e(T)^2} \tag{5.9}$$

y = T_c - T

x = (T_c - T)/T_c

b0 = 0.8

b1 = -2.2×10^{-7}

b2 = 1.95×10^{-13}
b3 = -1.3×10^{-17}
b4 = -4.0×10^{-23}
b5 = -$6.5076312364\times10^{-32}$

For $\mathbf{T} < \mathbf{T}_c$

$$\chi_{\parallel} = \frac{b0 \times T_c}{(T_c \times 4.0 \times \pi \times y) + (b1 \times y) + (b2 \times y^3) + (b3 \times y^4) + (b4 \times y^6) + (b5 \times y^9)} \tag{5.10}$$

$$m_e = (1.3 \times \sqrt{x}) - (0.12 \times x) - (0.51 \times x^2) + (0.37 \times x^3) - (0.01 \times x^4) - (0.03 \times x^8) \tag{5.11}$$

For $\mathbf{T} > \mathbf{T}_c$

$$\chi_{\parallel} = \frac{(0.00233333 \times T_c)}{((T - T_c) \times 4.0 \times \pi)} \tag{5.12}$$

$$m_e = 0.0 \tag{5.13}$$

Where m is the magnetisation length, m_s is the saturation magnetisation, V is the volume of the grain, m_e is the equilibrium magnetisation, $\chi_{\parallel}$ is the parallel susceptibility, T is the temperature and k_B is the Boltzmann constant.

5.5 Information on the thin film images

The LLB thin film model outputs an image of the thin films granular structure including the magnetic configuration at that instance. The initial set up of the thin film has all the individual magnetisations orientated entirely in the easy axis with a length 1, the thin then relaxes and the magnetisation reduces to the abient length (on what ever constant temperature is chosen). Under these conditions the image shows all the grains in bright blue, where the opposite conditions (the grains in the other orientation) show the grains in bright red. There is a shade scale where the shade of the grain dictates the magnitude of the component of the magnetisation in the z/easy axis, due to precessional reversal or a reduction in the length of the magnetisation due to elevated temperature, figure 5.4.

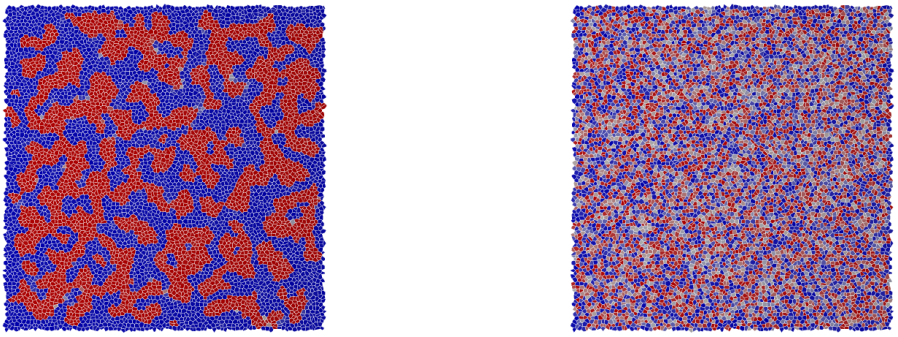

Figure. 5.4: Two images of the thin film output by the LLB model, showing the magnetic configuration of the thin films. The image in the left contains distinct domains of grains with the magnetisation sitting in both orientations (blue for positive and red for negative. The magnetisation of the grains in the image on the left are reduced in the z/easy axis, due to precessional reversal or the reduction in the magnetisation length due to thermal effect.

6. Static hysteresis properties and relaxation

To better understand the properties of the thin film, the LLB model was used to study the coercivity and magnetisation dynamics at constant temperature. The coercivity of the FePt thin film is calculated over a range anisotropies from 10% to 100.0% $L1_o$ ordered FePt and range of temperatures, 300 - 700 Kelvin, over the Curie point, 660 Kelvin and range for the exchange constant, 0 - 30000 Oe. And the saturation magnetisation (m_s) was set to 1150emu/cc throughout the study. The study was performed by generating hysteresis curves over the full range of the anisotropies, temperatures and exchange constants.

6.1 Anisotropy dependence

To investigate the anisotropy dependence of the coercivity, K_v was varied from 10% $L1_o$ ordered FePt (9.2×10^6ergs/cc) to 100% $L1_o$ ordered FePt (9.2×10^7ergs/cc). Note that with 6nm grains, 10% $L1_o$ ordered FePt is below the anisotropy requirements for magnetic data storage. An anisotropy of above 20% $L1_o$ grains is required to maintain n_o. At this point in the investigation the exchange energy constant was held at 4000Oe and the temperature of the thin film was held at 300K. As expected increasing K_v increases the coercivity of the thin film. Figure 6.1 shows the hysteresis curves generated over the full range of anisotropies studied, plotted as ($M_z(t = 6.0ns)$ vs H). The coercivity for the 20% $L1_o$ case was calculated to be 20599Oe. This highlights the need for new methods of magnetic data storage, as a coercive field, H_c, of 20599Oe is above what is achievable with current write head technologies. A larger applied field strength, H_r, is needed to fully reverse the magnetisation of the thin film, the 20% $L1_o$ case requires H_r to be above 39495Oe, almost double the coercivity, figure 6.1.

As expected H_c and H_r have an almost linear relationship with the anisotropy field. Increasing K_v, increases the energy barrier for reversal as in the S-W model. Figure 6.1 shows the coercivity and reversal field for the full range of anisotropies studied. Individual grains of equal size and shape in isolation would show an entirely linear relationship, as the anisotropy field would be the only barrier for reversal. The situation is more complex in the thin film. The exchange field and dipole field effect the reversal dynamics of the individual grains and therefore the system as a whole. The hysteresis curves for the lower anisotropy cases in figure 6.1 (10% - 40% $L1_o$) have a pronounced kink at negative M_z. This is caused by a slowing of the thin film reversal process brought about by the dipole field.

As the dipole field builds (generated by the magnetisation of the grains that have reversed and therefore acting in the opposite direction to the applied field) the effect of the applied field is reduced and if the dipole field builds to a sufficient level further reversal of the individual grains is slowed or even stopped.

The dipole field is generated by the individual grains magnetisation within the thin film, and acts in the opposite direction to the magnetisation that creates it. Therefore at the start of the simulation the dipole field works to lower the energy barrier of magnetisation reversal for individual grains, and is equal to H_D=-4π**M**. As the reversal process progresses the magnetic profile of the thin film changes, some of the grains remain in the initial positive position and some are now in the negative position after reversal. This alters H_{eff} locally on the thin film. The situation is therefore that when a single magnetisation that has not flipped, m_{nf}, (or small number grouped together) is surrounded by grains where the magnetisation has flipped, m_{hf}, the energy barrier for reversal for m_{nf} is raised. If the dipole field is sufficiently large in comparison to the applied field and/or anisotropy field then the barrier for reversal for m_{nf} is raised to a point where the grain/grains are much less likely to reverse, and some of the grains become trapped by the increased energy barrier created by the dipole field generated by m_{hf}. This causes the kink in the hysteresis curves at the lower anisotropies seen in figure 6.1. The effect is not seen in the higher anisotropy regimes, above 40% $L1_o$ ordered grains the hysteresis curves show a more linear relationship between the applied field and the magnetisation, figure 6.1. The dipole field generated is of course independent of K_v. As the higher anisotropies require a relatively larger applied field to reverse the magnetisation of the thin film, the dipole field is relatively smaller and therefore its effect is reduced.

In the 20% $L1_o$ regime, when the applied field is sufficiently large, a portion of the grains reverse quickly and the magnetisation enters a metastable state. This causes the reversal process to come to an abrupt halt, figure 6.2. In the higher anisotropy regimes the reversal process for the thin film is relatively slow and requires larger fields as shown in figure 6.2. The M_z time sequences for the 100% $L1_o$ case show a much slower reversal rate when compared with the 20% $L1_o$ case. This is caused by the diminished effect of the applied field.

For the lower anisotropies investigated the strength of the dipole field is of a similar order as the applied field strength and more importantly H_K. Therefore the dipole field has a significant effect in the reversal process. The initial set up of the thin film has all of the individual spins aligned, therefore the dipole interaction is reducing the energy barrier for each spin. In the 20% $L1_o$ case with zero exchange coupling the magnitude of the dipole field is sufficient to cause

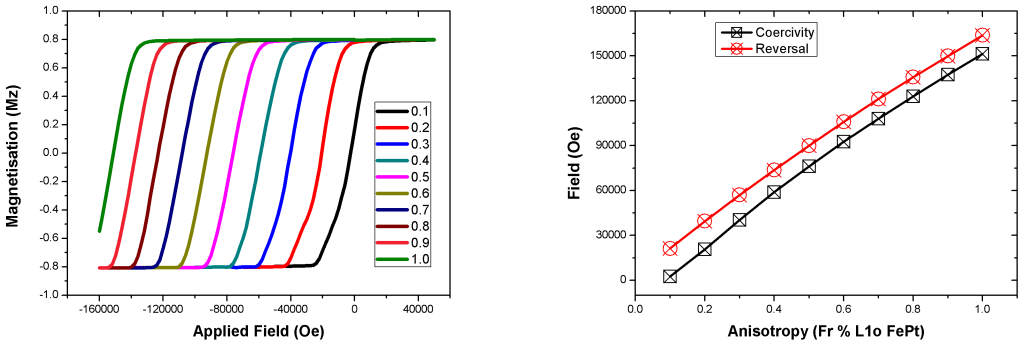

Figure. 6.1: On the left hand side: The effect on the hysteresis curves when increasing the anisotropy energy K_v. The anisotropy energy is given as the fractional percentage of $L1_o$ ordering of the FePt in the thin film. On the right hand side: A linear relationship between the anisotropy field the coercivity and reversal fields. The reversal field is taken from the graph on the right hand side. The exchange field is held constant at 4000Oe.

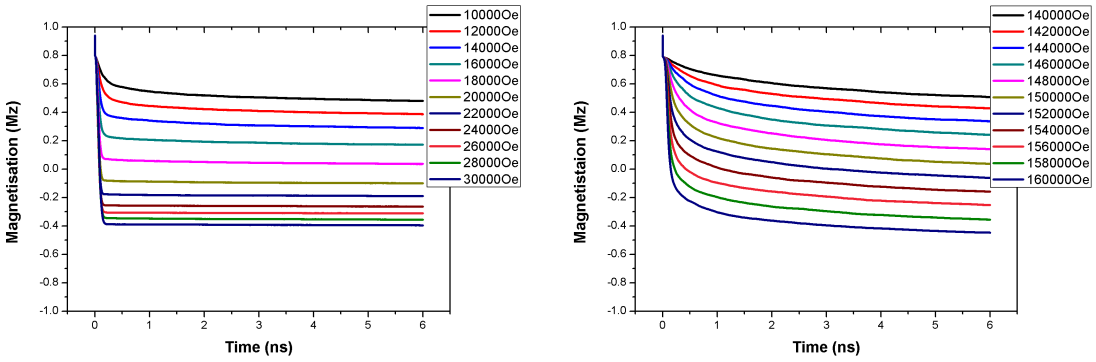

Figure. 6.2: A time sequence showing the magnetisation reversal process for the 20% $L1_o$ (left hand side) and 100% $L1_o$ (right hand side) cases, with a 4000Oe exchange field. In the 20% $L1_o$ the dipole field, generated by m_{hf}, is seen to stop the reversal process entirely. Where as the higher anisotropy regimes significantly slows the reversal process.

some of the grains to reverse in an otherwise thermally stable system. Figures 6.3 and 6.5 show a portion of the individual grains switching with no applied field. The dynamic motion of an individual magnetisation, $\mathbf{m}_i$, means the effective field acting on $\mathbf{m}_i$ is constantly changing. In the lower anisotropy regime the dipole field has a significant contribution to the effective field acting on $\mathbf{m}_i$ and can cause individual grains to switch. Increasing the exchange coupling between the grains reduces and even stops this from happening. With an exchange field above 4000Oe no spins reverse in zero field and the remanence is saturated.

6.2 Exchange dependence

The inter-granular exchange constant, H_{exc}, effects the magnetisation reversal process in a more complex manor than the anisotropy field. Figures 6.3, 6.4 and 6.5 help describe this relationship. The exchange field is only present when the magnetic grains are in ensemble. In the 0Oe exchange regime the precessional motion of the magnetisation of an individual grain is only weakly dependent on the motion of the neighbouring grains magnetisation through the dipole field. As mentioned above H_{exc} couples the precessional motion of the magnetisation of the neighbouring grains within the thin film, and therefore the reversal of the magnetisation is also coupled. The coupling effect of the exchange field is proportional to the magnitude of the exchange constant H_{exc}. Above a certain level of H_{exc} all the grains magnetisation are precessing together and the reversal process is no longer S-W switching and domain formation and subsequent domain wall motion switching is seen.

The hysteresis curves have three distinct points over the applied field range. The applied field which is capable of initiating magnetisation reversal (the initiation field H_I), the applied field which demagnetises the thin film (the coercive field H_c) and the minimum field which reverses the magnetisation (the reversal field H_r). Increasing the exchange field effects all three of these fields differently.

In both anisotropy regimes investigated increasing the exchange field increases H_I, figure 6.3, 6.4 and 6.5. The initiation field increases by a similar amount when increasing the exchange field from 0Oe to 30000Oe, roughly 17000Oe for the 20% $L1_o$ case and 20000Oe for the 100% $L1_o$ case. The grain size dispersion of the thin film is such that a small portion of the grains have a much lower thermal stability constant $K_v V/kT$ than the average for the thin film. Therefore the grains have different switching requirements. In the higher exchange regimes the smaller grains are coupled to the larger grains and visa versa. This raises the energy barrier for reversal for the smaller grains and also lowers the energy barrier for the larger grains, effectively averaging the energy barrier for reversal for the interacting grains. At the same time the exchange field counteracts the demagnetising tendency of the dipole field. As a result the field required to initiate magnetisation reversal increases, as seen in figures 6.3, 6.4 and 6.5.

Figure 6.4 shows a alternative way of viewing the hysteresis data from figure 6.3. The M_z(t=6.0ns,H_E >0) is plotted against M_z(t=6.0ns,H_{exc}=0) which shows the relative effect of H_{exc} on the reversal process. Initially the exchange

field has a more pronounced effect on H_I for the 20% $L1_o$ case verses the 100% $L1_o$ case. Initial increases in H_{exc} mean larger increases in H_I for the lower anisotropy, also the increase in H_I stops earlier (relative to H_{exc}). In the higher anisotropy regime H_{exc} is comparatively smaller (and therefore has less effect) which explains the initial larger increase in H_I at the lower anisotropy.

Exchange coupling has a more pronounced effect on the reversal field. In the 20% $L1_o$ simulations, increasing the exchange field from 0Oe to 30000Oe reduces the reversal field by approximately half, from ∼45000Oe to ∼22500Oe. In the larger anisotropy regime, 100% $L1_o$ ordered, the effect is not as pronounced. Over the same exchange field range the reversal field reduced from ∼166000Oe to ∼157000Oe, only 9000Oe or roughly a 5% reduction. Clearly the the reduction is going to be proportionally less, as H_I, H_c and H_r all scale with K_v. As mentioned above, in the 20% $L1_o$ case the lower exchange hysteresis curves have the apparent kink that is not seen in the 100% $L1_o$ case. As discussed above the kink is caused by the dipole field stopping the reversal process. Increasing the exchange field reduces the effect of the dipole field and removes the kink from the hysteresis curves. The exchange field effectively reduces the energy barrier for reversal for the neighbouring grains. In the lower anisotropy case, as H_D is of the order of K_v and H, the exchange field has two effects working together. It not only alters the reversal process by coupling the motion of the grains, it also reduces the effect of the dipole field. In the higher anisotropy regime, above 40% $L1_o$ ordered grains, the effect of the dipole field is already reduced therefore the exchange field can not further reduce this effect and as a result H_r is more weakly dependent on exchange at higher anisotropies.

The exchange field effects the coercivity in a more complex manor, than that discussed above, figures 6.3, 6.4 and 6.5. In the 20% $L1_o$ case first increasing the exchange field from 0Oe works to increase the coercivity of the thin film. With an exchange field above 10000Oe the opposite occurs and the coercivity begins to reduce. However, in the 100% $L1_o$ case increasing the exchange field increases the coercivity of the thin film. The dipole field effect (briefly discussed above) and the reduced effect of H_{exc}, explain the relationship between the coercivity and the exchange field over the different anisotropy regimes. In the 20% $L1_o$ case the dipole field has a pronounced effect on the reversal process, slowing and evening stopping magnetisation reversal.

A possible explanation is that the exchange field initially increases the coercivity by overcoming the demagnetising effect of the dipole field, with non-coherent reversal processes setting and reducing the coercivity for stronger exchange coupling. There is no observed peak in the coercivity for the 100%

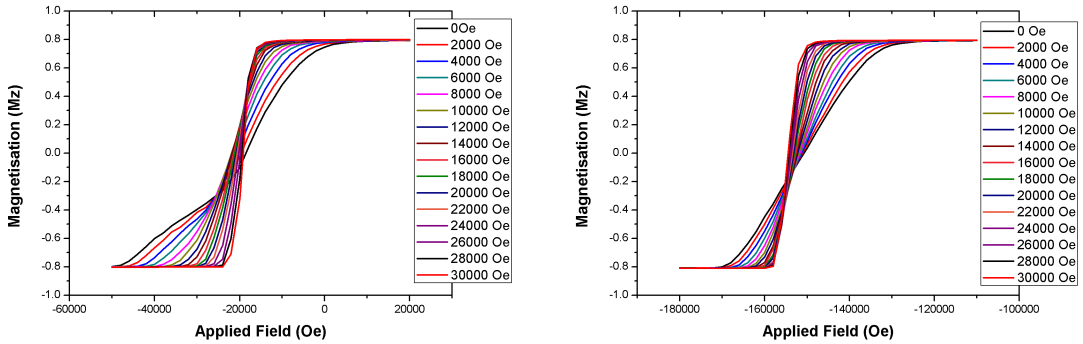

Figure. 6.3: The effect on the hysteresis curves when increasing the inter-granular exchange coupling. The anisotropy is 0.2 = 20% $L1_o$ on the left hand side and 1.0 = 100% $L1_o$ on the right hand side.

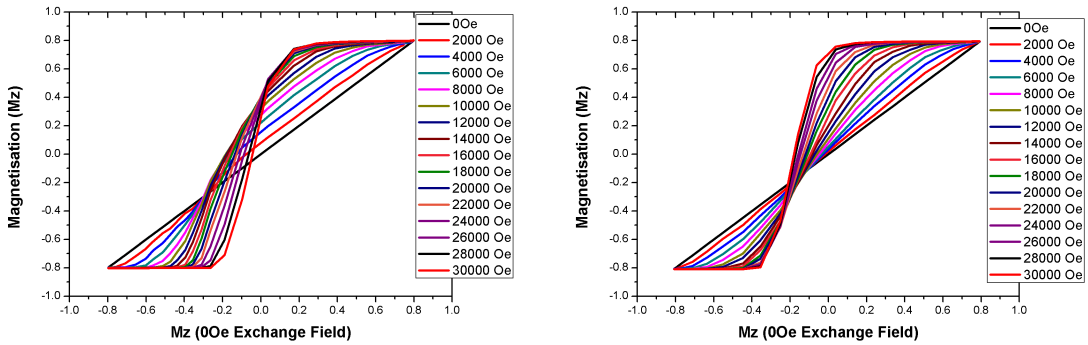

Figure. 6.4: An alternative way of analysis the hysteresis data from figure 6.3. The relative effect of the exchange field is determined by plotting $M_z(H_{exc} > 0)$ V's $M_z(H_{exc} = 0)$.

$L1_o$ case. The previous explanation suggests that there may be a peak at higher exchange, but such values would be non-physical in relation to practical media.

Figure 6.6 shows M_z time sequence diagrams for the two anisotropy regimes and for the full range of exchange constants. The effect of the anisotropy field is highlighted. The reduced component of M_{xy} at the higher anisotropy slows the reversal process markedly. The exchange field dramatically slows the thin film reversal process in the 100% $L1_o$ case. The size of the domains that form and the way they form are similar in both anisotropy regimes, only the time scale is relatively slower in the higher anisotropy regimes.

6.3 Domain formation and domain wall motion

As discussed above the exchange field alters the magnetisation reversal process. In the zero exchange regime the motion of the grains is coupled only by

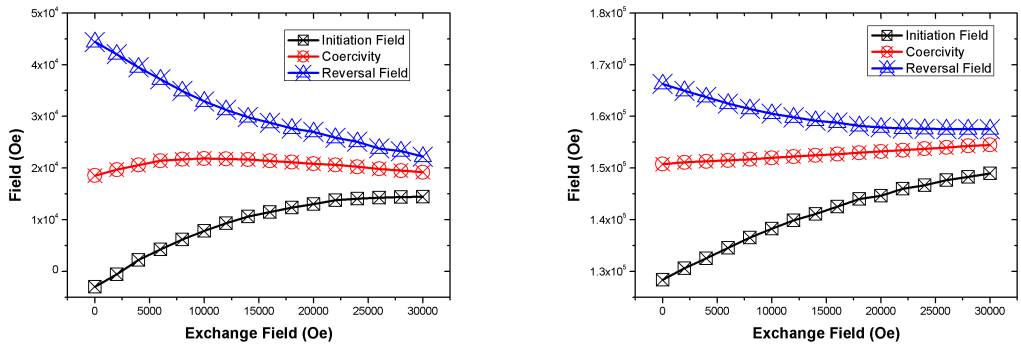

Figure. 6.5: A fit to H_I, H_c and H_r taken from the hysteresis data in figure 6.3. The exchange field has a similar effect in both anisotropy regimes.

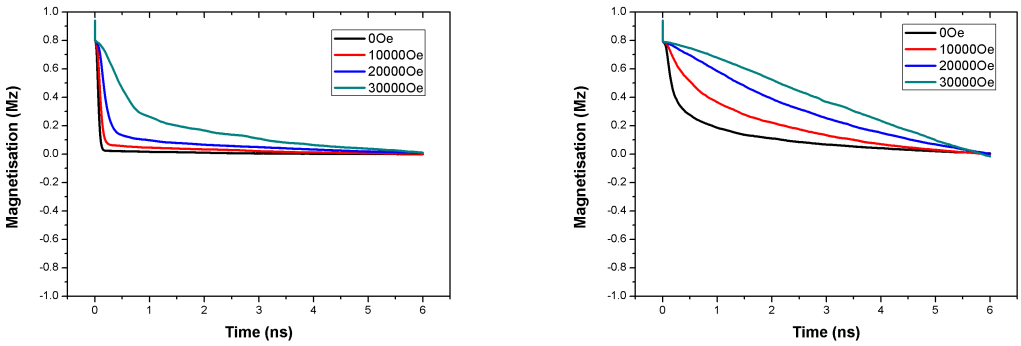

Figure. 6.6: Time sequence diagrams showing the reversal of the thin film magnetisation in the z-axis. On the left hand side: The 20% $L1_o$ thin film over a range for H_{exc}. On the right hand side: The 100% $L1_o$ thin film over the same range for H_{exc}. The exchange field slows the reversal process.

magnetostatics. In the larger exchange regimes the grains are coupled and individual grains do directly effect the motion of the neighbouring grains, by lowering the energy barrier for reversal. This effect causes the reversal process to nucleate on individual grains and then domains spread out across the thin film via domain wall motion. This effect can be seen in the two images at the top of figure 6.7. The images represent the magnetic configuration of two separate 20% $L1_o$ ordered thin films with different exchange constants. Each image was taken at 6.0ns. The image on the left has no exchange field and has a small amount of correlation between the grains. The images on the right have a 30000Oe exchange constant and show much larger domains forming. The progression of the reversal process for both exchange regimes is shown in full in appendix 1. The 30000Oe exchange coupled thin film clearly shows domain wall motion in action.

As mentioned above increasing the anisotropy field slows the reversal process

and this is seen to reduce the size of domains that form when the thin film is demagnetised. The top two images in figure 6.7 are the 20% $L1_o$ case (H_{exc} =0Oe on the left and H_{exc} = 30000Oe on the right) and the bottom two images are the 100% $L1_o$ case. The domains forming in the 100% $L1_o$ case are marginally smaller for both exchange regimes.

There is a noticeable grouping between the positive and negative magnetisation for the 20% $L1_o$ thin film with 0Oe exchange coupling, the top left hand side of figure 6.7. As no exchange field is present there was expected to be no domain formation between the magnetisation. To investigate this further the thin film was demagnetised by heating up to T_c then allowing to cool to ambient, allowing domains to form without an applied field. At T_c the magnetisation of the individual grains is destroyed and the magnetisation of the thin film is in a disordered state. The domains form as the system temperature returns back to ambient. Under these conditions the thin film with zero exchange shows no domain formation, figure 6.8 on the left hand side. The experiment was then repeated with a 30000Oe exchange, and the thin film formed relatively smaller domains. This implies the formation of domains is a dynamic process and domain formation is in part dependant on the path taken to form the domain. Therefore the formation of the domains in the 0Oe case is caused by the dipole field trapping regions of grains in a potential well with a higher energy barrier, as discussed for the lower exchange case above.

The rate at which the thin film is demagnetised alters the size of the domains that form at M_z=0. Figure 6.9 show two images of the 30000Oe exchange coupled thin film demagnetised at different rates. The demagnetisation was achieved in a simple way, by applying a field (of a given strength) until the thin film is demagnetised, then removing the field allowing the thin film to remain demagnetised. The image on the left was demagnetised with a 20000Oe applied field, taking 0.8526ns and the thin film on the right was demagnetised with a 26000Oe applied field taking 0.2101ns. Taking the 30000Oe image from figure 6.7 (demagnetised in 6.0ns) this gives three identical thin film demagnetised at different rates. The largest domains form in the thin film which was demagnetised slowest, where the applied field is equal to H_c. Raising the applied field strength above H_c increases the reversal rate which causes smaller domains to form. This effect is also seen in the 100% $L1_o$ thin film. Smaller domains form in the 100% $L1_o$ thin film that demagnetises slower than the 20% $L1_o$ thin film, left top and left bottom of figure 6.7.

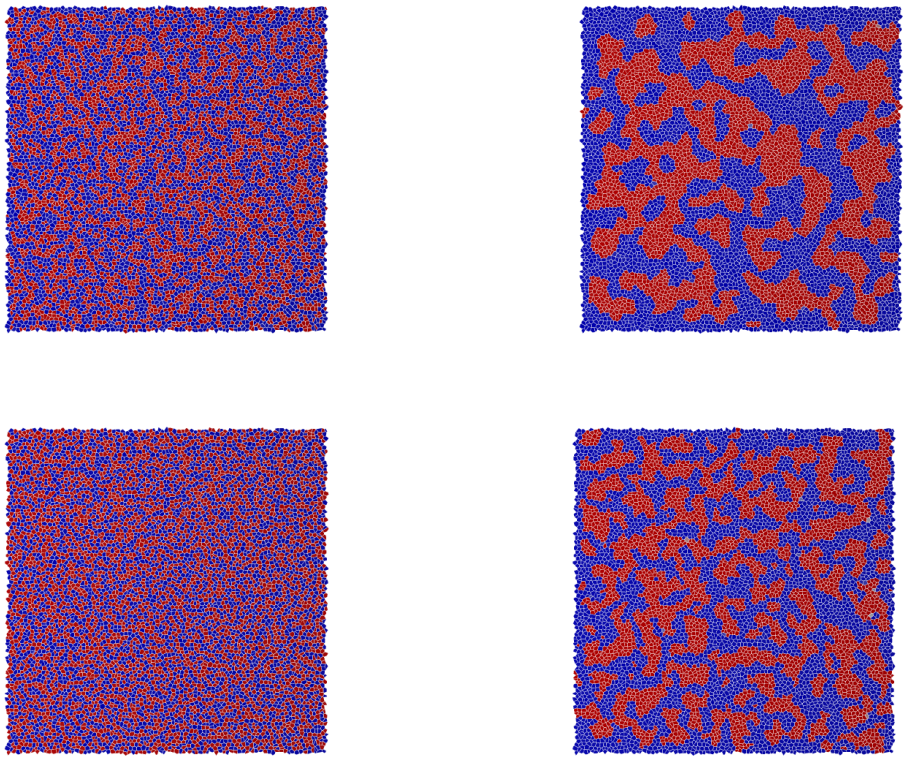

Figure. 6.7: AT THE TOP: On the left hand side: An image showing the magnetisation of the individual grains in a 20% $L1_o$ FePt thin film, with 0Oe exchange coupling, which has been demagnetised. On the right hand side: An image showing the magnetisation of the individual grains in a 20% $L1_o$ FePt thin film, with 30000Oe exchange coupling, which has been demagnetised. Note the formation of larger domains in the higher exchange regime and some grouping in the 0Oe exchange regime. AT THE BOTTOM: On the left hand side: An image showing the magnetisation of the individual grains in a 100% $L1_o$ FePt thin film, with 0Oe exchange coupling, which has been demagnetised. On the right hand side: An image showing the magnetisation of the individual grains in a 100% $L1_o$ FePt thin film, with 30000Oe exchange coupling, which has been demagnetised. Note the formation of larger domains in the higher exchange regime is still present, but they are smaller than the 20% $L1_o$ case.

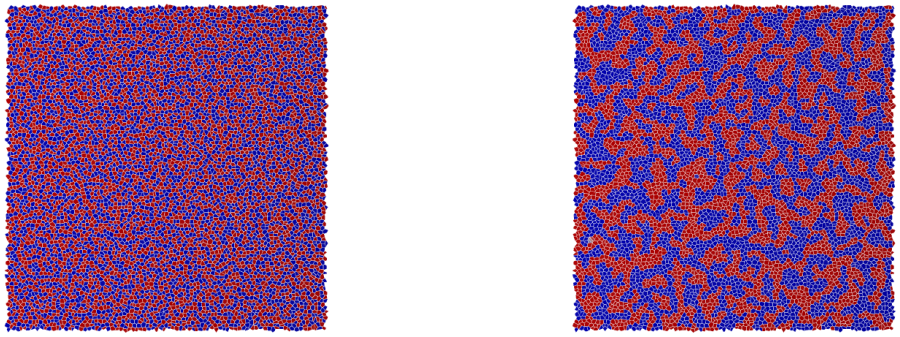

Figure. 6.8: On the left hand side: An image showing the magnetisation of the individual grains in a 20% $L1_o$ FePt thin film, with 0Oe exchange coupling, which has been demagnetised by heating up to T_c then allowing to cool to ambient. On the right hand side: An image showing the magnetisation of the individual grains in a 20% $L1_o$ FePt thin film, with 30000Oe exchange coupling, which has been demagnetised by heating up to T_c then allowing to cool to ambient. Note there is no domain formation in the 0Oe exchange coupled thin film.

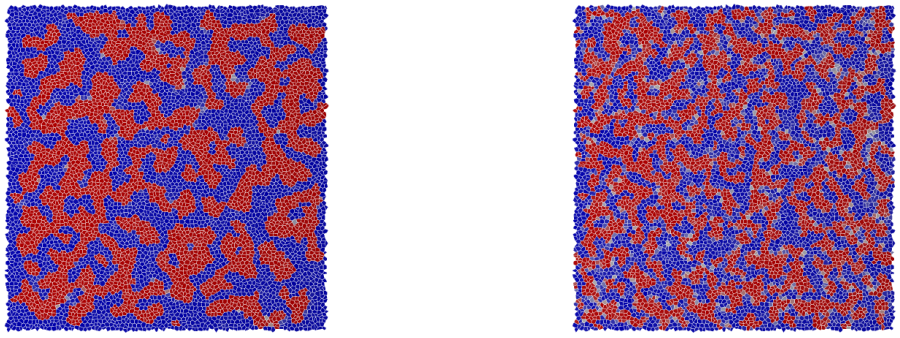

Figure. 6.9: On the left hand side: An image showing the magnetisation of the individual grains in a 20% $L1_o$ FePt thin film, with 30000Oe exchange coupling, which has been demagnetised with a 20000Oe applied field. On the right hand side: The 20% $L1_o$ thin film with 30000Oe exchange coupling that was demagnetised with a 26000Oe thin film. Smaller domain from at M_z = 0.0 when the system is demagnetised at a faster rate.

6.4 Coercivity at elevated temperature

Heat assisted magnetic recording (HAMR) hinges on the temperature dependence of the anisotropy energy leading to reduced reversal field. As expected the coercivity of the thin film drops as the temperature of the thin film is raised, figure 6.10. The fall in the coercivity is not linear and increases as the Curie temperature is approached, falling to effectively zero ∼10 - 60 Kelvin below T_c dependant on the anisotropy field. The coercivity has dropped to zero at a lower temperature than T_c, as the thermally activated switching is sufficient to demagnetise the thin film without an applied field. The temperature at which the film demagnetises without an applied field is dependant on K_v as a relatively larger component of K_v remains at higher anisotropies. The reduction in H_c and therefore H_r will not be as large under HAMR conditions as the elevated temperature regime is transient in HAMR and therefore the thermal assist is not as large.

The Sharrock law[27], equation 6.1, describes the time and temperature dependant change in the coercivity of single domain magnetic particles. To describe the case in figure 6.10 the time, (t), is fixed at 1.5ns which simplifies the equation so that it describes only the temperature dependant change in the coercivity, H_c.

$$H_c(t) = H_K(T)\left[1 - \left[\frac{k_B T}{K_{v(T)} V} ln\left(\frac{f_o t}{ln(2)}\right)\right]^{\frac{1}{2}}\right] \tag{6.1}$$

Where $H_K(T) = K_v(T)/2m_s(T)$, $K_v(0)$ and f_o is the attempt frequency equal to approximately $10^{10} H_z$ and t = 1.5ns (the time scale of the experiment), therefore the Sharrock law describes the temperature dependance of the coercivity in terms of the temperature dependant magnetisation, $m_s(T)$, and the temperature dependant anisotropy, $K_v(T)$, equation.

$$H_c(t) = \frac{2K_v(T)}{m_s(T)}\left[1 - \left[\frac{k_B T}{K_v(T) V} ln\left(\frac{f_o t}{ln(2)}\right)\right]^{\frac{1}{2}}\right] \tag{6.2}$$

The effect of the exchange field is reduced at higher temperature. The right hand side of figure 6.10 shows the coercivity for the 20% $L1_o$ case calculated over a range of exchange field strengths and temperatures. At higher system temperatures the magnetisation and anisotropy field are reduced and the thermal energy is raised. The raised thermal energy and reduced anisotropy effect the

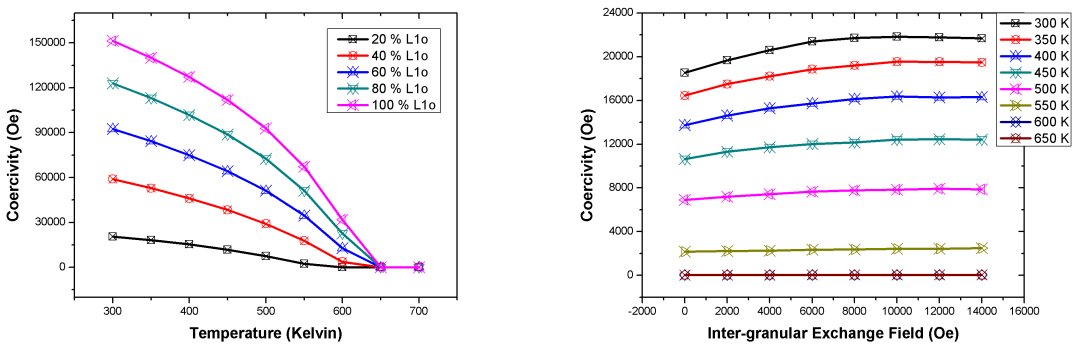

Figure. 6.10: On the left hand side: The coercivity for 20% $L1_o$ case calculated over a range of exchange field strengths and system temperatures. The effect of the exchange field is reduced at higher temperatures. On the right hand side: The coercivity dropping to zero at the system temperature rises and approaches the Curie point, over a range of anisotropies.

stability of the magnetisation, this puts the magnetic profile of the thin film in a disordered state which reduces the effect of the exchange field. The exchange coupling between each grain is reduced as the relative exchange coupling coupling between the grains is proportional to the magnitude of $\mathbf{m}_i$ and $\mathbf{m}_j$ is reduced at higher temperature.

6.5 Relaxation time calculations

The LLB model has been used to calculate the relaxation time of the modelled nano particles. Partially $L1_o$ ordered FePt hexagonal grains with volume 1.87061×10^{-19}cc are used to investigate the anisotropy and temperature dependence on the relaxation time, τ. The study is performed over a range on anisotropies, 0.05% - 4.0% $L1_o$ ordered FePt and range of temperatures, 300 - 700 Kelvin, over the Curie point. The LLB calculation is compared to the Arrhenius-Néel equation over the range of anisotropies and temperatures studied. The Arrhenius-Née'l law is found to fail at high temperatures.

6.5.1 Calculation method

The method uses a set of 'non interacting' identical hexagonal grains (simulated with the voronoi construction) each with a single spin (simulated by the LLB equation). The time evolution of each magnetisation is tracked over a 50ns period and the relaxation time determined. The transition of the magnetisation between 'fixed points', on the z-axis, is captured to determine the number of times the magnetisation has flipped in a given time. Figure 6.11 gives an example of the

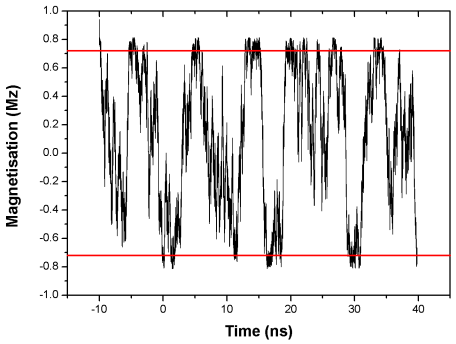

Figure. 6.11: An example of the transition of the magnetisation between stable positions, over a 50 nano second period.

dynamics of the magnetisation, m_z, over the 50 nanosecond period. The method allows the first 10 nano seconds for equilibration. A transition is recorded when the magnetisation changes sign and reaches a specified value , taken here as $|m_z|$=0.72. This technique avoids false counts being registered, as the m_z value was seen to oscillate in the region between the stable magnetisation positions; examples of which can be seen in fig. 6.11.

6.5.2 Anisotropy dependence

Firstly the relaxation time was calculated over a range of anisotropies from 0.05% - 2.0% $L1_o$ ordered FePt. Figure 6.12 shows the relaxation time calculated using the LLB model in comparison with the analytic solution from Arrhenius-N*é*el (A-N). The relaxation time calculated with LLB model (τ_{LLB}) increases exponentially with increasing anisotropy. Although τ_{LLB} has a different anisotropy dependence from the that calculated with the A-N equation (τ_{A-N}), τ_{A-N} increases at faster rate when compared with τ_{LLB}, figure 6.12.

$$\tau_n = \tau_o \exp\left(\frac{K_v V}{k_B T}\right) \tag{6.3}$$

To investigate higher anisotropies (0.05% - 4.0% $L1_o$ FePt) and improve the accuracy of the calculated relaxation time at the lower anisotropies, the simulation time was increased to 1000 nano seconds. The relaxation time is larger for the higher anisotropies, therefore a longer simulation is needed as the number of flips is much lower. Figure 6.12 shows the relaxation time over the larger range of anisotropies calculated using the 1000ns simulations and compares this with the 40 nano second result. The 40 nano second and 1000 nano second simulations are a close match, this result goes some way to validating the later 40 nano

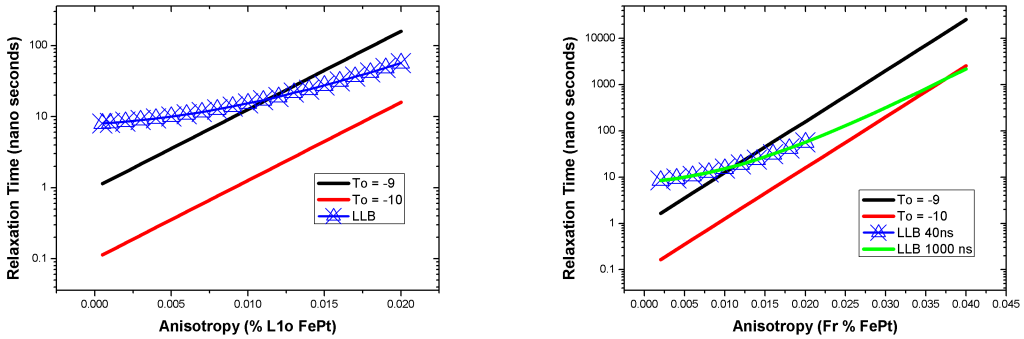

Figure. 6.12: On the left: The relaxation time of 6nm hexagonal grains calculated with the LLB model (calculated over 40ns), over a range of anisotropies between (0.05 - 2.0)% $L1_o$ ordered FePt, compared with τ_n. on the right: The relaxation time of 6nm hexagonal grains calculated with the LLB model (calculated over 1000ns to check the accuracy of the 40 nano), over a range of anisotropies between (0.05 - 4.0)% $L1_o$ ordered FePt, compared with τ_n. The 1000ns data is in accord with the 40ns data.

second simulations. τ_{LLB} still has a different dependence from τ_{A-N} at the higher anisotropies, although it is tending towards what is predicted by Arrhenius-Néel. A longer simulation time is need to investigate this dependence further, but this was not possible due to time constraints (as the simulations time would need to increase exponentially with K_v). As will be discussed later, the discrepancy for short relaxation times is probably due to a failure of the Arrhenius-Néel law, which is strictly valid only for large values of $K_v V/k_B T$.

6.5.3 Temperature dependence

To investigate the temperature dependence the calculation method had to be changed, as the the magnetisation length is less than 0.72. Therefore the condition was changed to, when the sign of m_z changes and $|m_z| > 0.95|m|$. To investigate the temperature dependence of τ_n the anisotropy was held at 1.4% $L1_o$ ordered FePt, only as the relaxation time calculated with the LLB model at this anisotropy lies between that predicted by Arrhenius-Néel. The LLB calculated temperature dependant relaxation time (τ_{LLB}) is in good agreement with the Arrhenius-Néel relaxation time (τ_{A-N}) at temperatures below 500K ($T \lesssim 3T_c/4$). Above 500K τ_{LLB} begins to decrease rapidly, where as τ_{A-N} decreases at a constant rate over the range of temperatures investigated, figure 6.13. At T_c τ_{LLB} is two to three orders of magnitude smaller than τ_{A-N}. This is very important result as the Arrhenius-Néel law can be used to calculate the energy barrier for reversal. Clearly the energy barriers calculated at higher temperatures will be incorrect.

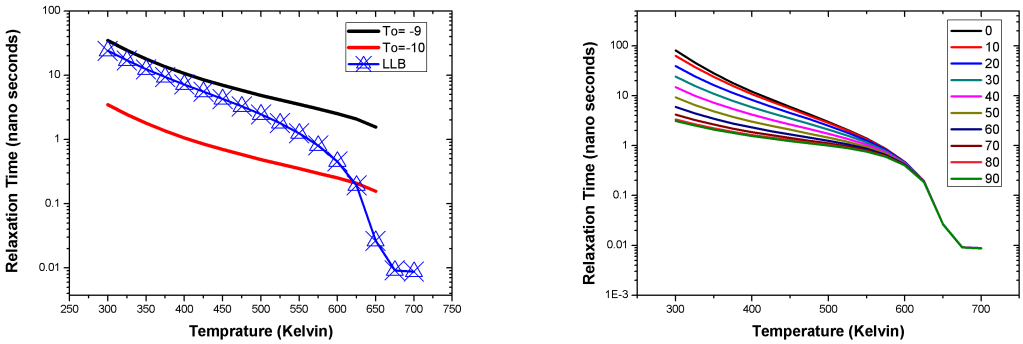

Figure. 6.13: The left hand side: The temperature dependence of relaxation time approximated by the LLB model, over a range of temperatures, 300 - 700 Kelvin. Taken from 40 nano second simulations. For comparison the analytic solution as by Arrhenius-Néel. The right hand side: The angular dependance of the relaxation time, due to an applied field of 500Oe, over a range of field angles and system temperatures.

6.5.4 Applied field: Angular dependence

The relaxation time, when an external field is a applied, is investigated to determine the effect of the field magnitude and orientation. The relaxation time is calculated over a range of system temperatures and applied field angles (the angle is given in degrees from the easy or z axis, an angle of 0° means the applied field is anti-parallel with the easy axis). Figure 6.13 shows the approximated relaxation time with a 500Oe applied field. As expected the relaxation time decreases as the temperature is raised, as seen in the zero applied field case. When the applied field makes an angle of 0° with the easy axis (aligned anti-parallel) the relaxation time is slowed from ∼24 to ∼80 nano seconds, compared with the zero applied field simulation, figure 6.13. The relaxation time is slowed as the applied field changes the energy profile for the grains, similar to what was seen in the simple S-W analysis.

At lower temperatures there is a significant dependence of the relaxation time on the applied field angle. At 300K τ_n has range of ∼80 nano seconds figure 6.13. Increasing the angle made by the applied field (from 0°) speeds up the relaxation time, at 30° the relaxation time is comparable with the no applied field case. Increasing the applied field angle above 30° further speeds up the relaxation time. When the applied field makes an angle with the easy axis there is a component in the xy-plane. This pushes the magnetisation away from the easy axis which raises the energy of the grain (by increasing the anisotropy energy and zeeman energy) which effectively lowers the energy barrier for reversal. The component of the applied field in the z axis is less (with increasing angle) which raises the

depth of the energy well at π rads. These two effects reduce τ_n. The relaxation time is at a maximum when the applied field angle is at a maximum (90°), where there is no component of the applied field in the z axis.

At higher temperatures the field angle no longer effects the relaxation time. At the higher temperatures, 500K and above for the 100Oe applied field case and 600K and above for the 500Oe case, the applied field strength is not able to overcome the thermal energy of the grains. This probably reflects the transition into the elliptical and linear reversal regimes where the energy barrier becomes independent of anisotropy.

6.6 Summary and further work

As expected, increasing K_v increases the coercivity and reversal field of the thin film. The increase is not entirely linear and is effected by the dipole and exchange fields. The dipole field generated by each grain has a significant impact on the reversal process for thin films where H_D is of the same order as K_v. The reversal process comes to a complete halt when the dipole field is sufficiently large and this raises the field required to fully reverse the magnetisation of the thin film. The effect is reduced at higher anisotropies as the dipole field is relatively smaller compared to the applied field needed to reverse the grains. Increasing the exchange coupling also reduces the effect of the dipole field. In the higher exchange regimes reversal of an individual grain lowers the energy barrier for reversal for the neighbouring grains, which offsets the increased energy barrier that the dipole field generated by the grain that has switched. The reversal process is slower in the higher exchange regimes, as reversal of the individual grains is not independent and happens via domain wall motion. Also increasing the anisotropy slows the reversal process. Increasing the exchange field changes the way the thin film reverses. The individual grains motion is not independent and the reversal of individual grains lowers the energy barrier for reversal for the neighbouring grains. This causes the reversal process to nucleate on individual grains across the thin film. Reversal then spreads from these grains via domain wall motion. The size of the domains that form is effected by the rate of system reversal. Higher reversal rates cause smaller domains to form.

The relative effect of the exchange field in the different anisotropy regimes is difficult to determine. The effect of the exchange coupling does, on first inspection, appear to be reduced. The initial increase of H_{exc} in the lower anisotropy regime has a larger effect on the reversal process, but the effect of the exchange field continues to alter the reversal process into higher values of H_{exc}.

The higher anisotropy effects the reversal process in a subtle way, by slowing the thin film reversal process. This changes the reversal dynamics, making the relative effect of the exchange field difficult to determine.

For low temperatures the relaxation time calculated using the LLB model has a close match to theory, in the form of the Arrhenius-Néel law. The anisotropy dependence is exponential and is tending toward A-N theory at the highest anisotropies studied. This is because the A-N law is valid only for large values of KV/k_BT. A continued investigation is required to determine the anisotropy dependence on τ_{LLB} at the higher anisotropy regimes. The LLB model showed a good agreement with A-N between 300K and 500K. Above this the agreement is lost and τ_{LLB} reduces at a much faster rate than τ_{A-N}. This is important in terms of the understanding of the HAMR process since the A-N law cannot be used in simple analytical models of HAMR.

7. Heat assisted magnetic recording

Heat assisted magnetic recording (HAMR) uses a laser pulse to locally heat the recording medium to reduce the anisotropy of the constituent grains to a level that can be recorded on. To simulate the temperature conditions of HAMR the following temperature profile is implemented. The temperature rise associated with the laser pulse is simulated as a step change from ambient (300K) to a maximum (Tmax) then following a gaussian back to ambient at a characteristic cooling rate, figure 7.1. The standard cooling rate used in the investigation is 0.5ns, which returns the system temperature back to ambient in approximately 1.0ns. The simulation time was reduced to 1.7ns, including a 0.2ns equilibration period before the simulated temperature rise at t=0.0, and then a 1.5ns HAMR simulation time. The simulation time was reduced to 1.7ns as the thermal assist has all but disappeared by this point.

The HAMR process is investigated over a range of maximum temperatures up to and above T_c and anisotropies 20% to 100% $L1_o$ ordered FePt to determine the affect on the magnetisation reversal process. The effect of inter-granular exchange coupling and the cooling rate are also investigated.

7.1 Thin Film Reversal process

The initial study concentrated on the 20% $L1_o$ case as this gives the minimum anisotropy required to hold a permanent magnetisation for 6nm grains (to

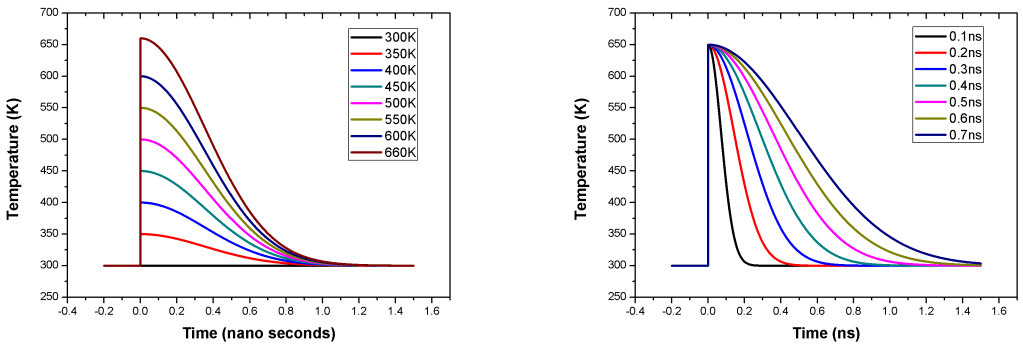

Figure. 7.1: The temperature profile of the thin film used to simulate HAMR style heating and cooling. On the right hand side: The temperature profile over a range of maximum temperatures up to T_c with a 0.5ns cooling rate. On the right: The temperature profile over a range of cooling rates heated up to T_c.

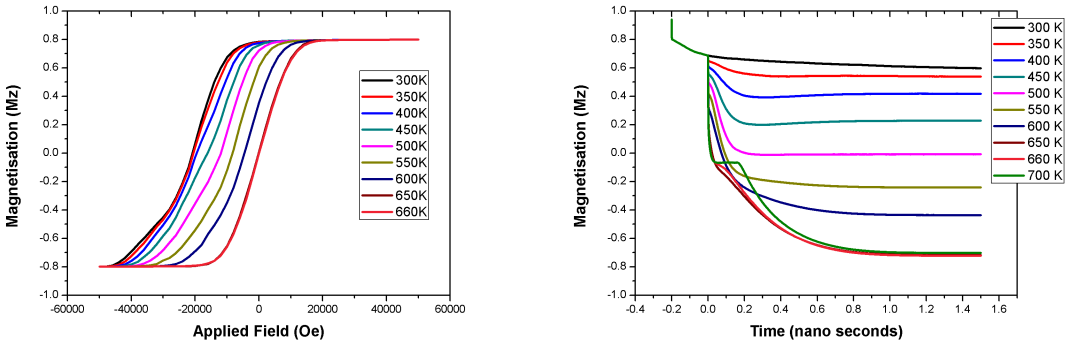

Figure. 7.2: On the left: Hysteresis curves for the 20% $L1_o$ case. Increasing the maximum temperature during the HAMR process reduces the applied field required to reverse the magnetisation of the thin film, shifting the hysteresis curves toward the positive end of the applied field range. On the right: Time sequences for the 20% $L1_o$ case, with a 12000Oe applied field. Magnetisation reversal increases as the maximum temperature is increased over successive simulation. The whole system reverses the magnetisation when the system temperature is raised to T_c during the HAMR process.

maintain n_o) and the exchange field was held at 4000Oe. To gain a general picture of the thin film response to the applied field at different maximum temperatures hysteresis curves were generated by plotting M_z(t=1.5ns) vs H. Increasing the temperature of the thin film during HAMR momentarily lowers the anisotropy of the individual grains increasing the effect of the applied field, which reduces the coercivity and reversal field, figure 7.2. The hysteresis curves show an applied field in the region of 12000Oe and a temperature approaching T_c are required to reverse 95% of the thin film magnetisation within the 1.5ns simulation time, figure 7.2. The reversal field has reduced by a significant amount when compared with the ambient temperature situation, but still remains at the upper limit of what is achievable [22].

Figure 7.2 shows the full M_z time sequence for the 20% $L1_o$ simulations with the 12000Oe applied field, over the range of maximum system temperatures investigated. Raising the temperature by only 50K increases the number of grains that reverse. For the 20% $L1_o$ case the dipole field effects the stability of the individual spins and can cause switching to occur in a thermally stable system where no applied field is present, as seen in the ambient temperature case with no exchange coupling. Therefore any small assist to the reversal process (be that an applied field or heat) will increase the number of grains that switch. At ambient temperature roughly 12.5% of the individual grains switch the magnetisation within the 1.5ns simulation time, due to the effect of the 12000Oe applied field alone. The simulation time was increased to 20.0ns to observe the

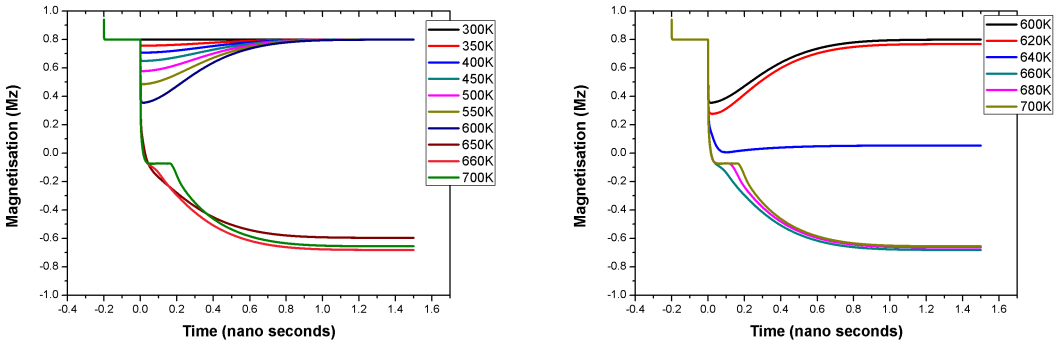

Figure. 7.3: On the left hand side: An M_z time sequence of the whole system, for 100% $L1_o$ grains. Showing the effect of increased temperature, during the HAMR simulations. On the right hand side: An M_z time sequence of the whole system, for 100% $L1_o$ grains. Over a narrower range of temperature.

continued switching of the grains and a total of 18.5% reversed by this time. Therefore when the temperature of the thin film is increased by a small amount the number of individual spins that switch increases, figure 7.2. The increase in the reversal percentage (brought on by the increase in the maximum temperature) is approximately linear, and as already stated the whole system is reversed when the maximum system temperature reached T_c.

The temperature required to initiate reversal is much higher for the 100% $L1_o$ ordered grains, than the 20% $L1_o$ case, figure 7.3 shows the M_z time sequence for the 100% $L1_o$ case, again with a 12000O applied field. This is due to a larger component of the anisotropy being present, relative to the 20% $L1_o$ case at the same temperature. Therefore a higher temperature is required to lower the anisotropy to a level where an equal applied field is capable of initiating the reversal process. In the simulation where the temperature reached 600K the anisotropy is sufficient to resist the applied field and as the system temperature returns back to ambient the magnetisation returns back to the initial state, showing effectively zero system reversal. The right hand side of figure 7.3 better highlights the effect of the thermal assist. At 620K the thin film shows a small portion of the grains reversing, approximately 2%. By increasing the maximum temperature to 640K almost half of the grains have reversed their magnetisation. Again increasing the maximum temperature by a further 20K to T_c, 660K, and now all of the grains have effectively reversed and the thin film has roughly 95% of it's overall magnetisation in the negative direction.

In the 20% $L1_o$ case the temperature increase effects the reversal percentage almost linearly, figure 7.2. The grain size dispersion of the thin film is such that

a relatively small portion of the grains reverse with the 12000Oe applied field alone. This can be seen in the initial 0.2ns of the 300K constant temperature simulation on the right hand side of figure 7.2. The rate of reversal drops off quickly, as the larger grains on average do not flip their magnetisation with only the applied field, figure 7.6. This result is in agreement with A-N theory (discussed in the theory section) as small decreases in the volume of the grains (at this scale) will drastically effect the stability of the magnetisation. The situation is therefore, that any small increase in the maximum temperature during the simulation will increase the number of grains that reverse as a function of the temperature increase. The rate of increase of the reversal percentage is not entirely linear, and increases as the maximum temperature approaches T_c. Increasing the anisotropy increases the temperature required to initiate reversal, as the magnitude of the anisotropy is a function of the temperature and therefore the higher the anisotropy the higher the temperature must be to allow an equal applied to overcome the anisotropy, figure 7.7. In the higher anisotropy regimes and at ambient temperature the associated thermal energy of the thin film is sufficiently lower than the region where reversal of the individual grains is likely to occur and no grains are seen to reverse the magnetisation with only the applied field. This effect means initial small increases in the temperature rise are not sufficient to lower the anisotropy to a level where reversal is likely. Therefore a higher increase in the temperature is required for any reversal to happen.

When the maximum temperature of the system exceeds T_c the reversal process is slowed, figure 7.2 and figure 7.3. Above T_c the grains are no longer ferromagnetic and the magnetisation fluctuates only existing spontaneously. The period of time where the system temperature is above T_c is dictated by the maximum system temperature and the cooling rate of the system, as all of the current simulation have a cooling rate of 0.5ns, the maximum system temperature alone dictates the time period above T_c. Therefore the magnetisation is rebuilt, aligned with the applied at a later point in the simulation, when the temperature drops below T_c. This effectively slows the reversal process. The rate at which the temperature reduces (dT/dt) is also dictated by the maximum temperature, as the system returns to ambient in the same time, roughly 1.0ns. Therefore when the system temperature is above T_c dT/dt is relatively large, so the system changes from an anisotropy that can be recorded on, to an anisotropy that can not be recorded on, relatively quickly. As a result the magnetisation that is in the positive direction, when T drops below the critical temperature, is held in that position, which marginally reduces the number of grains that reverse.

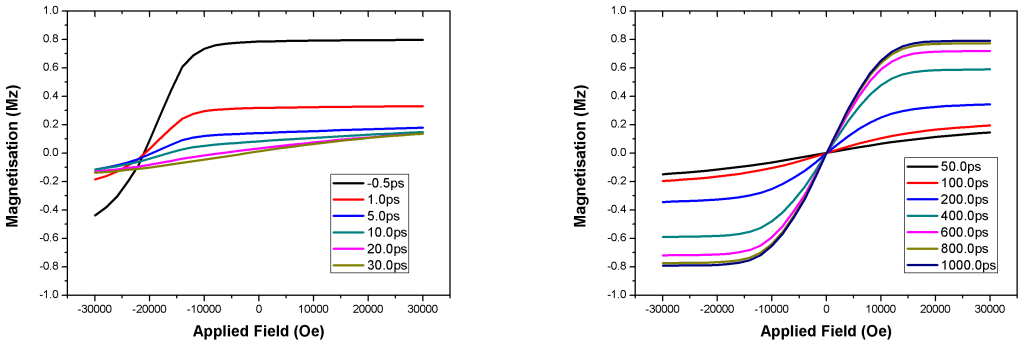

Figure. 7.4: Hysteresis curves for the 20% $L1_o$ case that was heated up to T_c, generated as M_z(t) vs H where t is a succession of time throughout the HAMR simulation. On the left hand side: The demagnetisation process over the first 30 pico-seconds after the temperature rise. On the right hand side: The reformation of the magnetisation as the system temperature cools, dictated by the applied field.

7.1.1 Time evolution of the thin film magnetisation

The magnetisation reversal process, under HAMR conditions, is a dynamic and variable process. Figure 7.4 shows hysteresis curves for the 20% $L1_o$ case where the thin film was heated up to T_c at a succession of times after the temperature rise (the hysteresis curves were generated by plotting M_z(t) vs H where t is a succession of times throughout the simulation). The magnetisation of the individual grains within the LLB model undertake both parallel and transverse relaxation. Parallel relaxation occurs due to the reduction in the magnetisation induced by the increased temperature, and is fast acting taking only pico-seconds. The transverse relaxation happens as the magnetisation precesses from one stable orientation to the other and the precessional motion is relatively slower than the reduction in the magnetisation and therefore transverse relaxation happens over a relatively longer time scale than the parallel relaxation. The parallel relaxation acts within the initial few pico-seconds after the temperature increase, causing the magnetisation to rapidly reduce in magnitude. This can be seen in the hysteresis curves in figure 7.4. The magnetisation reduces in magnitude similarly over the range of H investigated in the initial few pico-seconds after the temperature increase. At 5.0ps the individual grains magnetisation have reduced to the effective temperature dependant minimum, and at this point in the simulation there has been no further reversal of the grains brought about by the slower acting transverse relaxation mode. Beyond 5.0ps the shape of the hysteresis curves begin to change as individual grains begin to switch the magnetisation dictated by the applied field. In high positive fields the magnetisation of the grains do not flip and remain in the initial positive position and equally the high negative

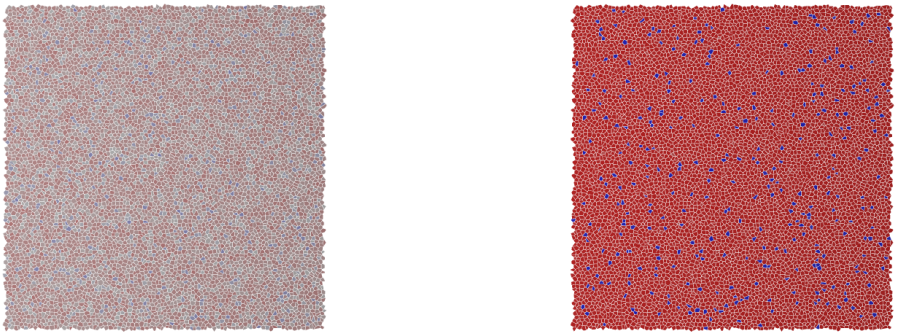

Figure. 7.5: Images a thin film that was heated up to T_c and a 12000Oe applied field was present, showing the demagnetisation and reformation process. On the left hand side: 100ps after the temperature rise the magnetisation of the individual grains are reduced and are showing a majority of grains having reversed. On the right hand side: 500ps after the temperature rise the magnetisation is reforming in the negative direction.

fields holds the magnetisation in the negative position after reversal. At 20.0ps the temperature still remains high and the applied field is controlling the shape of the hysteresis curves. Beyond 50.0ps the temperature of the thin film begins to drop sufficiently below T_c and the magnetisation of the individual grains returns. Where no applied field is present the thin film becomes demagnetised as an equal number of grains are in both orientations. If the applied field strength is sufficient then the magnetisation of the grains is rebuilt in the direction of the applied field, resulting in the characteristic shape seen in the T_c simulation in figure 7.2 and at 1000ps in figure 7.4.

7.1.2 Further HAMR effects

At T_c the magnetisation of all the grains are destroyed momentarily and then rebuilt in the applied field direction in about 1.0ns. Figure 7.5 shows two images of the thin film that was heated to T_c, at 100ps and 500ps after the temperature rise. The 100ps image is much fainter than the standard image, which indicates the magnetisation is at a reduced magnitude. Although the image is fainter the general red colour of the grains can be seen which show the majority of the grains have switched by this point. At 500ps the magnetisation of the grains has increased in magnitude considerably, and can be seen as the image on the right hand side is much fuller in colour.

Raising the temperature of the thin film during the HAMR process reduces and removes the effect of the dipole field. The higher temperature hysteresis

curves in figure 7.2 do not have the kink caused by the dipole field seen at ambient temperature. At elevated temperature the magnetisation of the individual grains are reduced, which therefore reduces the dipole field allowing the individual grains to switch unaffected by the magnetisation of the neighbouring grains. Then the magnetisation is rebuilt in the direction of the applied field at roughly the same time.

The time scale for reversal is notably faster via HAMR than the standard ambient reversal process. The reversal process is complete within the 1.0ns period, where the temperature of the thin film is elevated, and the timescale for reversal is dictated by the cooling rate of the system. At ambient temperature for the 20% $L1_o$ case with relatively low exchange coupling (4000Oe in this case) the reversal of all the grains takes roughly 6ns, although a majority (90%) of the grains have switched by 250ps, the remaining 5% is slowed by the dipole field.

7.1.3 Grain Size Dependence

The reversal of individual grains has effectively stopped by 1.5ns in almost all of the simulations, figure 7.2. The ambient temperature simulation has approximately 12.5% of the magnetisation reversing within the 1.5ns simulation time. When the simulation time is increased to 20.0ns a further 6% of the magnetisation is seen to reverse. By increasing the temperature during the simulation, more individual grains are seen to reverse their magnetisation by the end of the 1.5ns simulation. This slows down any further reversal after this point. The 350K simulation has 16% of the magnetisation reversing by the end of the 1.5ns simulation and then a further 4% is seen to reverse by 20.0ns. Further increasing the temperature during the simulation to 400K causes roughly 24% of the individual grains to reverse by 1.5ns and this time only a further 1% is seen to reverse by 20.0ns. When the maximum temperature reaches 450K the reversal process has stopped entirely by 1.5ns and no further grains are seen to reverse their magnetisation after this point.

In all temperature regimes the reversal process stops as the relatively smaller grains with lower anisotropy energy have flipped the magnetisation, by this point in the simulation. The grain size dispersion of the thin film is such that the applied field and temperature required to cause reversal for each grain is different. Therefore if the thermalised decrease in the anisotropy energy is sufficient then the applied field is capable of reversing the magnetisation of that grain. This means that the portion of grains that are below a certain volume are more likely to reverse due to the thermal assist, figure 7.6.

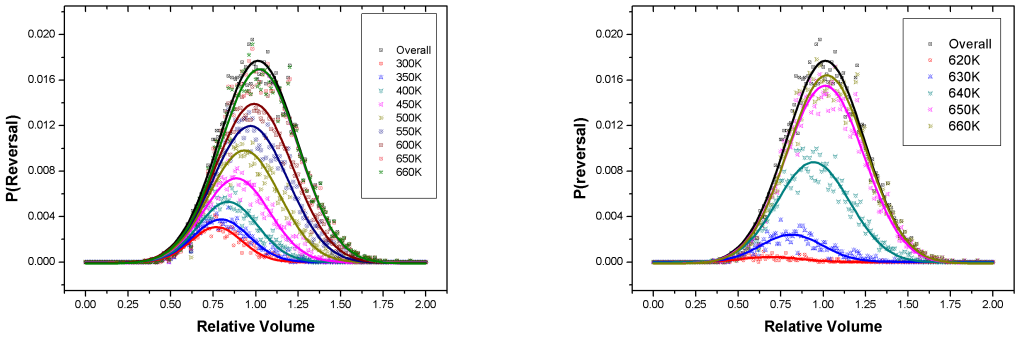

Figure. 7.6: The spread of the relative volume of the FePt grains within the thin film, showing the spread of the volume for the grains which have reversed their magnetisation over a range of maximum system temperatures during the HAMR process. On the left hand side: The 20% $L1_o$ case. On the right hand side: The 100% $L1_o$ case.

Figure 7.6 shows the relative volume of the grains that have switched by 1.5ns after the temperature rise for the 20% $L1_o$ and 100% $L1_o$ cases. The average volume of the grains that reverse for the 20% $L1_o$ case in the ambient temperature situation, in figure 7.2, is roughly 75% of the overall average volume for the thin film, figure 7.6. As the maximum temperature is raised over successive simulations the volume spread for the grains that reverse becomes larger, moving towards the overall spread for the thin film. In the highest temperature simulations the volume spread is marginally shifted towards the larger end of the scale. The smaller grains have lower anisotropy energy, $K_v V$, which are therefore more susceptible to the associated thermal energy. This causes the smaller grains magnetisation to behave more erratically at lower temperatures and therefore for a longer period during the simulation. The system cools at a faster rate for higher temperatures (high dT/dt), which means the system changes from a position where the anisotropy is low enough to allow reversal, to an anisotropy where reversal is forbidden at a much faster rate, as discussed above for the case above T_c. This increases the chance for the magnetisation becoming caught in the positive direction when the system cools. The same process happens for both anisotropy regimes, only the temperature that initiates the reversal process is much higher for the 100% $L1_o$ case.

7.1.4 Probability of Magnetisation Reversal

The probability of an individual grain reversing the magnetisation within 1.5ns after the temperature rise is shown in figure 7.7. The data was calculated using the initial ($M_z I$) (initial being the M_z value after the system has equilibrated and

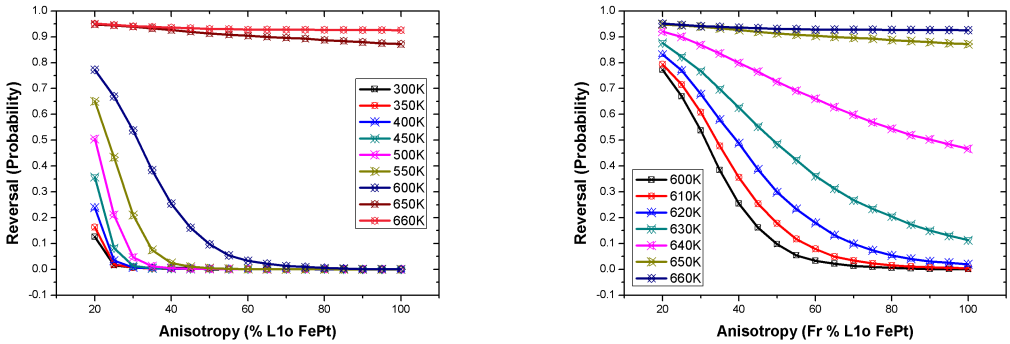

Figure. 7.7: On the left hand side: The reversal probability of the whole system with a 12000Oe applied field, over a range of maximum system temperatures (300K - T_c) and anisotropies (20% - 100% $L1_o$ ordered FePt grains). on the right hand side: The reversal probability of the whole system with a 12000Oe applied field, over a range of maximum system temperatures (600K - T_c) and anisotropies (20% - 100% $L1_o$ ordered FePt grains).

before the temperature rise) and final (M_zF) M_z values (ie (M_zI)-(M_zF)/(2M_zI)). This approach assumes zero reversal before the temperature rise and that all the individual grains are is a stable position at t=1.5ns. The data covers a range of anisotropies and maximum system temperatures. They neatly show the increase in the temperature required to initiate the reversal process in the higher anisotropy simulations. Above an anisotropy of 60% $L1_o$ ordered grains and a temperature of 600K the system shows very low or zero magnetisation reversal. When the maximum system temperature reaches T_c, during the simulation, all anisotropies, 20% to 100% $L1_o$ ordered grains, will achieve a similar level of magnetisation reversal. An individual grain, for the 20% $L1_o$ case, has a probability of 0.951 of reversing by the end of the simulation time. Where as the 100% $L1_o$ case has a marginally lower probability of magnetisation reversal, 0.926.

These two constraints; the higher anisotropy regimes needing increasingly higher temperatures (approaching towards T_c with increased anisotropy) to initiate reversal and all the anisotropies having achieved the maximum reversal at T_c, means that the temperature range where reversal is seen is reduced as the anisotropy is raised. This is a significant result for HAMR, as a narrower range of temperature where magnetisation reversal is seen means the reversal process is more controllable. This would reduces unwanted reversal of the grains that neighbour the current bit that is being recorded.

7.1.5 Cooling Rate

So far all the HAMR simulations have had a cooling rate (CR) of 0.5ns, which returns the system temperature to ambient in around 1.0ns. To investigate the effect of the cooling rate on the magnetisation reversal process the thin film was heated up to T_c while a 12000Oe field was applied, and allowed to cool at different rates. Changing the length of CR effects the reversal process in a subtle way, which changes the length of time taken for the thin films magnetisation to fully reverse, figure 7.8. When the cooling rate is relatively short (compared with 0.5ns CR) the temperature of system reduces faster and the anisotropy rebuilds at an equally quick rate. Therefore the period of time where reversal can occur (in the thermally activated lower anisotropy regime) is reduced. With a 0.1ns cooling rate all of the magnetisation does not have time to reverse before the temperature has dropped to a point where reversal is stopped, figure 7.8 and 7.9. The M_z time sequence diagrams in figure 7.8 show the reversal process stopping relatively early for the 0.1ns and 0.2ns CR cases when compared to the systems with longer cooling rates. This effect is also seen in the hysteresis curves in figure 7.9. The 0.1ns CR case requires a negative applied field to demagnetise the thin film, where as with slower cooling rates the system demagnetises with no applied field. With a CR less than 0.2ns there is not sufficient time to allow the slower acting transverse relaxation mode to fully reverse the magnetisation of all the grains. When the cooling rate is above 0.2ns the amount of grains that reverse is not effected and only the time taken for the reversal process is changed. This is an interesting result. The thin film requires a CR above 0.2ns to fully respond to the increased temperature, and therefore removing the temperature any faster reduces the reversal process. At 0.1ns after the temperature rise and with a CR of 0.1ns the system temperature has dropped to $\sim$425K where as with a 0.5ns CR the temperature is much closer to T_c, $\sim$640K. This indicates that the thin film requires roughly 0.2ns to fully respond to the reduced anisotropy.

Increasing CR beyond 0.5ns slows the reversal process, as the temperature of the thin film is raised for a longer period. The reversal percentage of the thin film is not effected when the temperature has returned to ambient. All cooling rates above 0.2ns show the same level of magnetisation reversal when the thin film temperature has returned to ambient, figure 7.9. For the higher cooling rates dT/dt is much lower and therefore the reversal process is not constrained by a rapidly increasing anisotropy.

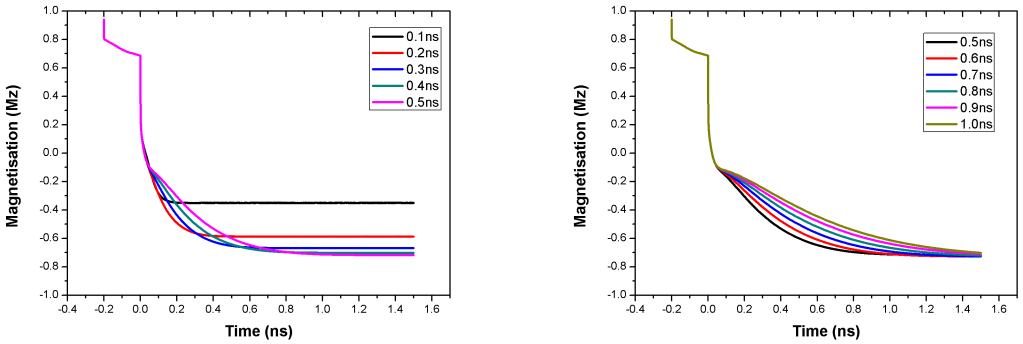

Figure. 7.8: M_z time sequence diagrams with different cooling rates, for the 20% $L1_o$ case with a 12000Oe applied field where the maximum system temperature reached T_c. On the left hand side: Cooling rates 0.1ns to 0.5ns. On the right hand side: Cooling rates 0.5ns to 1.0ns. The 0.1 and 0.2 nano second cooling rate cases show a reduction in magnetisation reversal.

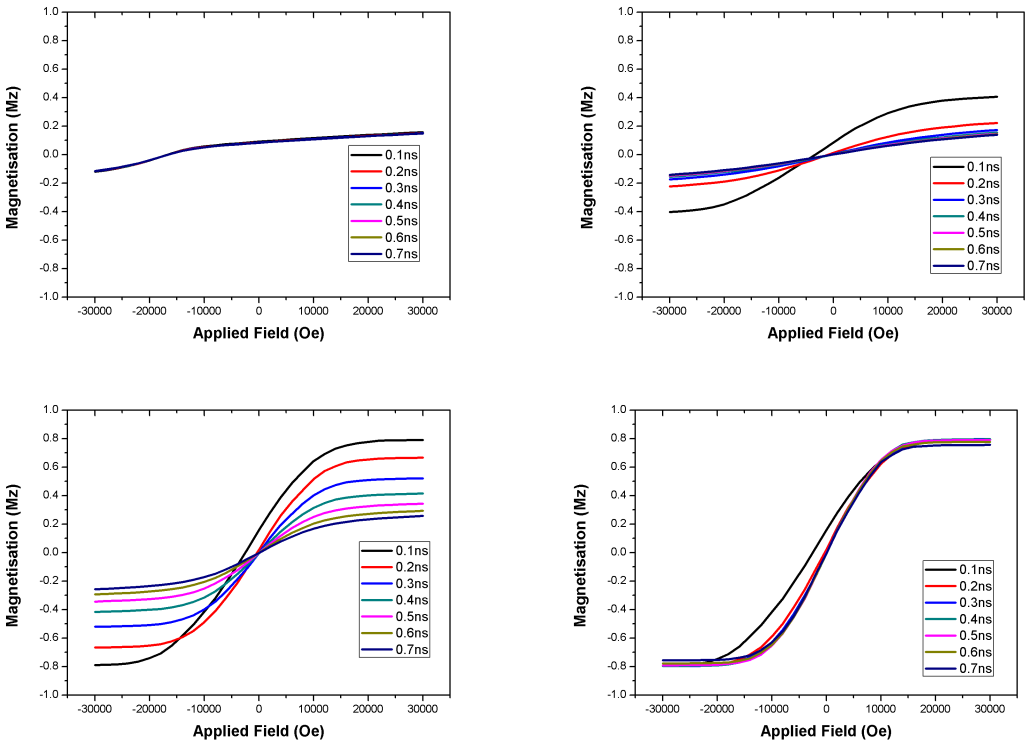

Figure. 7.9: Hysteresis curves with different cooling rates, for the 20% $L1_o$ case with a 12000Oe applied field where the maximum system temperature reached T_c. On the top left: 10ps, right: 50ps. On the bottom left: 200ps, right: 1000ps. The 0.1ns cooling rate case requires an applied field to demagnetise the thin film.

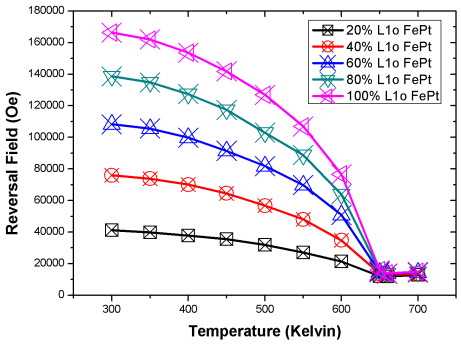

Figure. 7.10: The reversal field (the field required to reverse 95% of the thin film magnetisation) over a range of anisotropies and maximum temperatures during the HAMR simulations. All anisotropies need to be heated to T_c and require a minimum applied field in the region of 13000Oe to reverse the magnetistion of the thin film.

7.1.6 Reversal Field

The reversal field (H_r) drops for all anisotopies in a similar way, as the maximum temperature is raised towards T_c. Figure 7.10 shows (H_r) over a range of anisotropies and maximum system temperatures. For all anisotropies H_r falls to a mimimum value at T_c, and is approximately equal (11932Oe for the 20% $L1_o$ case and 13811Oe for the 100% $L1_o$ case). This highlights the effect of HAMR, all anisotropy regimes reduce in a similar way up to T_c, requiring similar conditions to reverse the magnetisation.

To reverse the magnetisation of the thin film using H_r(T), the reversal process happens in an unfamiliar manner. For the 20% $L1_o$ case (at lower temperature and therefore with a larger applied field) a portion of the individual grains must flip the magnetisation before the temperature rise, if full reversal of the thin film magnetisation is to happen. Figure 7.11 show the M_z time sequences for the 20% and 100% $L1_o$ cases. The ambient temperature H_r is equal to 41242Oe, raising the temperature only marginally during the HAMR process reduced H_r. In the 350K simulation the magnetisation of the thin film reverses almost entirely before the thermal assist, only falling marginally short due to the dipole effects discussed earlier. The thermal assist then reduces the magnetisation of the thin film in the opposite direction to what is normally observed (ie the magnetisation of the thin film reduces in magnitude in negative direction), as almost all of the individual grains have reversed at this point. Increasing the temperature over successive simulations (and by implication, lowering the applied field) reverts the simulations to a more typically seen reversal type, where the anisotropy resists the applied field and the thermal assist is required to reverse any of the

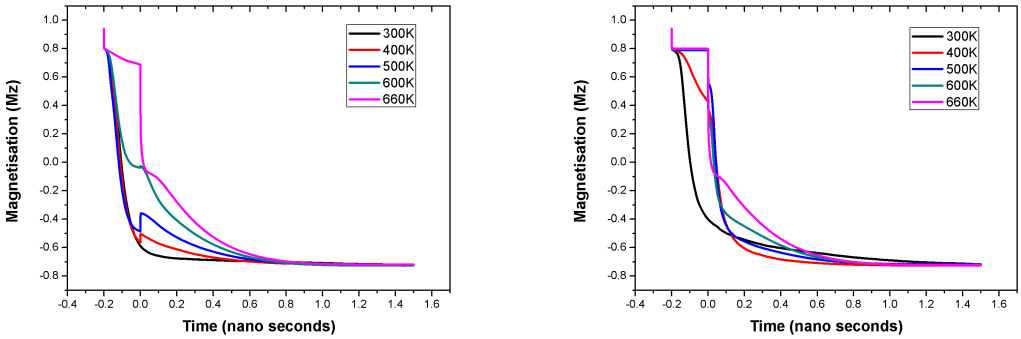

Figure. 7.11: On the left hand side: Time sequence diagrams for the 20% $L1_o$ case, showing the reversal process beginning before the temperature rise associated with HAMR. On the right hand side: Time sequence diagrams for the 100% $L1_o$ case, showing the reversal process beginning before the temperature rise associated with HAMR.

grains magnetisation.

This effect is caused by a number of factors, namely the grain size dispersion and the dipole field. The grain size dispersion causes the smaller grains to reverse with a relatively small applied field. The reversal of individual grains causes the dipole field to build in the opposite direction (the positive direction apposed to the initial negative direction) which is seen to slow and stop the reversal process. In the lower temperature cases the thermal assist is only required to over come the effect of the dipole induced freezing of magnetisation reversal.

In the higher anisotropy regime things happen a little differently. The reversal field is sufficient to reverse a portion of the individual magnetisations of the grains before the thermal assist, only in the lower temperature regimes. The lowest (400K and below) temperature simulations show reversal before the heat assist. The applied field required to reverse the magnetisation scales with K_v, but the grains size dispersion and dipole field generated by the magnetisations that have flipped remains the same as in the 20% $L1_o$ case. Therefore the effect of the dipole field is smaller when compared to the reversal field and its effect is reduced. This changes the reversal process and lowers the reversal field to a point where it doesn't reverse grains before the thermal assist. This effect would be of use in HAMR, as both the heat and applied field are required to successfully reverse any of the magnetisation, making the process easier to control.

7.1.7 Exchange Field at Elevated Temperature

The exchange field has a similar effect under HAMR conditions as at ambient temperature, although the magnitude of its effect is reduced. Increasing the

exchange field binds the motion of the individual spins, which alters the reversal process. Increasing the exchange coupling effects H_I, H_c and H_r in a similar way to what is seen at ambient temperature. H_I and H_c increase as the exchange field increases and H_r reduces in similar manor (the similarity is only when discounting the dipole effects seen in the 20% $L1_o$ case at ambient temperature). At elevated temperatures the effect of the dipole field is removed and therefore the lower exchange regimes do not have the kink below the M_z=0.0 point seen at ambient temperature. Figure 7.12 shows hysteresis curves for the 20% $L1_o$ case generated over a range of exchange fields (from 0Oe to 30000Oe), where the maximum temperature reached 620K. The strength of the exchange field is dependant on the overall state of the magnetisation of the thin film. When the temperature of the thin film is raised the magnetisation of the grains is reduced, which reduces the strength of the exchange coupling. This allows the reduced magnetisation to reverse more independently and over a shorter period (when compared with ambient temperature situation). As the temperature of the thin film falls the magnetisation is rebuilt and the effect of the exchange field increases.

A simple way to view the effect of the exchange coupling on the reversal process is based on the M_z value at t=1.5ns for the 0Oe exchange case. This analysis is not rigorous and only gives an impression of what is happening. If M_z(t=1.5ns) $\gtrsim$ -0.1 then increasing the exchange field reduces the reversal percentage and if M_z(t=1.5ns) $\lesssim$ -0.1 then the opposite is true, and increasing the exchange coupling increases the reversal percentage. The original assumption was the exchange field would increase the reversal percentage when M_z(t=1.5) $<$ 0.0, as the exchange field acts in the direction of the average magnetisation of the thin film, but the dynamics of the reversal process permit this from happening. Figure 7.12 shows the M_z time sequences for 4 different exchange regimes where the maximum system temperature was 620K. In the 0Oe exchange case M_z(t=1.5) = -0.5, therefore increasing the exchange field works to increase the reversal of the magnetisation. The magnitude of the exchange coupling dictates the increase in the reversal percentage.

The left hand side of figure 7.13 shows the probability of an individual spin having reversed by 1.5ns after the temperature rise. The effect of the exchange field is clearly displayed, only increasing the reversal probability of an individual grain when the zero exchange case has a probability greater than $\sim$0.65. This relationship is not entirely fixed. As mentioned above there are additional factors that effect the exchange coupling. The point where the different exchange regimes cross (ie when the exchange field assists the reversal process rather than hindering it) increases with increased anisotropy, figure 7.13. The higher

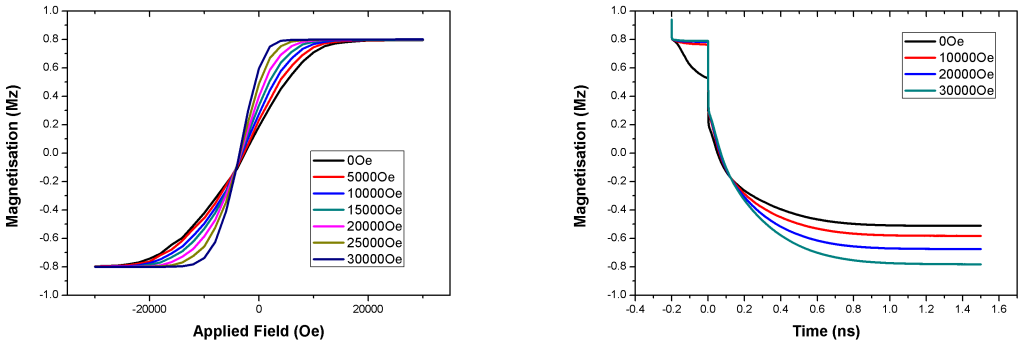

Figure. 7.12: On the left hand side: Hysteresis curves for the 20% $L1_o$ case that was heat to 620K with a range of exchange constants, 0Oe to 30000Oe. Increasing the exchange coupling squares off the hysteresis curves. On the left hand side: M_z time sequence diagrams for the 20% $L1_o$ case with a range of exchange constants, with a 12000Oe applied field, that was heated to 620K.

anisotropy regimes reduces the effect of the effect of the exchange field. The right hand side of figure 7.13 shows hysteresis curves for a range of anisotropies with a 30000Oe exchange constant, where the thin film was heated up to 620K. The lowest anisotropy (20% $L1_o$ case) is much squarer when compared to the higher anisotopies. This show that the exchange field has a larger effect at lower anisotropy. The magnitude of the exchange coupling is reduced at elevated temperature and increases as the temperature falls. Equally the magnitude of the anisotropy field is reduced at elevated temperature and also increases as the temperature falls. The returning anisotropy overpowers the returning exchange coupling and reduces its effect and smaller domain are see to form when the thin film is demagnetised. Figure 7.14 shows the images of two thin films (20% $L1_o$ ordered on the left and 100% $L1_o$ on the right) at 1.5ns that were heat up to T_c and they both have a 30000Oe exchange constant. Both thin films were demagnetised with a field equal to H_c. The 20% $L1_o$ ordered thin film has larger grains forming when the thin film is demagnetised, showing the reduced effect of the exchange field at higher anisotropies.

7.2 Single Grain Dynamics

The LLB model simulates the reduction in **m** associated with elevated system temperatures. The instantaneous temperature dependence of **m** for a 6nm grain is shown in the model section of the report. The temperature dependence of the magnetisation shows a critical decrease to 0.0 as the temperature approaches T_c, which is not seen in LLG calculations. Above T_c the magnetisation appears

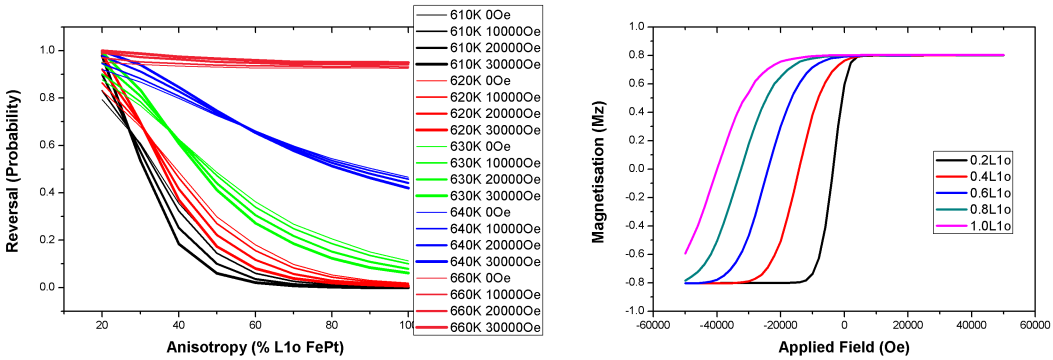

Figure. 7.13: On the left hand side: The probability of an individual grain reversing within 1.5ns after the temperature rise. The data is over a range of anisotropies (20% to 100% $L1_o$ ordered FePt), exchange constants (0Oe to 30000Oe), and range of maximum system temperatures from 610K - T_c. The effect on the reversal probability of inter-granular exchange coupling is neatly displayed. On the right hand side: Hysteresis curves for a range of anisotropies heated to 620K.

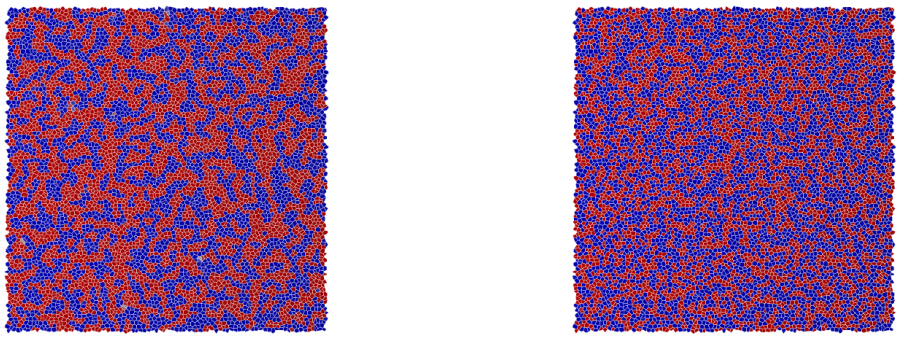

Figure. 7.14: Two images of the thin film at 1.5ns, that was heated up to T_c. On the left hand side: An image of the 20% $L1_o$ thin film with a 30000Oe exchange constant. On the right hand side: An image of the 100% $L1_o$ thin film with a 30000Oe exchange constant.

spontaneously, oscillating between 0.0 and 0.2.

During the HAMR process the magnetisation of each grain reduces rapidly to a temperature dependant minimum, on heating, then increases in magnitude following the temperature profile of the system in a characteristic time. Figure 7.15 shows the $\mathbf{m}_z$ time sequences, for the 20% $L1_o$ case in figure 7.2, for an individual magnetisation over a range of maximum system temperatures up to T_c. The left hand side shows the reversal process for a grain that required the thermal assist to reverse. The right hand side shows a grain that switched in all temperature regimes. In both cases the magnetisation reduces rapidly to a temperature dependent minimum, then is rebuilt (in either direction) following the temperature profile of the system. The magnetisation of the individual grains undergoes two distinct relaxation modes, over the range of temperatures investigated. The increased temperature causes a parallel relaxation which reduces the magnetisation to a temperature dependent minimum in approximately 2 - 3ns. Also the increased temperature reduces the energy barrier for reversal causing the magnetisation to precess for one orientation to the other in approximately 50ps. An individual grain achieves full reversal (from one stable position to the other) faster at ambient temperature. This is only true as the magnetisation, at higher temperatures, takes time to rebuild into the stable position. At ambient temperature the individual grain selected is fully reversed within approximately 70ps (from one orientation to the other). This in no way dictates the time scale for the whole system to reverse. In the ambient temperature case where the applied field is equal to H_r the whole system takes approximately 6ns to reverse. The time only indicates the time taken for an individual grain to switch at ambient temperature. When the system temperature is raised as in HAMR the individual grains switch orientation over a relatively shorter time scale (first predicted using the LLB equation, by N. Kazantseva et al, the University of York, Uk [13]). At T_c the individual grain selected takes roughly 8ps to switch orientation, but the magnetisation of that grain takes almost a further 1.0ns to fully recover in length. The faster switching time is as result of the dramatic decrease in the relaxation time at T_c. The faster switching happens via a new reversal mechanism, in the form of linear reversal, figure 7.16.

7.2.1 Linear Magnetisation Reversal of the Individual Grains

At ambient temperature the magnetisation of the individual grains remains at an approximately constant magnitude throughout the reversal process. This means the magnetisation of the individual grains precess through the xy plane during

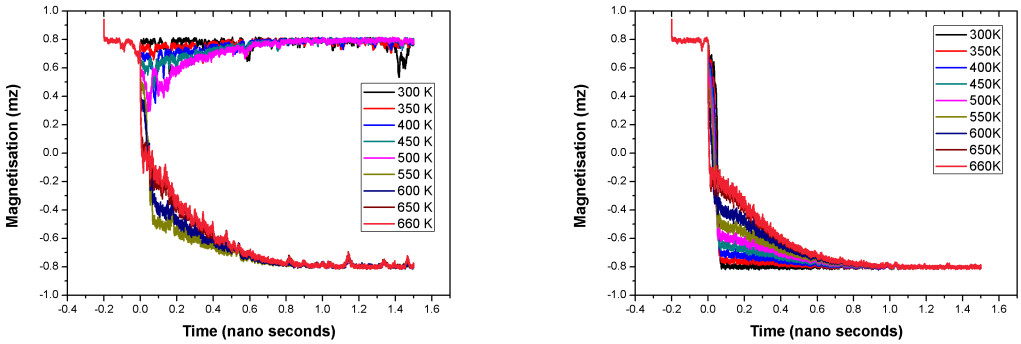

Figure. 7.15: On the left hand side: A time sequence showing the magnetisation reducing in length as the system temperature is raised during the HAMR simulations. On the right hand side: The temperature dependance of the magnetisation magnitude.

the reversal process, figure 7.16 (on the right hand side) shows the reversal type for the 20% $L1_o$ case where the temperature dependent reversal field is used to induce magnetisation reversal . The ambient temperature and low temperature rise simulations show purely precessional reversal, although there is a reduction in the magnetisation during reversal, to fit the associated temperature rise. The magnetisation shrinks on introduction of the heat, then reverses and is rebuilt in the opposite direction. In the higher temperature simulations (still sufficiently below T_c) the reversal takes an elliptical form. The reversal of the magnetisation begins while the magnetisation is shrinking and then the magnetisation rebuild as reversal completes. This gives the elliptical pattern seen between 500K and 600K in figures 7.16. In the highest temperature regimes, 650K and above, the magnetisation reverses linearly, never really entering the xy-plane. The combination of the applied field and the rapid reduction in the magnetisation length at such high temperatures result in fast acting linear reversal process. The magnetisation reduces so quickly and to such a point that it has been effectively destroyed before the applied field has had time to push the magnetisation into the xy-plane. After the magnetisation has been destroyed the applied field causes the it to rebuild in the opposite direction. The speed of reversal is then only constrained by the thermal energy remaining from the heat assist.

The linear reversal type recovered from the LLB calculations are in strong agreement with recently performed spin model calculations [13]. Figure 7.16 also show the results from atomistic calculations by J Barker et al, at the University of York, UK. The ab initio characterization within the spin model gives a Curie point of 700K, which is larger than the 660K used for the LLB model and therefore the linear reversal mode is seen at a higher temperature in the spin model calculations.

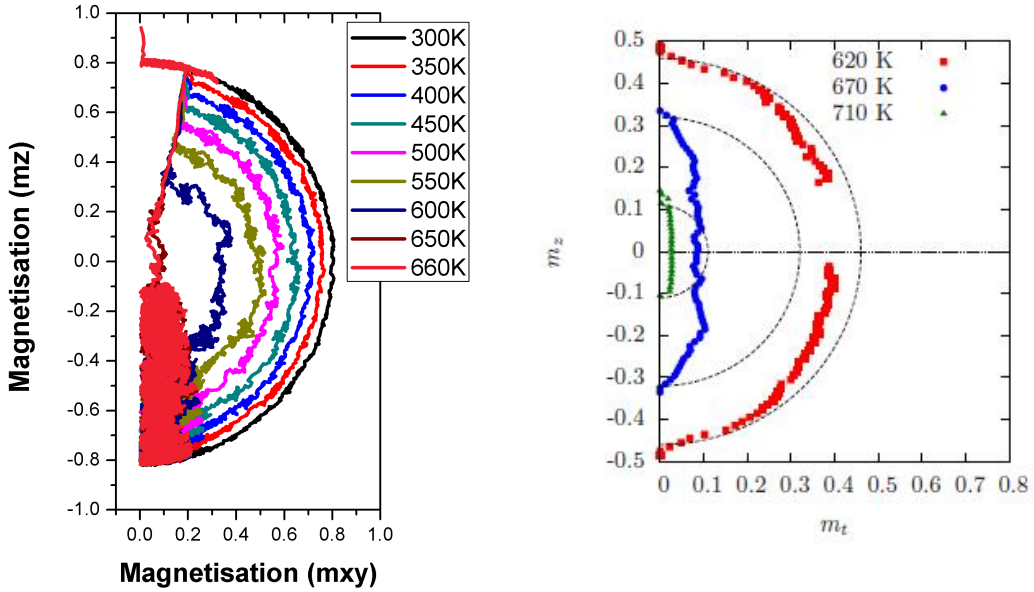

Figure. 7.16: On the left hand side: The reversal of the individual grains magnetisation for the 20% $L1_o$ ordered case, over a range of maximum system temperatures. With an applied field equal to the reversal field taken from figure 7.10. On the right hand side: spin model calculations by J Barker et al, showing the same linear reversal mechanism at high temperatures approaching T_c. T_c is approximately 700K for the spin model calculation, therefore the linear reversal mode is seen at a higher temperature.

7.3 Summary and Further Work

The LLB model has shown the potential for HAMR as successor to standard magnetic recording. To achieve the desired level of magnetisation reversal via the HAMR process requires very high temperatures approaching T_c and an applied field strength that is at the upper limit and beyond of what is achievable with magnetic solids, 12000Oe - 14000Oe. The reversal process is notably faster in HAMR when compared with the reversal rate at constant temperature. The time scale for reversal results from the temperature rise causing the individual spins to demagnetise and then reverse all at roughly the same time via the newly observed linear reversal mode. But the decreased switching time brought about by the linear reversal mode is not the limiting factor for the time scale for reversal of the overall magnetisation. The completion of the reversal process is dictated by the cooling rate of the system, taking approximately 1.0ns following the reduction in the system temperature. The time scale for an individual grain to switch from one stable orientation to the other is effectively slower at high temperature, as the stable position isn't recovered until the anisotropy has returned to a level

that can sustain a permanent magnetisation. At ambient temperature the time between switching events, with an applied field equal to H_r, is sufficiently greater then that at T_c with a 12000Oe applied field, therefore the thin film magnetisation reversal process is faster under HAMR conditions. This could lead to higher recording speeds, even faster than the 1.0ns reversal time, as the applied field is only required until the anisotropy has rebuilt to a level where reversal is forbidden. In the higher anisotropy regimes reversal is forbidden at a relatively high temperature, up to 600K. Therefore very high recording rate could be achieved. The length of time the applied field is required for to maintain an equal amount of magnetisation reversal is currently being investigated to determine the minimum time for the reversal process to complete.

8. Laser pulse induced reversal in perpendicular $L1_o$ FePt thin films; theory vs experiment.

The LLB model has been used to replicate a newly formulated pump probe experiment performed to measure the dynamic photoinduced magnetisation reversal in a perpendicular nanogranular FePt thin film. The experiment was undertaken by S. M. Zhou et al., the Department of Physics, Fudan University, Shanghai, China [30]. The conventional TR-MOKE technique for determining the magnetistion of the thin film has been shown to be inadequate as the measurement process delivers the transient magnetisation to the subsequent data point, due to the effect of the preceding pump-probe pair, and therefore the magnetisation can not be accurately determined during dynamic photoinduced magnetisation reversal using this technique. S. M. Zhou et al. have demonstrated a new photo magnetic synchronised TR-MOKE measurement method which recovers the magnetisation to the same state before each pump probe measurement, removing the effect of the previous pump probe measurement. The method generates a static 'no pump' hysteresis loop to be used as the 'same state' conditions for initialisation before each pump probe measurement, figure 8.1. The alternating magnetic field (AMF) and laser pulse used for the experiment are synchronised, so that the magnetisation is recovered to the static hysteresis loop before the following laser pulse and measurement. This removes any effect on the magnetisation from the previous laser pulse and measurement. The alternating magnetic field can be considered static from the point of view of the experiment as the measurement times are at least six orders of magnitude smaller than the oscillation period of the AMF.

8.1 No Pump Case

The FePt thin film used in the Fudan experiment has a coercivity of approximately 3300Oe, therefore the degree of $L1_o$ ordering of the thin film must be relatively low. Also the hysteresis loop is very square indicating very large exchange coupling, figure 8.1.

To investigate the static 'no pump' case, hysteresis loops were generated by plotting M_z(t=4.0ns) vs H. After a considerable search varying both the

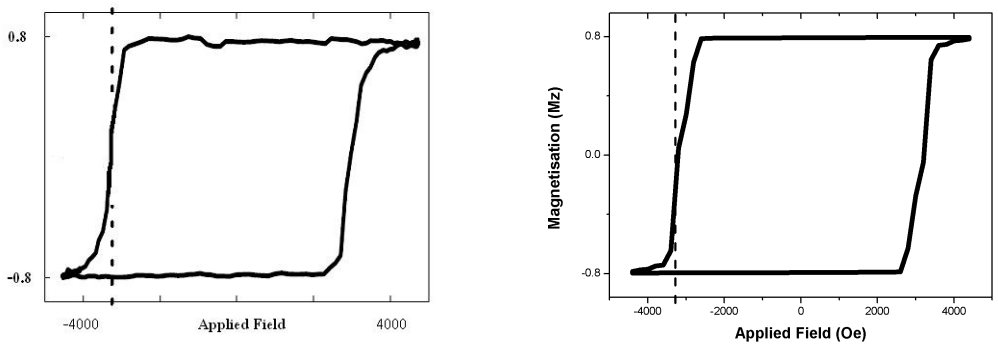

Figure. 8.1: The static hysteresis loop for the FePt thin film determined at Fudan, on the left hand side, compared with the result replicated with LLB model. The perpendicular anisotropy constant is calculated as K_v = 1.2604×10^7 ergs/cc and the inter-granular exchange constant is 32000Oe. The coercivity for the LLB calculated thin film is 3300Oe.

anisotropy and exchange fields the 'best fit' to the Fudan experiment was found to be 13.7% $L1_o$ ordered FePt (this gives an anisotropy of $K_v = 1.2604\times10^7$ergs/cc) and the exchange field was found to be 32000Oe. Figure 8.1 shows the 'static case' from the Fudan experiment and the closest fit found with the LLB model. The coercivity with the LLB model is calculated as 3274Oe, equal to that determined by the Fudan experiment (3300Oe) and the hysteresis loop has a similar square shape due to the high exchange coupling.

Determining the anisotropy and exchange parameters to fit a given coercivity is relatively straight forward in high anisotropy regimes as the coercivity scales with K_v and the exchange field doesn't alter the coercivity by a significant amount. In the low anisotropy regime required to reproduce the static hysteresis loop from the Fudan experiment, both the anisotropy and exchange fields shift the coercivity by a relatively large amount, which made determining the correct parameters relatively difficult. Figure 8.2 shows the anisotropy and exchange dependence on the coercivity at levels close to that determined for the static case. Changing the anisotropy from 12% to 14% $L1_o$ FePt, with a 32000Oe exchange field, increases the coercivity from a few hundred Oe to roughly 4000Oe. With an anisotropy equal to 13.7% $L1_o$ FePt change the exchange constant from 26000Oe to 30000Oe moves the coercivity by 1000Oe from $\sim$4300Oe to $\sim$3300Oe. This made determining the correct parameters to reproduce the static hysteresis loop a difficult process.

The researchers at Fudan proposed a dynamic reversal process accompanied by domain nucleation and barrierless transient domain wall motion (DWM), to account for the shape of the static hysteresis loop. This is found to be true in the

LLB model. The reversal process nucleates on individual grains (or small groups) and reversal spreads via domain wall motion (for the full time evolution of the reversal process via DWM, displayed pictorially using the images of the thin at 100.0ps increments, see appendix 2.0. The data are shown for the switching field case and the reversal field case). The reversal process, under the switching field, shows extreme DWM. Reversal nucleates at 4 different points on one side of the thin film and spreads via DWM until almost one half of the thin film has reversed in to one large domain. DWM is again seen with the reversal field and in this case reversal nucleates at a number of points all across the thin film, and continues to completion via DWM.

The applied field required to initiate the reversal process is only marginally lower than the switching field and reversal field. With an applied field of -2600Oe no reversal of the thin film is seen. Increasing the applied field strength to -3600Oe reverses all the magnetisation within the 4.0ns simulation. This however is not the entire picture. Figure 8.3 (on the left hand side) shows the M_z time sequences over a range of H fields around the switching field. In all cases (barring the -2600Oe case) the reversal process appears to continue beyond the time frame of the simulations. The right hand side of figure 8.3 shows the same data as the -2800Oe applied field case shown on the left hand side of the same figure, but where the simulation was allowed to run for 20.0ns. In the 4.0ns case the magnetisation reversal process initiates at roughly 2.5ns and the thin film is partially reversed by the end of the simulation. The thin film then continues to reverse via DWM over the next 17.5ns until reversal is complete. This implies that with such high exchange coupling the reversal process will continue to completion once it has been initiated. This also means that the 'static loop' isn't static and the coercivity would marginally reduce had the simulation continued beyond 4.0ns.

8.2 Femto second laser pump simulation.

To simulate the pump probe case the temperature rise associated with the laser pulse is simulated as in the HAMR section of the investigation. The temperature rises from ambient (300K) to the maximum temperature (Tmax) in a single time step. The temperature then returns back to ambient following a gaussian in a characteristic time. The LLB model is capable of reproducing the dynamic photoinduced reduction in the magnetisation seen in the Fudan experiment, due to the addition of the longitudinal relaxation parameter not seen in the LLG model. The aim of this portion of the investigation is to reproduce the hysteresis loops determined by the Fudan experiment, at the specific times after the laser

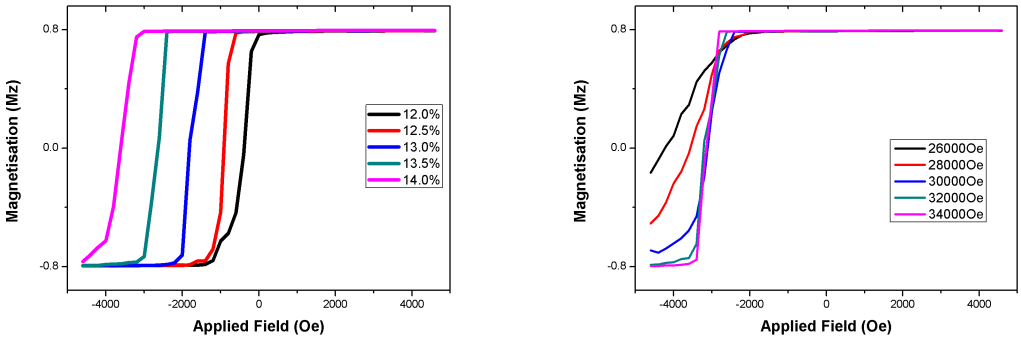

Figure. 8.2: On the left hand side: The anisotropy dependence of the coercivity calculated with LLB model with an exchange constant of 32000Oe. On the right hand side: The exchange constant dependence of the coercivity calculated with the LLB model with an anisotropy equal to 13.7% $L1_o$ ordered FePt.

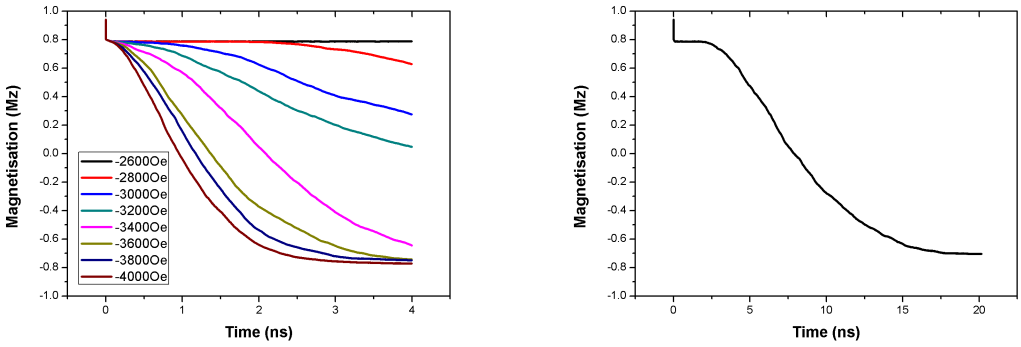

Figure. 8.3: M_z time sequences taken from the static case over a range of applied fields around H_c. The right hand side shows the case with a -2600Oe applied that over a 20.0ns simulation time, showing the continued reversal of the magnetisation due to DWM.

pulse; 0.5ps, 50.0ps and 600.0ps shown in figures 8.5, 8.6 and 8.7. This was achieved by varying the maximum temperature and cooling rate during the simulation. An accurate reproduction of the Fudan results will give information about the conclusions made by the team at Fudan and confirm the ability of the LLB models predictive power.

8.2.1 0.5ps after the laser pulse

The magnetisation of the thin film in the Fudan experiments reduces rapidly in the z-axis within the first pico-second after the laser pulse, and has reduced to approximately 30% of the ambient magnitude at 0.5ps after the laser pulse, figure 8.5. The level of magnetisation reduction in the z-axis (M_z), at this point after the laser pulse, is in the main dictated by the maximum temperature

reached by the thin film, as the magnitude of the magnetisation (**m**) is a function of the temperature. The reduction in the magnetisation in the z-axis is caused by the longitudinal and transverse relaxation modes. The longitudinal relaxation is induced by the associated temperature rise and occurs within 1.0ps after the temperature rise. The transverse relaxation is caused by the reduced anisotropy and thermally reduced relaxation time causing the magnetisation of the individual grains to switch orientation, which happens over a longer time scale than the longitudinal relaxation mode. This is apparent as the magnetisation has reduced in a similar way over the range of H, indicating that no grains switched. Figure 8.5 also compares the 'best fit' hysteresis loop generated by the LLB model to that generated by the Fudan experiment.

To achieve a similar level of reduction in the magnetisation (M_z), with the LLB model, the temperature was raised to approximately 640K. At this point in the investigation the cooling rate remains at the standard 0.5ns, as the cooling rate does not affect the recovery of magnetisation, as at 0.5ps after the temperature rise the temperature remains approximately equal for all cooling rates. The magnetisation is affected by the temperature rise similarly in the Fudan experiment as with the LLB model. The magnetisation reduces rapidly within the first pico-second after the temperature rise, due to the thermal effect of the longitudinal relaxation. Figure 8.4 shows the M_z time sequence for a single grain, over the 10.0ps after the temperature rise, for the 620K and 640K maximum temperature cases with a 0Oe applied field. The data shows both the magnetisation for the thin film and a single grain. The magnetisation is seen to reduce via two different modes. The magnetisation of a single grain reduces very rapidly within the first pico-second, following the magnetisation of the thin film, and then oscillates to a temperature dependant minimum at around 3.0ps. The reduction in the magnetisation is affected by a number of factors beyond the effect of the longitudinal relaxation. At high temperature the parallel susceptibility is a significant factor which affects the magnitude of the magnetisation. The combined affect of the anisotropy, exchange and dipole fields causes the magnetisation to oscillate in magnitude after the initial reduction caused by the longitudinal relaxation. This affect causes the reduction in the magnetisation to happen at a different rate in the LLB model when compared with what was seen in the Fudan experiment.

This affect causes the magnetisation in the LLB model to take a longer time to show a similar level of reduction and therefore a similar hysteresis loop was generated at 3.0ps after the temperature rise. Figure 8.4 shows the hysteresis curves at 0.5ps and 3.0ps after the laser pulse, for a range of maximum

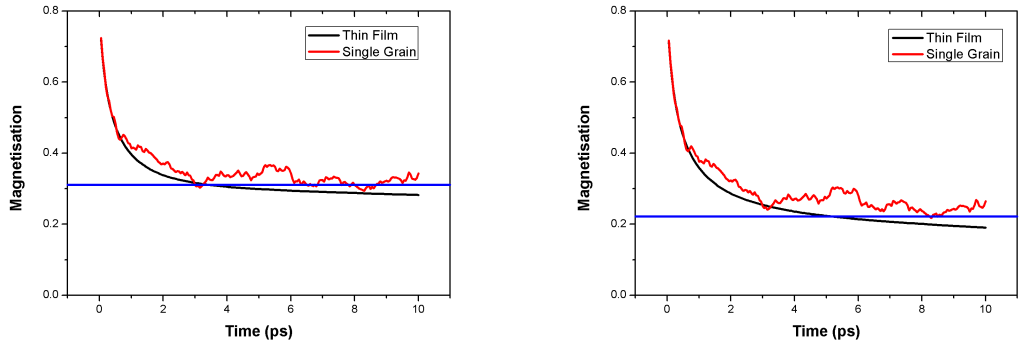

Figure. 8.4: M_z time sequences for the 620K (on the left) and 640K (on the right) cases with a 0Oe applied field, showing rapid reduction in the magnetisation in the z-axis due to the longitudinal relaxation. The reduction in the magnetisation, caused by the longitudinal relaxation, is interupted caused by the effective field acting on the magnetisation of the individual grains.

temperatures. The lower temperature cases do not achieve the level of reduction seen in the Fudan experiment, as the reduction in **m** caused by the longitudinal relaxation is not as large at lower temperatures. At this point, in both cases, the reduction in M_z is entirely caused by the thermally induced longitudinal relaxation in the magnetisation. At this point no reversal of the individual grains magnetisation is seen in the thin film. This is apparent as the magnetisation has reduced similarly over the range of H. The magnetisation, M_z, of the thin film would vary in magnitude over the range of H (dictated by the H field) had transverse relaxation begun to occur. The cooling rate (CR) of the system has no effect on the state of the magnetisation at this stage in the reversal process, as the temperature remains similarly high for all CR regimes.

8.2.2 50.0ps after the laser pulse

At 50.0ps the effect of the applied field and the thermally reduced anisotropy is becoming more apparent in the Fudan experiment, figure 8.6. The shape of the hysteresis loop is being dictated by the different relaxation modes. The longitudinal relaxation is reducing the magnitude of the individual grains magnetisation and the transverse relaxation is switching the individual grains magnetisation, dictated by the applied field. As mentioned above the two relaxation modes happen at different rates. As seen the longitudinal relaxation is very fast acting and reduces the magnitude of the magnetisation within the first pico-second after the temperature rise. The transverse relaxation happens over a longer time scale and takes around 50.0ps for the magnetisation of the individual grains to start switching. The longitudinal relaxation affects the magnetisation

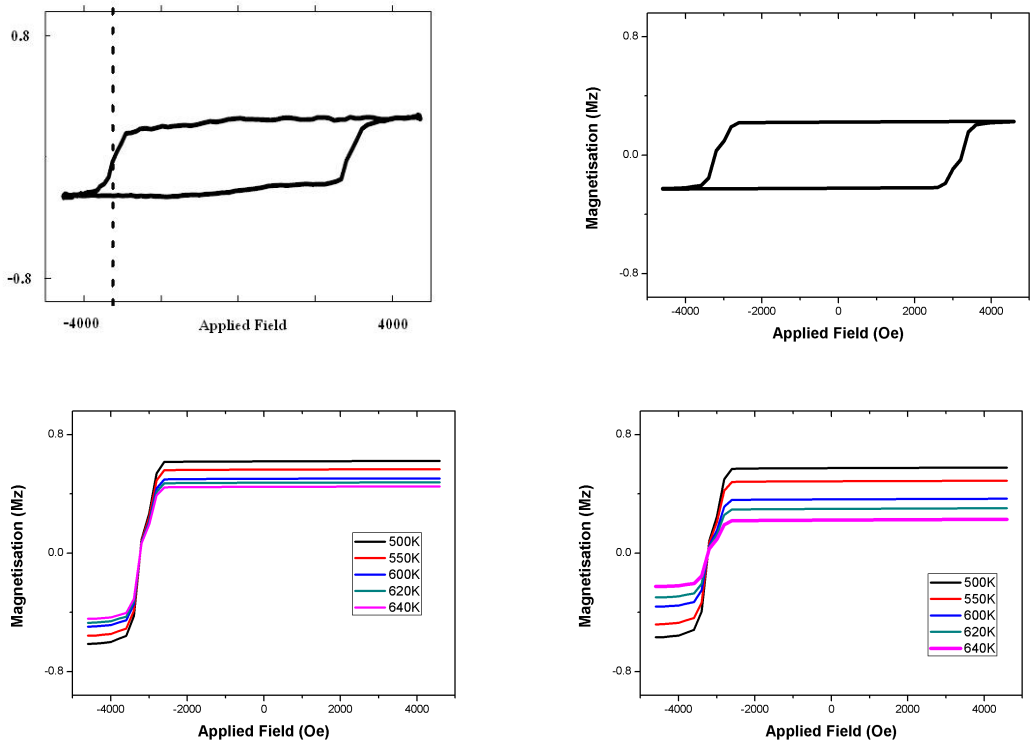

Figure. 8.5: Top left: The dynamic hysteresis loop for FePt thin film determined at Fudan at 0.5ps after the laser pulse. Top right: The 'best fit' found with the LLB model taken at 3.0ps. The thin film is heated up to 640K and the cooling rate is 0.5ns. Bottom left: The hysteresis curves generated with the LLB model at 0.5ps over a range of maximum temperatures. Note the thin film hasn't reduced to the same level as seen in the Fudan thin film at this point. Bottom left: The LLB hysteresis curves at 3.0ps, show a similar level of reduction in the magnetisation above a maximum temperature of 620K.

consistently over the range of H used in the investigation, as an applied field at these strengths does not have a significant affect on the magnitude of the magnetisation which would keep the square shape to the hysteresis loop, but the transverse relaxation mode causes switching to occur, dictated by the applied field, giving the characteristic shape seen at 50.0ps after the temperature rise. In the higher positive and negative fields the magnetisation is held at a temperature dependant saturation, and the beginnings of reversal can be seen in the region around the switching field for the static case. Again the best fit to the Fudan result was achieved by heating the thin film up to 640K, and the time scale for reversal is correct at this stage (ie the LLB 'best fit' is also taken at 50.0ps after the laser pulse).

The 50.0ps case is a little more difficult to replicate as the cooling rate and time frame for reversal is beginning to take an effect on the reversal process.

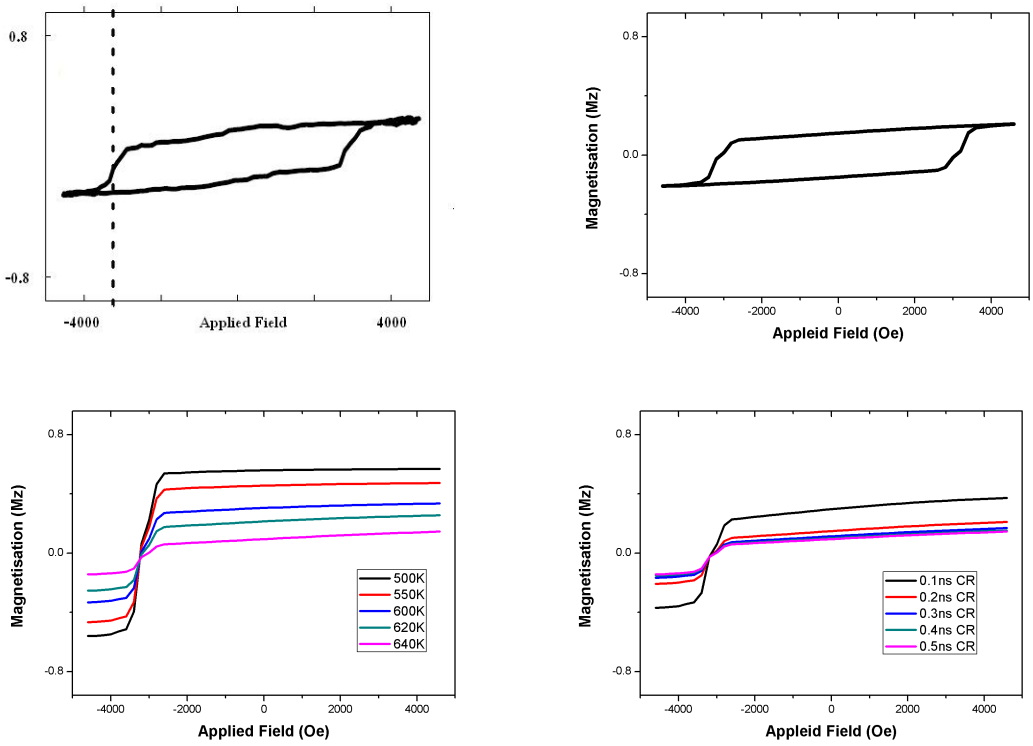

Figure. 8.6: Top left: The dynamic hysteresis loop for FePt thin film determined at Fudan at 50.0ps after the laser pulse. Top right: The 'best fit' found with the LLB model, also taken at 50.0ps after the laser pulse. The thin film was heated up to 640K and the cooling rate is 0.2ns. Bottom left: The hysteresis curves generated with the LLB model at 50.0ps over a range of maximum temperatures, showing a similar level of reduction in the magnetisation above 620K. Bottom right: Hysteresis curves generated at 50.0ps with the LLB model, that was raised to 640K, over a range of cooing rates.

The standard cooling rate used in the HAMR simulations (and in the results in figures 8.5) causes the magnetisation to reverse at a marginally faster rate in the region around H_c than was seen in Fudan experiment, figure 8.6. The 0.1ns CR case is showing the largest variation from the Fudan experiment at 50.0ps. The magnetisation is recovering at an increased rate as the temperature of the thin film is markedly lower at 50.0ps (550K for the 0.1ns CR and 610K - 625K for the 0.2ns - 0.5ns CR cases) when compared to the other cooling rates. A maximum temperature of 640K and a cooling rate of 0.2ns gives the best fit at 50.0ps, figure 8.6 (the 0.2ns was chosen as it gives better results at the later stages of the simulations). Although all cooling rates do give a similar result at this point.

8.2.3 600.0ps after the laser pulse

At 600.0ps the magnetisation (M_z) of the Fudan thin film has began to recover and the shape of the hysteresis loop is being dictated by the applied field, figure 8.7. The magnetisation is being held a temperature dependant saturation in the high positive and negative fields, equal to $|M_z| \simeq 0.6$. The magnetisation in the region around H_c has remained fairly constant over the time frame of the experiment being roughly equal at 0.5ps, 50.0ps and 600.0ps, giving the hysteresis loops the characteristic squaring. Before the laser pulse the effect of the transverse relaxation has stopped and the thin film magnetisation has reached an equilibrium state and reversal has all but stopped. The laser pulse causes a reduction in the magnetisation (**m**) and the reversal process to re-initiate which causes the individual grains which have already reversed to switch back to the initial position, via domain wall motion caused by the strong exchange coupling overcoming the affect of the applied field. This causes reversal in both direction to be approximately equal, which gives a constant value for M_z over this period.

The 600.0ps result is by far the most difficult to replicate. The maximum temperature is reasonably fixed, at this point, by the magnetic state of the 0.5ps and 3.0ps hysteresis loops (at 620K to 640K). Beyond 50.0ps the cooling rate has a dramatic effect on the reversal process, which was not seen within the first 50.0ps. With the standard 0.5ns CR the magnetiation collapses in the region around H_c, as the associated thermal energy is sufficient to allow an increased rate of reversal. Figure 8.7 (on the bottom) shows the 620K and 640K cases, at 600.0ps, with a range of cooling rates (0.1ns to 0.5ns). Reducing CR removes the thermal energy at a faster rate, this slows the rate of magnetisation reversal, stoping the magnetisation from collapsing, but also causes the magnetisation to recover relatively to fast. At 600.0ps with a 0.1ns CR and a maximum temperature of (620K to 640K) the magnetisation has recovered, but not in similar way to Fudan. The recovery is to apparent. The magnetisation has returned to the ambient length in the high positive and negative H fields, where as the Fudan data still shows a level of reduction at this point. Figure 8.8 (on the top) shows hysteresis curves for the 620K and 640K cases with a 0.1ns cooling over a range of times from 100.0ps to 600.0ps in 50.0ps increments. The magnetisation (M_z) recovers much faster than in the Fudan experiment, as the thermal energy is removed much faster which reduces the longitudinal relaxation and slows the transverse relaxation. As a result with a 0.1ns CR the magnetic state of the Fudan thin film (at 600.0ps) is not recovered by the LLB model at any point during the simulation. With a 0.2ns CR the the thermal energy remains for a longer period which allows the longitudinal and transverse relaxation modes to have an increased affect.

Figure 8.8 (on the bottom) also shows the same data as the hysteresis curves on the top of the same figure, but with a longer 0.2ns CR. Under these conditions the magnetisation recovers at a slower rate and a similar magnetic state to the 600.0ps Fudan experiment is recovered at between 150 and 200 pico-seconds. The 'best fit' to the 600.0ps Fudan result, calculated with the LLB model, shown in figure 8.7 on the top, was calculated with a maximum temperature of 620K, and a cooling rate of 0.2ns and was taken at 190.0ps after the laser pulse. It would be of use to see the magnetic state of the Fudan thin film at times beyond 600.0ps, to determine if the later time evolution of the magnetisation is in accordance with what is seen with the LLB model.

The time evolved shape of the Fudan hysteresis loop is dictated by a number of factors; the maximum temperature reached during the experiment, the rate of longitudinal and transverse relaxation and the rate of domain wall motion. As seen above the longitudinal and transverse relaxation modes initially occur over a similar time scale in the Fudan experiment and the LLB model. Beyond 50.0ps the magnetisation of the individual grains are bgining to recover and are reversing via DWM. These two factors happen at different rate in the LLB model compared with what is seen in the Fudan experiment. To maintain a similar level of reduction in **m** the cooling rate must be around 0.5ns which maintains a higher system temperature for a longer period. But in the LLB model this increases the level of DWM, which allows the magnetisation to collapse and the magnetisation does not recover in similar manor to what was seen in the Fudan experiment. Increasing the cooling rate, so that the temperature is removed faster, slows the rate of DWN but increase the rate at which **m** recovers, which reduces the time frame for experiment.

The reversal process is markedly different with the addition of the thermal energy from the laser pulse. Appendix 3 shows the reversal process altered by the excitation from the laser pulse, using the thin film images at 100.0ps intervals as before. The magnetisation reduces rapidly and by 100.0ps the magnetisation of the thin film is in a disordered state, showing the reduced magnetisation in both orientations. As the reversal process proceeds, a domain pattern has formed at 300.0ps which grow rapidly via DWM until the thin film is reversed at 1400.0ps. The rate of reversal is slowed after the temperature has returned to ambient, but continues to completion via DWM.

8.2.4 Summary and Best Fit to the Fudan data

The parameters that gave the best overall fit to the Fudan data over the whole time frame of the experiment was a maximum temperature of 620K and a 0.2ns

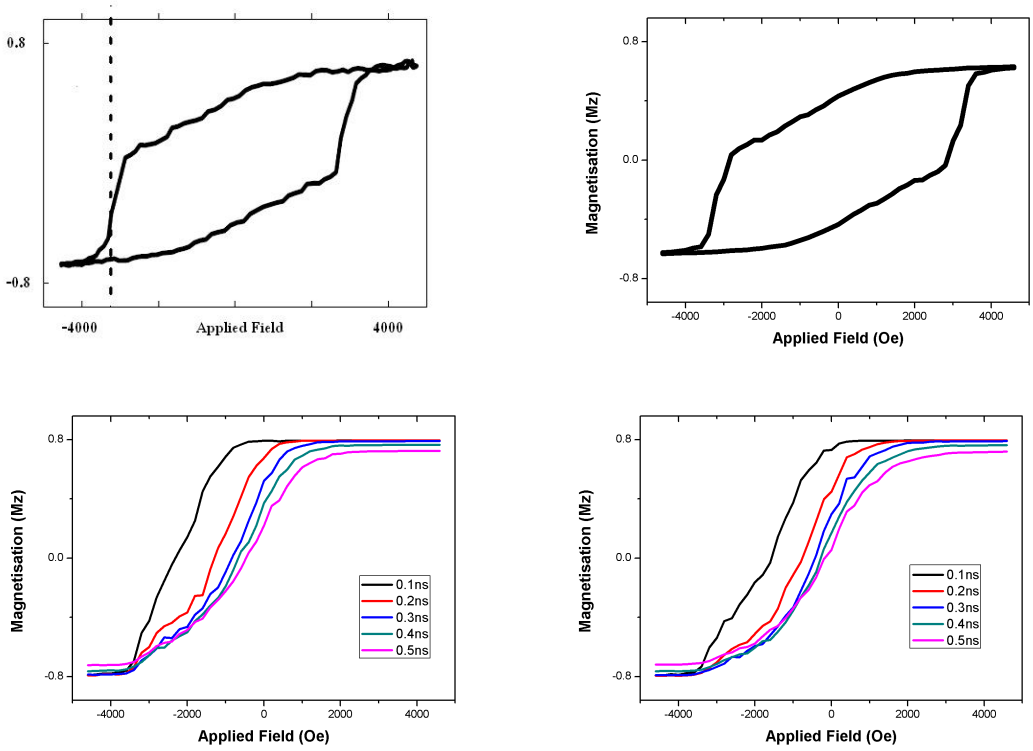

Figure. 8.7: Top left: The dynamic hysteresis loop for FePt thin film determined at Fudan at 600.0ps after the laser pulse. Top right: The 'best fit' found with the LLB model, taken at the early time of 190.0ps after the laser pulse. The thin film was heated up to 620K and the cooling rate is 0.2ns. Bottom left: Hysteresis curves generated with the LLB model, with a maximum temperature of 620K, at 600.0ps, over a range of cooling rates (0.1ns to 0.5ns). Bottom right: Hysteresis curves generated with the LLB model, with a maximum temperature of 640K, at 600.0ps, over a range of cooling rates (0.1ns to 0.5ns).

cooling rate (for a complete overview of the 'best fit' data see appendix 2). With a maximum temperature of 620K the thin film in the LLB model doesn't see the same level of reduction in the magnetisation over the first 50.0ps, as was seen at Fudan. To achieve and equal level of reduction the system temperature was raised to 640K, but, as seen, this temperature caused the magnetisation to collapse and the magnetic state of the thin film, in the latter stages (seen at Fudan), was not recovered. The grains in the LLB modelled thin film do not show the same response to the thermal energy, introduced by the laser pulse, as was seen in the Fudan thin film. The LLB model takes marginally longer (3.0ps for the LLB apposed to 0.5ps for the Fudan thin film) to achieve a similar level of reduction of the magnetisation, although the longitudinal relaxation happens over a similar time frame. Over the next 50.0ps the LLB model is in good agreement with Fudan results. The magnetisation reduces in a similar way and shows a similar response to the applied field. The magnetisation of both thin films begins to reverse at

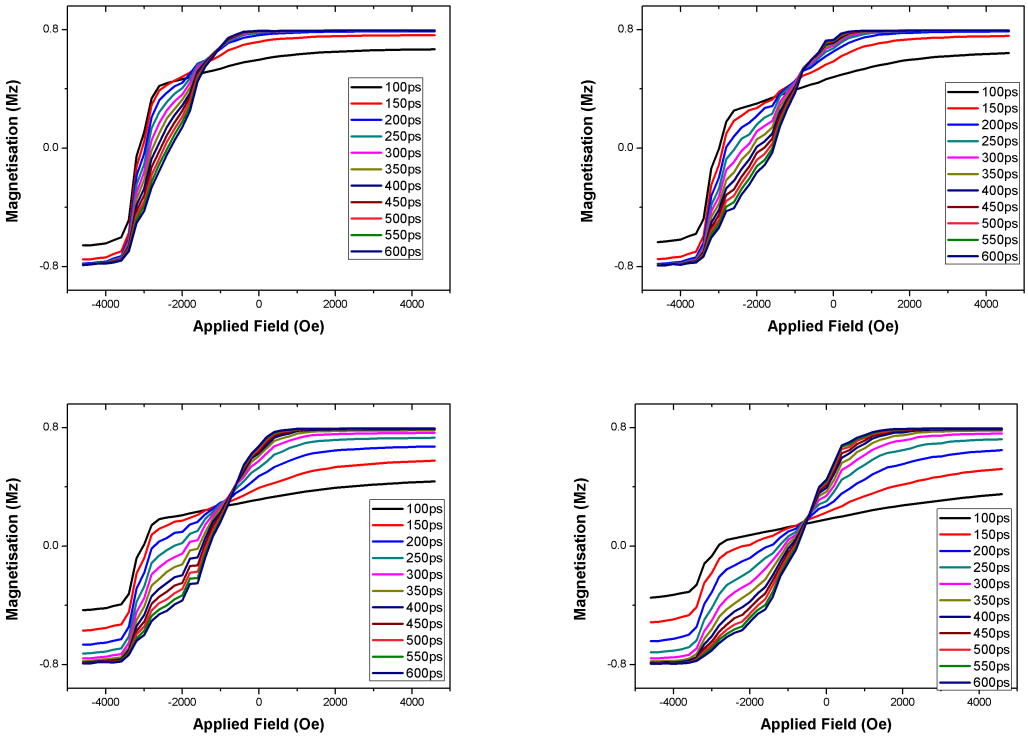

Figure. 8.8: Top left: The dynamic hysteresis loops for FePt thin film generated with LLB model, where the temperature is raised to 620K with a cooling rate of 0.1ns over a range of time after the laser pulse, from 100.0ps to 600.0ps. Top right: The dynamic hysteresis loops for FePt thin film generated with LLB model, where the temperature is raised to 640K with a cooling rate of 0.1ns over a range of time after the laser pulse, from 100.0ps to 600.0ps. Top left: The dynamic hysteresis loops for FePt thin film generated with LLB model, where the temperature is raised to 620K with a cooling rate of 0.2ns over a range of time after the laser pulse, from 100.0ps to 600.0ps. Top left: The dynamic hysteresis loops for FePt thin film generated with LLB model, where the temperature is raised to 640K with a cooling rate of 0.2ns over a range of time after the laser pulse, from 100.0ps to 600.0ps.

roughly the same time caused by the transverse relaxation mode (somewhere between 0.5ps and 50.0ps). Beyond 50.0ps the differences between the two reversal process becomes more apparent. The LLB model demagnetises in the z-axis at an increased rate, compared to Fudan thin film and the magnetisation is seen to collapse in the latter stage of the LLB simulations. The thin film in both the Fudan experiment and the LLB model show magnetisation reversal via domain wall motion. In the LLB model the DWM happens at an increased velocity compared with the Fudan thin which causes the magnetisation to collapse at an increase rate. To achieve a similar magnetic state as the 600.0ps Fudan result, takes a relatively shorter period; 190.0ps for the LLB model.

9. Conclusion and further work

9.1 Conclusion

This body of work describes the heat assisted magnetic recording process (HAMR), including a macro spin model of a nano-granular high anisotropy $L1_o$ FePt thin film for use as recording media. The 80 x 80 x 1 granular thin film is modelled using a voronoi construction, which gives a realistic grain size dispersion and microstructural disorder. The thin film is comprised of 6nm magnetic FePt grains with perpendicular orientated uniaxial anisotropy. The voronoi model also includes the granular magnetic interactions associated with the thin film format. The dynamic motion of the magnetisation of each grain is independently described with the stochastic form of the Landau-Lifshitz-Bloch (LLB) equation. The LLB equation is capable of describing the magnetisation at elevated temperatures up to and above the Curie point T_c.

The static hysteresis and relaxation properties are determined for comparison with theory. The coercivity of the thin film has an approximately linear relationship with the anisotropy energy, which is shifted from linear by the dipole and exchange fields. When the dipole field, generated by an individual grain, is of the same order as the anisotropy and applied fields the magnetisation dynamics are impacted. The dipole interaction between neighbouring magnetisations causes instability in an otherwise thermally stable system and unwanted magnetisation reversal can occur causing loss of data. The dipole field (in the lower anisotropy regime, the than 20% $L1_o$ FePt) is shown to slow and stop the reversal process, as individual grains magnetisation (and small groups) become stuck by the increased energy barrier created by the dipole field generated by the grains that have already reversed. The dipole slowing/stopping is reduced at higher anisotropies as the effect of the dipole field is minimised by the increased anisotropy field and switching field associated with large values of K_v.

Inter-granular exchange coupling alters the reversal process for the thin film. In higher exchange regimes the motion of the individual grains magnetisation is dependant on the neighbouring grains, which causes the component magnetisation of the thin film to precess together. Therefore the reversal process is also bound, which impacts in a number of ways. The reversal process nucleates on grains across the thin film and the energy barrier is then lowered for the neighbouring grains, causing domains to form and the reversal

process continues via DWM. This reduces the coercivity and reversal field in all anisotropy regimes and causes larger domains to form when the thin film is demagnetised. The exchange field is also shown to reduces the effect of the dipole field (at lower anisotropies) during the reversal process. The increased energy barrier brought about by the dipole interaction is offset by the effect of domain wall motion (DWM).

The LLB model is also used to determine the relaxation time of an ensemble of non interacting grains. The LLB calculated relaxation time is shown to have a different anisotropy dependence from Arrhenius-Néel (A-N), as A-N is only valid for large values of KV/kT. The value determined by the LLB model is tending (with the highest anisotropies) toward a similar trend as A-N, which is still to be determined. The LLB model is in good agreement with A-N at temperatures below $3T_c/4$. Above this temperature the LLB relaxation time shows a critical decrease from what is predicted by Arrhenius-Néel, as the A-N equation is based on the LLG approach and is therefore incorrect at temperature approaching T_c. This is an important result as the A-N law will be insufficient for modelling high temperature regimes like in the HAMR process.

In addition to the constant temperature study, the LLB model is used to describe the magnetic profile of the thin film due to application of an applied field and further excitation with a laser pulse. The magnetisation of the thin film responds to the increased temperature with a dramatic decrease in the magnetisation taking only tens of pico-seconds. If the temperature is raised sufficiently and for long enough the thin film will demagnetise. At this point the magnetisation of the grains are in a disordered state, with roughly an equal number sat in both orientations. As the temperature drops the magnetisation of the grains reform and with an applied field the magnetisation is guide in the field direction. To reverse the magnetisation of the thin film to the desired level required an applied of roughly 13000Oe and a maximum temperature of T_c. This is far lower than at ambient, but still remains at the limit of what is achievable with inductive technologies. The level of anisotropy dictates the temperature 'window' for reversal. Higher anisotropies requires higher temperatures to lower the anisotropy to a level where an applied field can reverse the magnetisation. Combined with the constraint that maximum reversal happens with a maximum temperature of T_c, results in a narrower temperature range where reversal will happen. This is a significant result, as the grains around the edge of the heating area will be less likely to reverse, reducing the loss of data due to thermal effects.

The LLB model is used to accurately replicate the magnetic configuration of an 6nm thin continuous partially $L1_o$ ordered FePt thin film, both due to

a static applied field and when further magnetisation reversal is induced by excitation with a fs laser pulse. The original pump-prob experiments with the FePt thin film where undertaken by Zhou etal at Fudan University, China. The experiment employed a new photo-magnetic synchronized magneto-optical Kerr effect technique for determining the magnetic state of the thin on the femto time scale. The dynamic hysteresis loops obtain by Zhou retain a characteristic squareness thought 600.0ps after excitation, which the team at Fudan explained by assuming domain nucleation and subsequent domain wall motion as the prominent reversal mechanism.

9.2 Further work

Work is continuing to modify the LLB model to replicate LLG dynamics, to continue the work on the relaxation time. A direct comparison between LLB and LLG dynamics will highlight the restrictions imposed by the LLG approach. The anisotropy dependence for higher values of KV/KT are also underway to confirm the relationship with the Arrhenius-Néel law.

Work is also continuing to determine the minimum time scale for reversal process under HAMR conditions. The time frame for reversal is dictated by the cooling rate of the thin film, essentially the time taken for the anisotropy to rebuild to a level where reversal is forbidden and the magnetisation reversal process is complete. The anisotropy rebuilds at a faster rate in higher K_v regimes and should therefore be stable at an early stage in the process.

Colleagues at the University of York are in the process of completing an extension to the LLB thin film model, to enable the simulated recording of bits. The recording model uses the same principles to generate and FePt thin film like in the standard LLB model, but the recording model will include a temperature and applied strength profile. To accurately simulate excitation with a laser pulse and the magnetic field profile generated by a modern write head. This will result in a model capable of simulating the recording of bits, including the disturbance to neighbouring bits when recording.

10. Appendix 1

10.1 Domain formation due to inter-granular exchange coupling

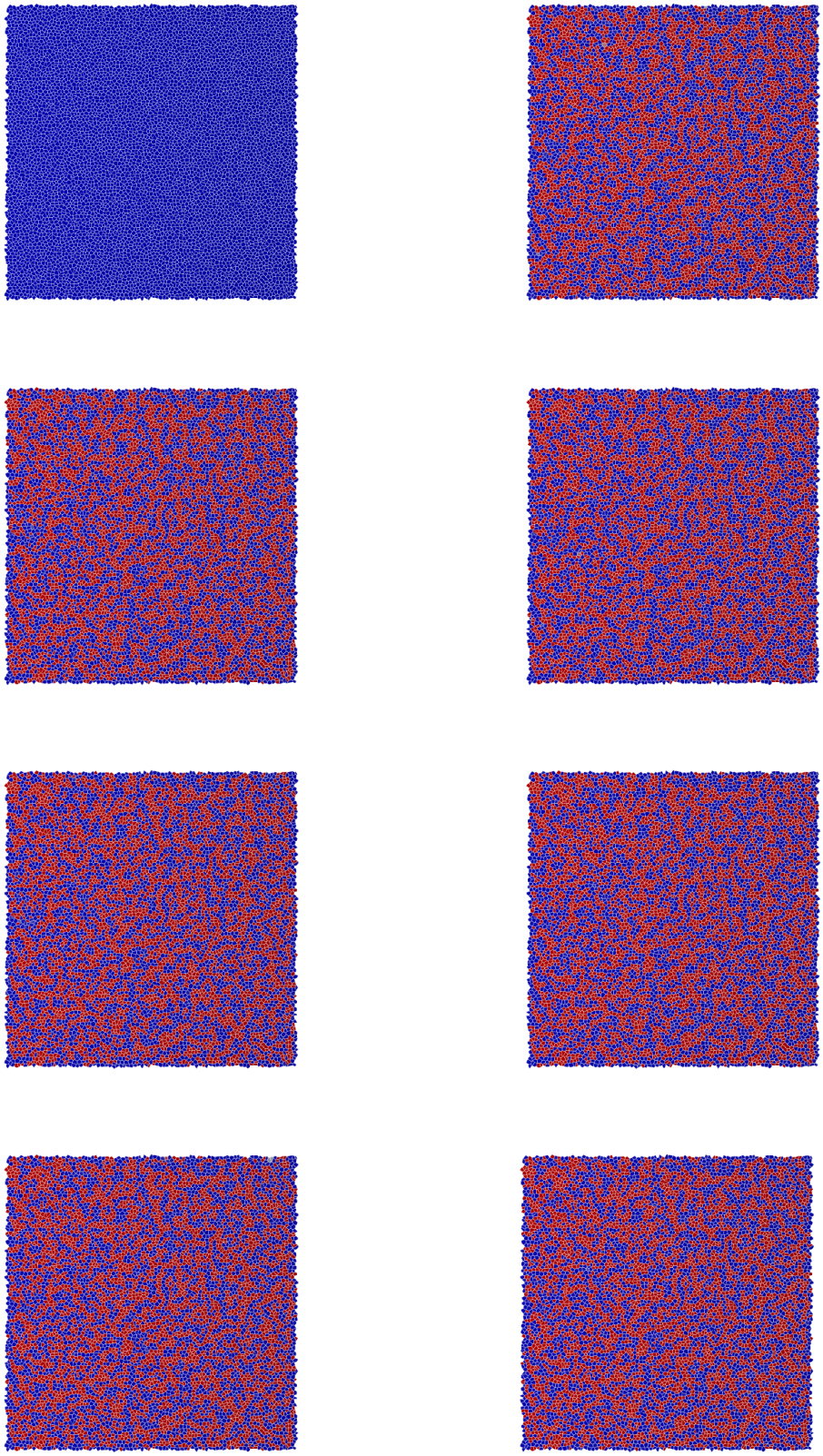

Figure. 10.1: The time evolution of magnetisation of the thin film for the static case with a 0Oe exchange field (note the formation of small domains caused by the dipole field) with an applied field equal to H_c, using the thin film images taken at 100.0ps increments, starting from 0.0ps on the top left and then moving left to right, working down the page to 700.0ps.

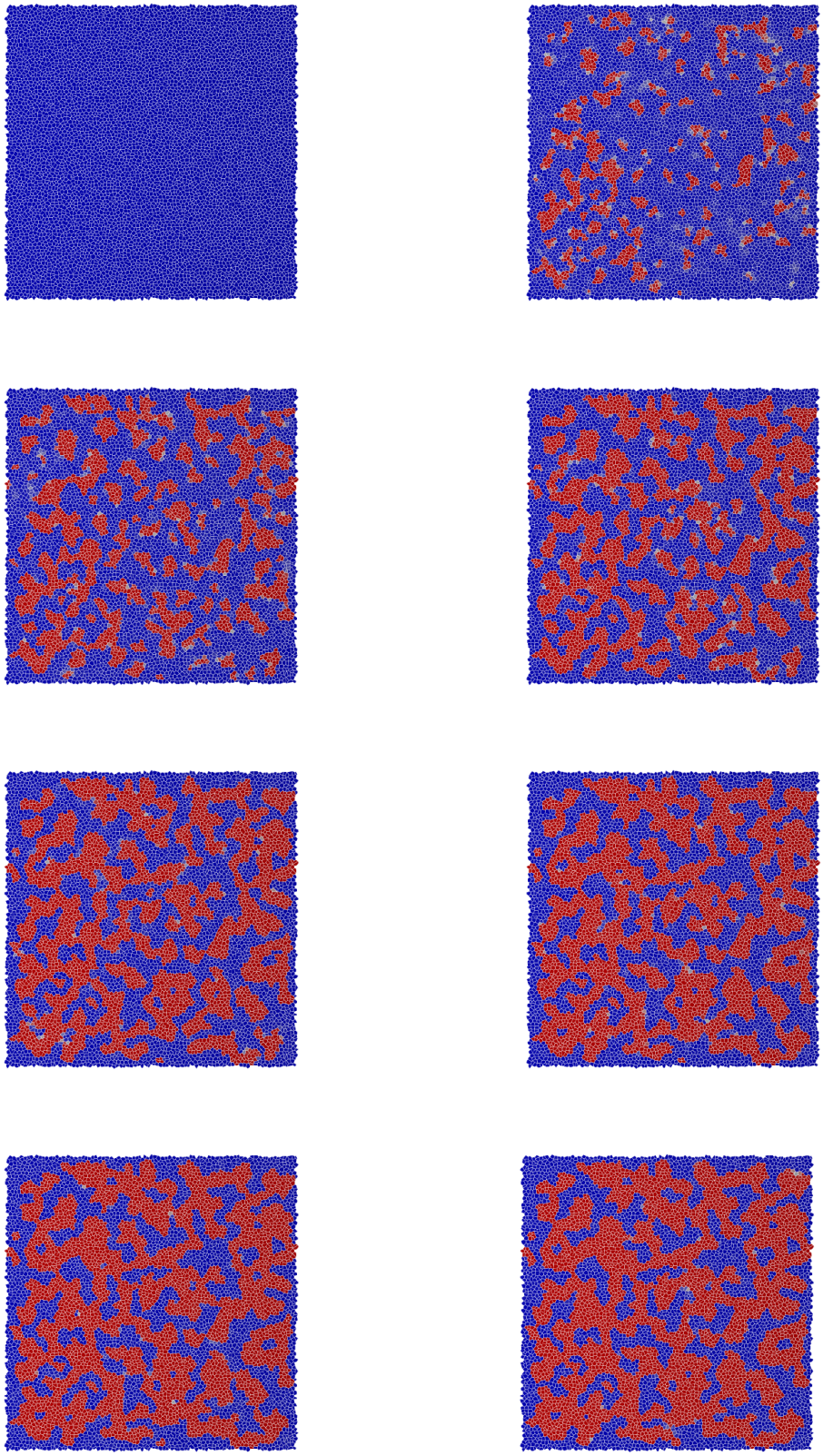

Figure. 10.2: The time evolution of magnetisation of the thin film for the static case with a 30000Oe exchange field with an applied field equal to H_c, using the thin film images taken at 100.0ps increments, starting from 0.0ps on the top left and then moving left to right, working down the page to 700.0ps.

11. Appendix 2

11.1 Best Fit to the Fudan Results Determined with the LLB Model

The 'best fit' to the Fudan FePt pump prob experiments, generated with the LLB model over the time frame for the experiment. The two images on the top are the Fudan and LLB modelled static loop. Where the LLB modelled thin film has an anisotropy equal to 13.7% $L1_o$ ordered FePt and the exchange constant is 32000Oe. To replicate the laser pulse experiment the maximum temperature is raised to 620K and the cooling rate is 0.2ns. Second from the top: The 0.5ps case from Fudan and the LLB modelled result, respectively. Note the LLB modelled result is taken at 5.0ps as the modelled magnetisation didn't reduce as fast on excitation with the laser pulse. Second from the bottom: the 50.0ps case from Fudan and the LLB modelled result respectively, both at 50.0ps. On the bottom: The 600.0ps case for the Fudan case and the LLB modelled result. Note the LLB modelled results was taken at 190.0ps, as the magnetisation of the thin film collapsed beyond this point via DWM.

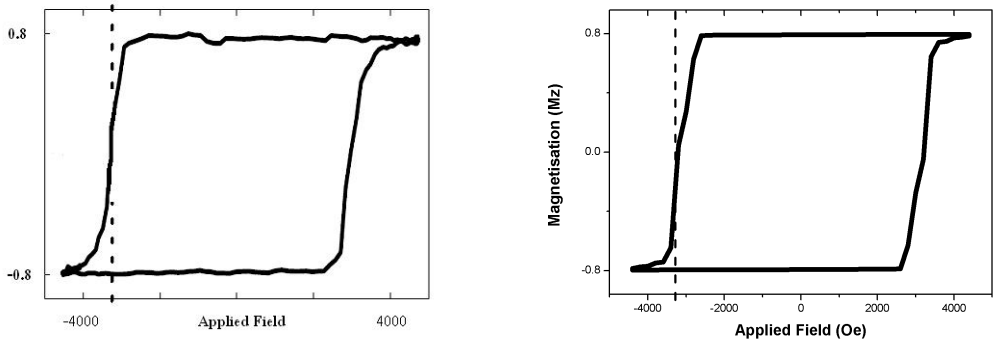

Figure. 11.1: The left had side: The static loop determined by experiment at Fudan. The right hand side: The static loop determined using the LLB model using an anisotropy of 0.137% $L1_o$ ordered grains and an inter-granular exchange field of 32000Oe.

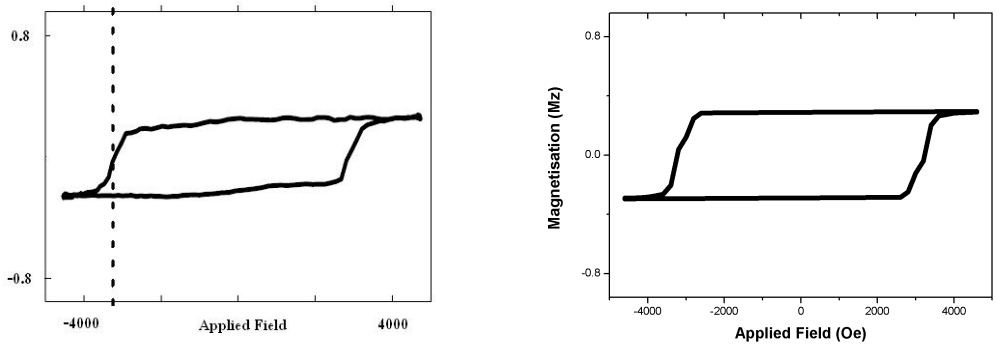

Figure. 11.2: The left had side: The Dynamic loop determined by experiment at Fudan 0.5ps after the laser pulse. The right hand side: The dynamic loop determined using the LLB model at 5ps, using a maximum temperature of 620K and a cooling rate of 0.2ns.

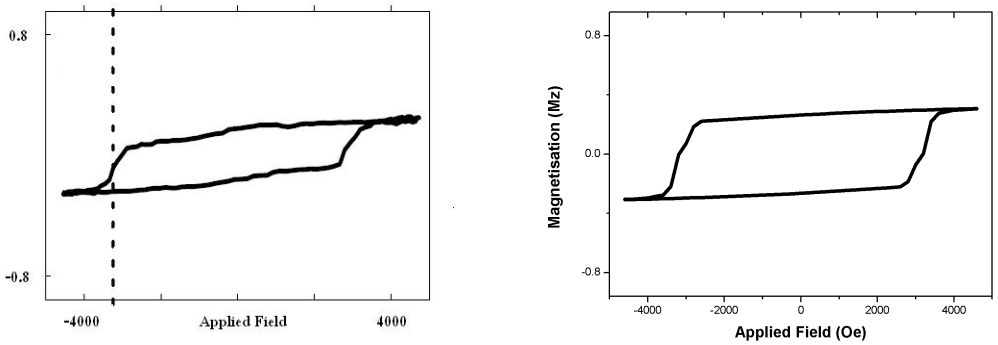

Figure. 11.3: The left had side: The Dynamic loop determined by experiment at Fudan 50ps after the laser pulse. The right hand side: The dynamic loop determined using the LLB model at 50ps, using a maximum temperature of 620K and a cooling rate of 0.2ns.

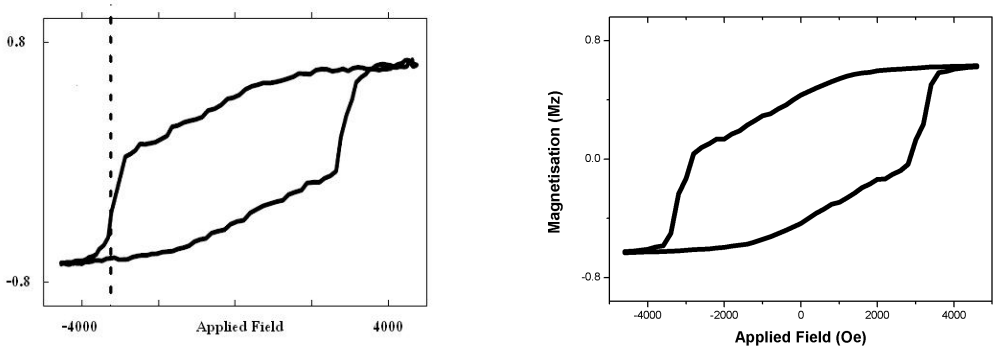

Figure. 11.4: The left had side: The Dynamic loop determined by experiment at Fudan 600ps after the laser pulse. The right hand side: The dynamic loop determined using the LLB model at 190ps, using a maximum temperature of 620K and a cooling rate of 0.2ns.

12. Appendix 3

12.1 Domain Wall Motion in the Fudan thin film

12.1.1 Static Case -3300Oe applied field case

The time evolution of magnetisation of the thin film for the no pump case with a -3300Oe applied field (equal to H_c), using the thin film images taken at 100.0ps increments, starting from 0.0ps on the top left and then moving left to right, working down the page to 2300.0ps.

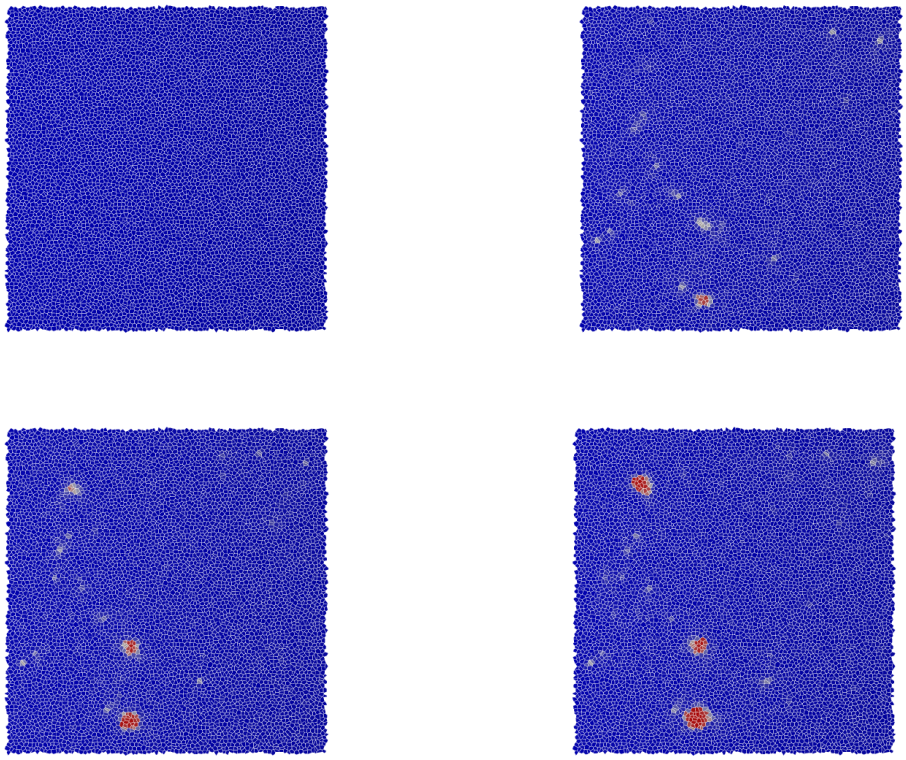

Figure. 12.1: The time evolution of magnetisation of the thin film for the no pump case with a -3300Oe applied field (equal to H_c), using the thin film images taken at 100.0ps increments, starting from 0.0ps on the top left and then moving left to right, working down the page to 300.0ps.

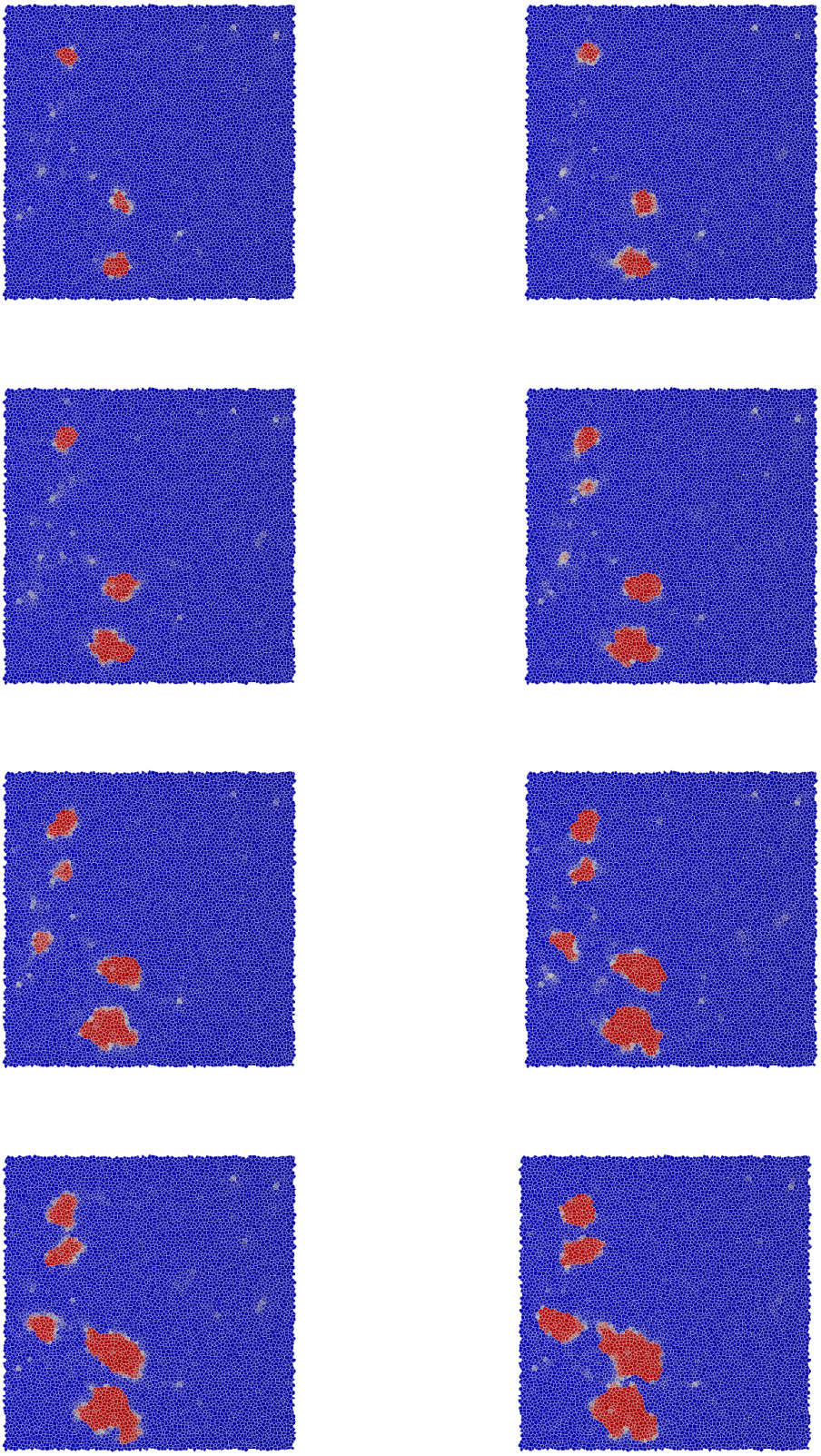

Figure. 12.2: The time evolution of magnetisation of the thin film for the no pump case with a -3300Oe applied field (equal to H_c), using the thin film images taken at 100.0ps increments, starting from 400.0ps on the top left and then moving left to right, working down the page to 1100.0ps.

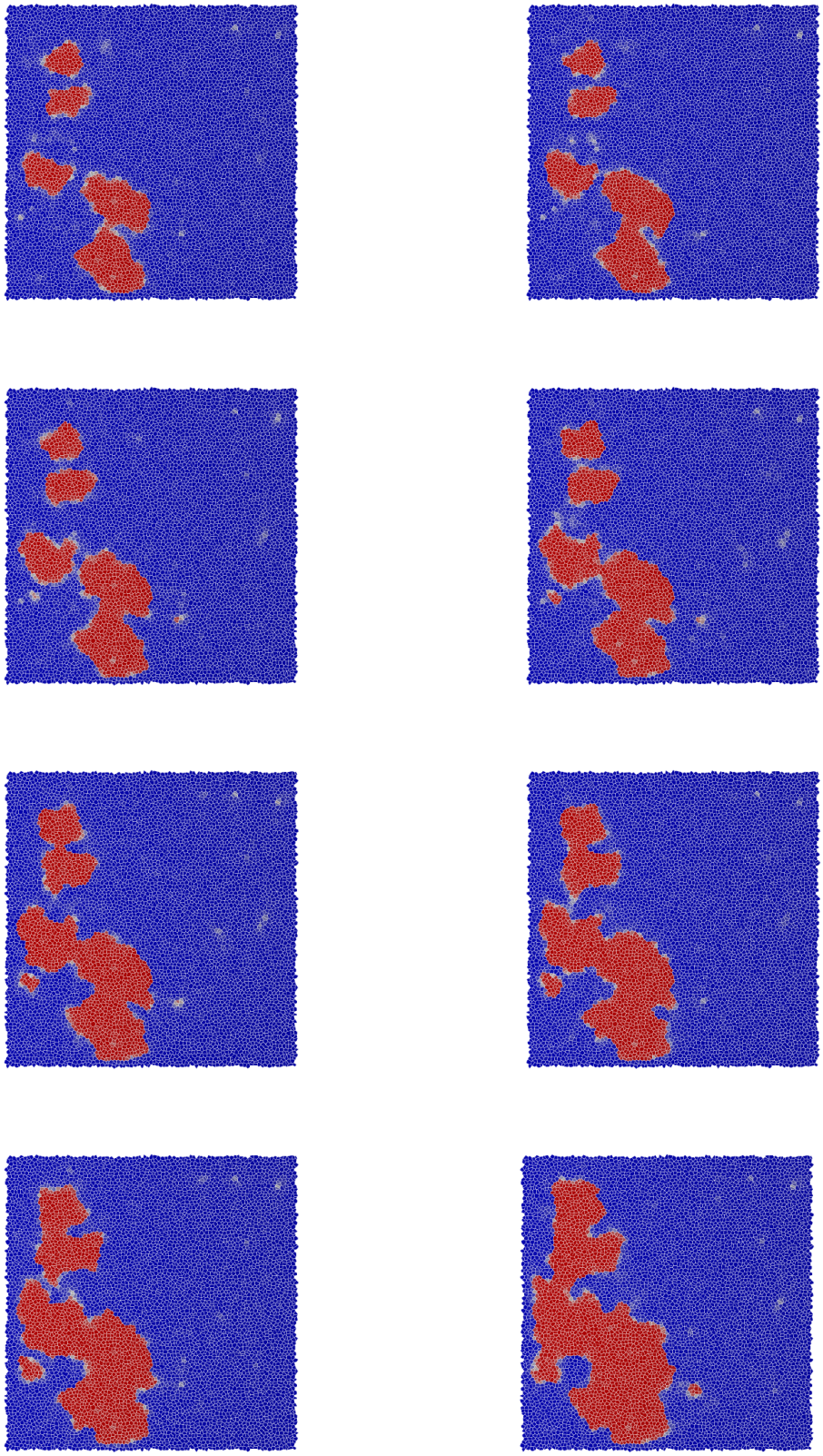

Figure. 12.3: The time evolution of magnetisation of the thin film for the no pump case with a -3300Oe applied field (equal to H_c), using the thin film images taken at 100.0ps increments, starting from 1200.0ps on the top left and then moving left to right, working down the page to 1900.0ps.

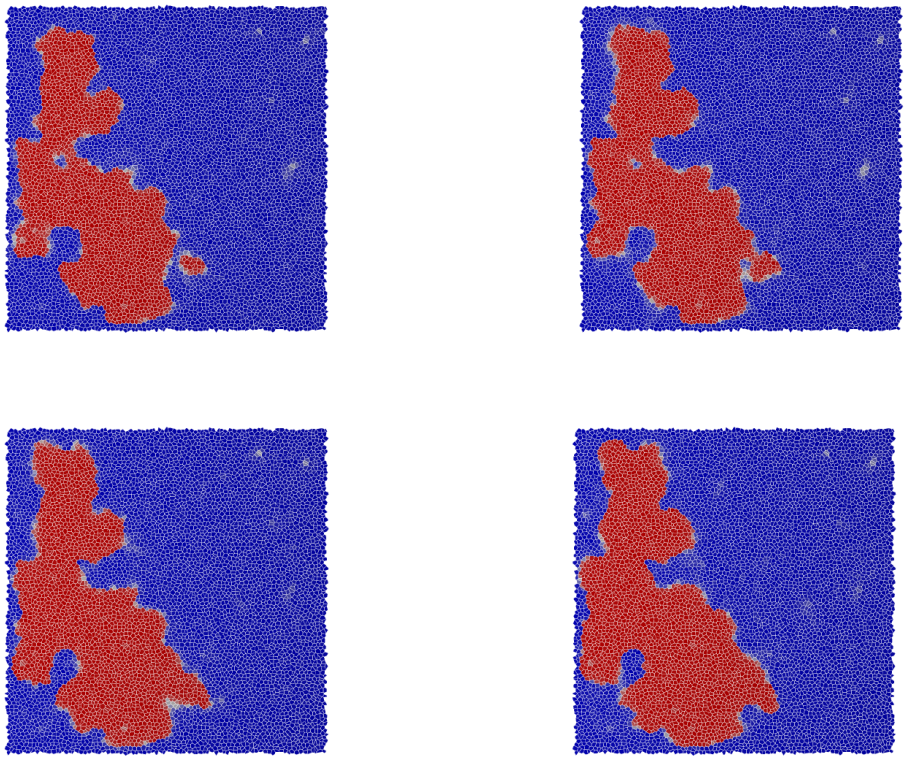

Figure. 12.4: The time evolution of magnetisation of the thin film for the no pump case with a -3300Oe applied field (equal to H_c), using the thin film images taken at 100.0ps increments, starting from 2000.0ps on the top left and then moving left to right, working down the page to 2300.0ps.

13. Appendix 4

13.1 Domain Wall Motion in the Fudan thin film

13.1.1 Static Case -4000Oe applied field case

The time evolution of magnetisation of the thin film for the no pump case with a -4000Oe applied field (equal to H_c), using the thin film images taken at 100.0ps increments, starting from 0.0ps on the top left and then moving left to right, working down the page to 2300.0ps.

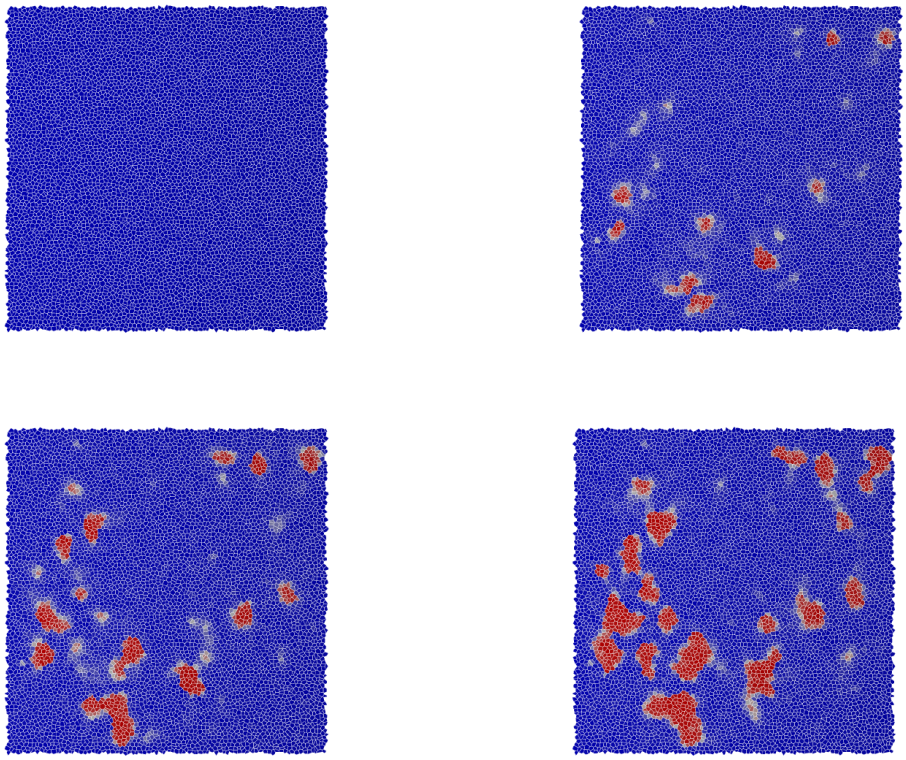

Figure. 13.1: The time evolution of magnetisation of the thin film for the no pump case with a -4000Oe applied field (equal to H_r), using the thin film images taken at 100.0ps increments, starting from 0.0ps on the top left and then moving left to right, working down the page to 300.0ps.

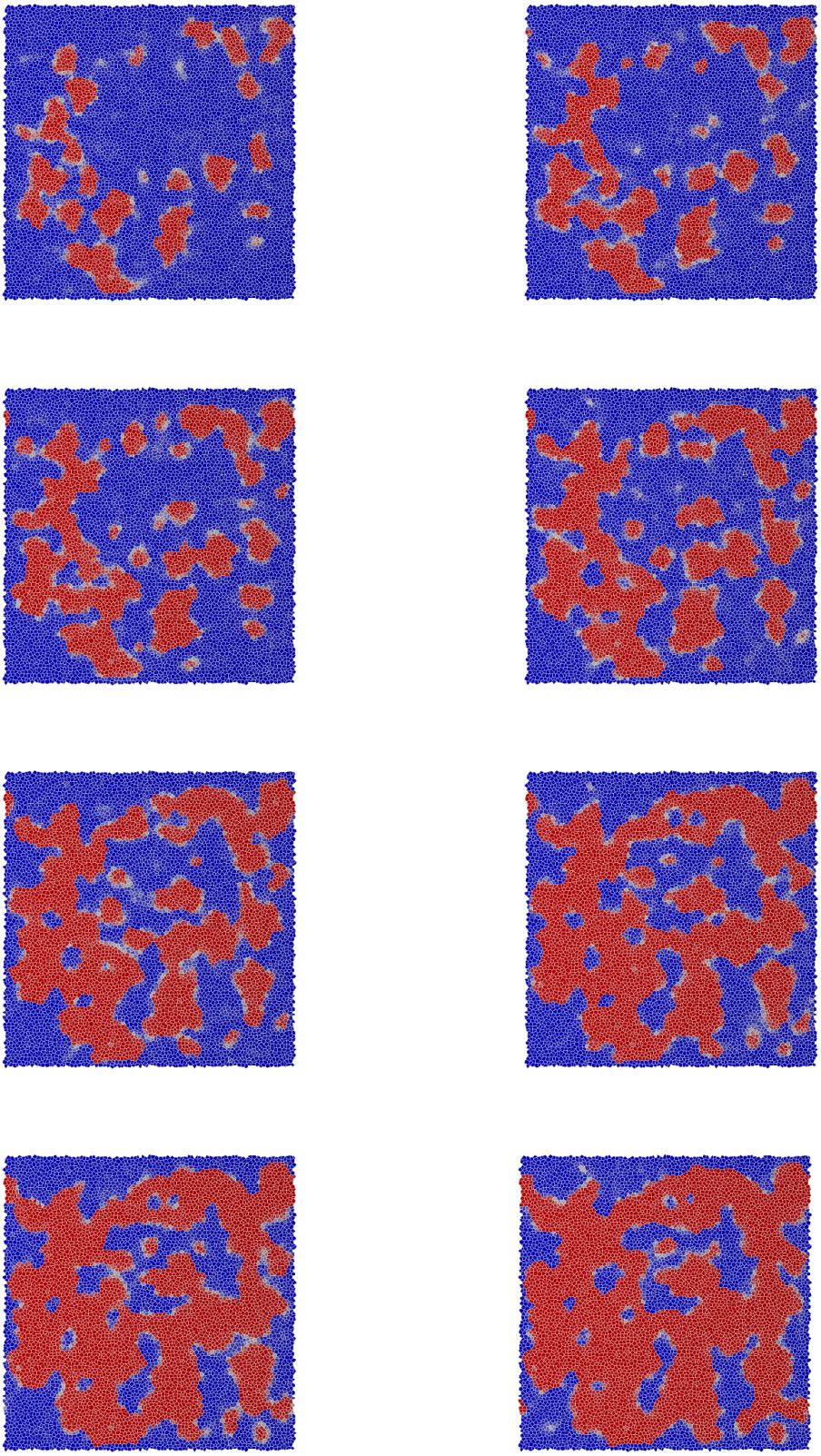

Figure. 13.2: The time evolution of magnetisation of the thin film for the no pump case with a -4000Oe applied field (equal to H_r), using the thin film images taken at 100.0ps increments, starting from 400.0ps on the top left and then moving left to right, working down the page to 1100.0ps.

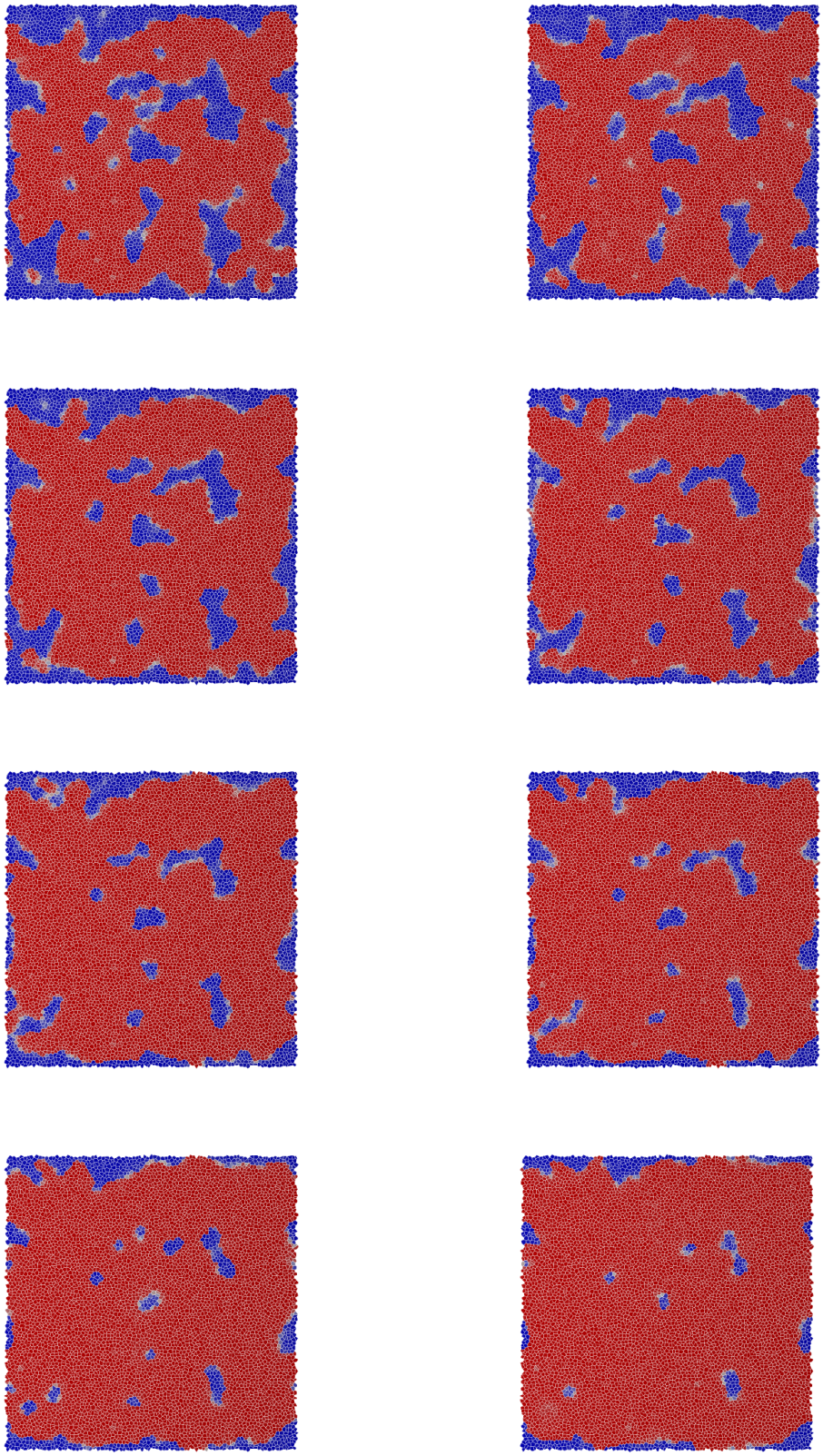

Figure. 13.3: The time evolution of magnetisation of the thin film for the no pump case with a -4000Oe applied field (equal to H_r), using the thin film images taken at 100.0ps increments, starting from 1200.0ps on the top left and then moving left to right, working down the page to 1900.0ps.

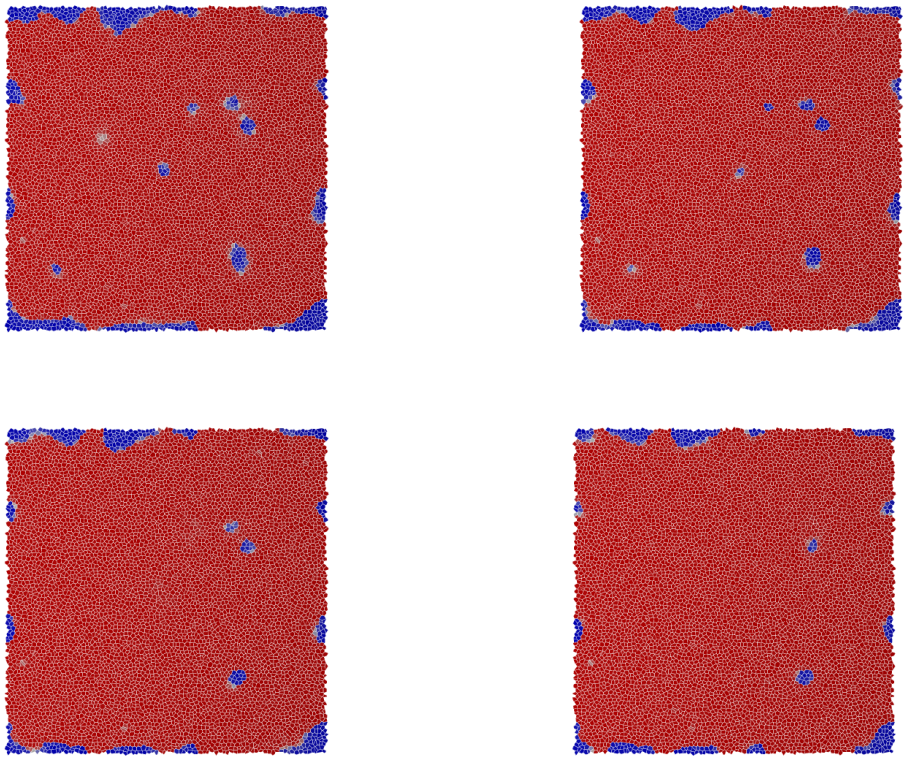

Figure. 13.4: The time evolution of magnetisation of the thin film for the no pump case with a -4000Oe applied field (equal to H_r), using the thin film images taken at 100.0ps increments, starting from 2000.0ps on the top left and then moving left to right, working down the page to 2300.0ps.

14. Appendix 5

14.1 Magnetisation reversal in the Fudan thin film, due to the laser assist

14.1.1 Dynamics Case, 620K maximum temperature and a 0.2ns cooling rate

The time evolution of magnetisation of the thin film for the laser pump case with a -2600Oe applied field (equal to H_c), with a maximum temperature of 620K and a 0.2ns cooling rate, using the thin film images taken at 100.0ps increments, starting from 100.0ps before the laser pulse on the top left and then moving left to right, working down the page to 1300.0ps after the laser pulse.

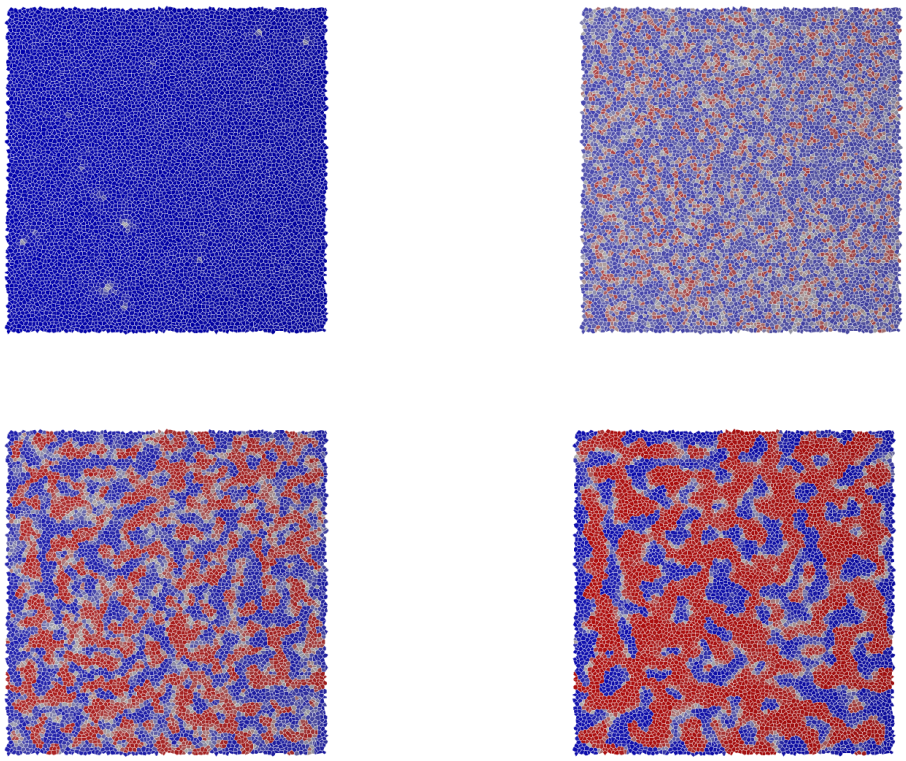

Figure. 14.1: The time evolution of magnetisation of the thin film for the laser pulse pump case with a -2600Oe applied field which was heated to 620K, using the thin film images taken at 100.0ps increments, starting from 100.0ps before the laser pulse, on the top left and then moving left to right, working down the page to 200.0ps.

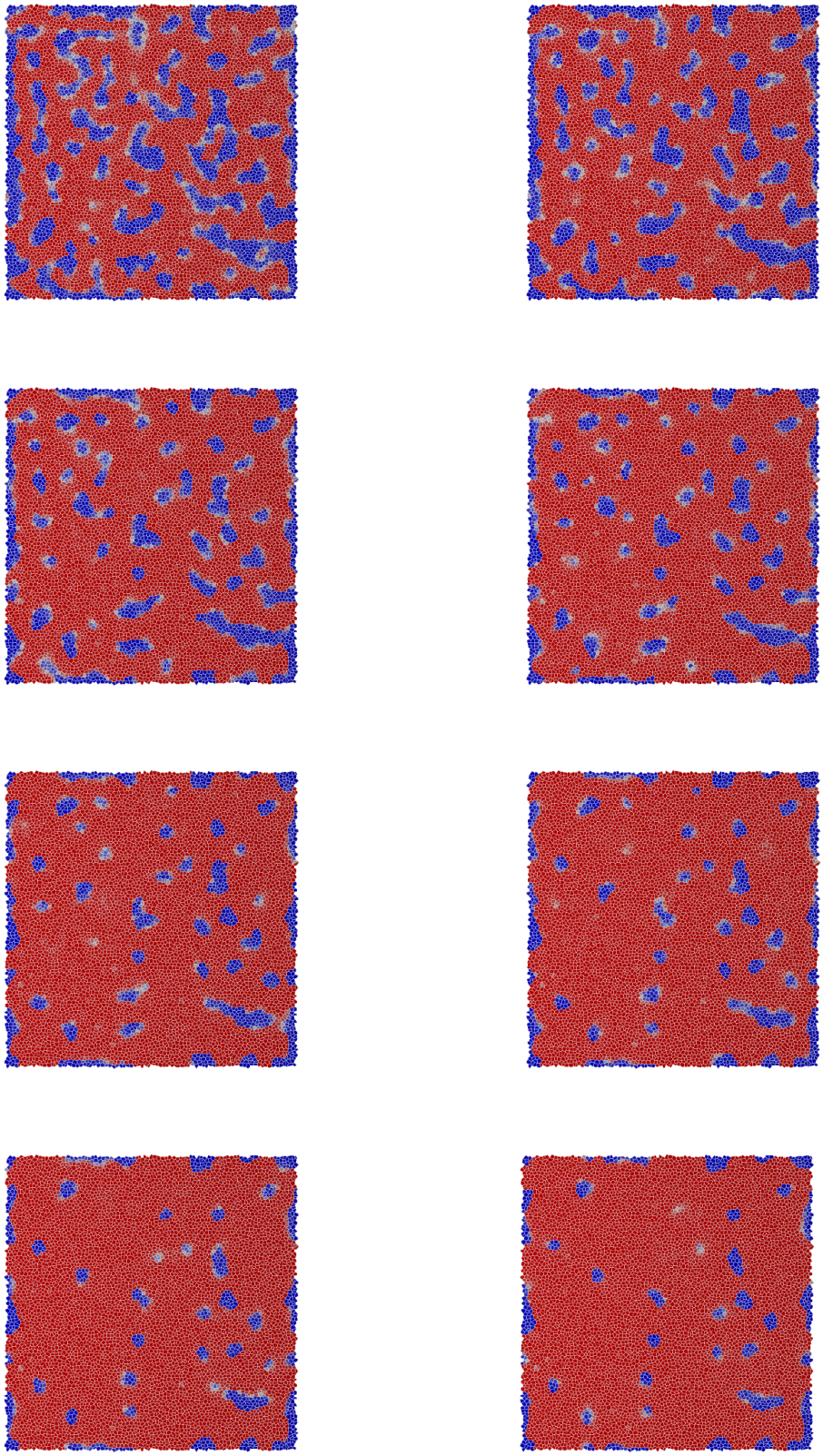

Figure. 14.2: The time evolution of magnetisation of the thin film for the laser pulse pump case with a -2600Oe applied field which was heated to 620K, using the thin film images taken at 100.0ps increments, starting from 300.0ps after the laser pulse, on the top left and then moving left to right, working down the page to 1000.0ps after the laser pulse.

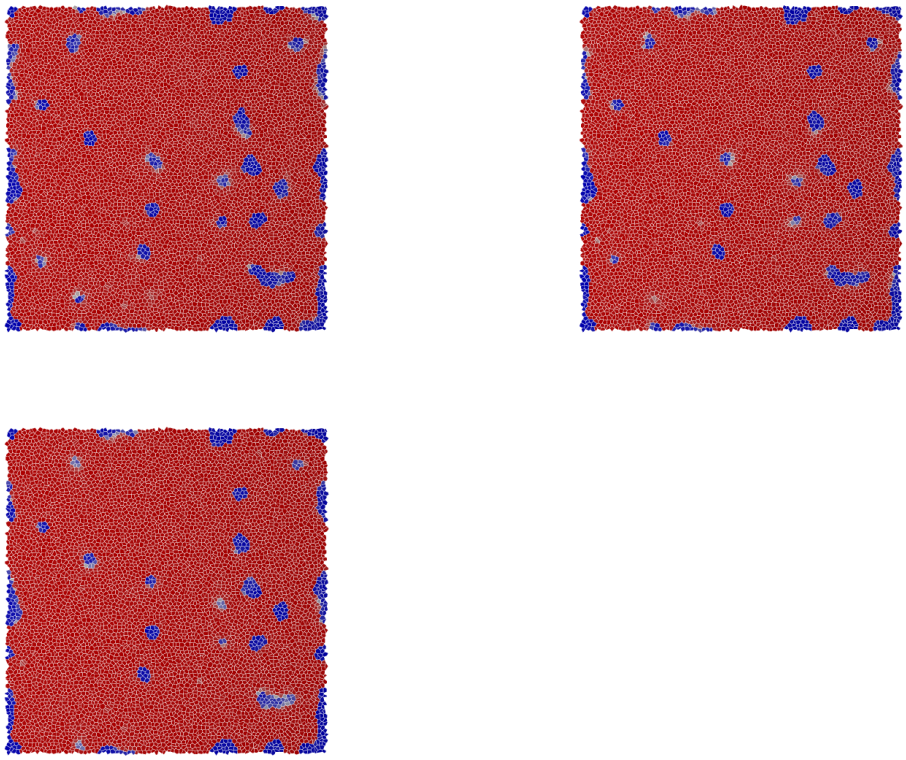

Figure. 14.3: The time evolution of magnetisation of the thin film for the laser pulse pump case with a -2600Oe applied field which was heated to 620K, using the thin film images taken at 100.0ps increments, starting from 1100.0ps after the laser pulse, on the top left and then moving left to right, working down the page to 1300.0ps.

References

[1] V. M. Kalita A. F. Lozenko P. A. Trotsenko et al A. A. Timopheev, S. M. Ryabchenko. The influence of intergranular interaction on the magnetization of the ensemble of oriented stonerwohlfarth nanoparticles. *J. Appl. Phys*, 105:083905, 2009.

[2] G. Hrkac T. Schrefl Y. Ikeda et al C. Morrison, L. Saharan. Inter/intra granular exchange and thermal activation in nanoscale granular magnetic materials. *Appl. Phys. Lett*, 99:132507, 2011.

[3] J. D. Livingston C. P. Bean. Superparamagnetism. *J. Apl. Phys*, S30:120S–129S, 1959.

[4] Chorpa. *Thin Film Phenomena*. McGraw Hill, 1969.

[5] O Chubykalo-Fesenko D Hinzke, U Nowak and RW Chantrell. Llb micromagnetic models for ultrafast magnetisation processes. *HYSTERESIS MODELING AND MICROMAGNETICS*, page 101, 2009.

[6] P Erdos. Theory of ion pairs coupled by exchange interaction. *Phys. Chem. Solids*, 27:1705–1720, 1966.

[7] J. Frenkel and J. Dorfman. Spontaneous and induced magnetisation in ferromagnetic bodies. *Nature*, 126:274–275, 1930.

[8] P. J. Kelly G. H. O. Daalderop and M. F. H. Schuurmans. Magnetocrystalline anisotropy and orbital moment in transition metal compounds. *Phys. Rev. B*, 44:12054–12057, 1991.

[9] D. A. Garanin. Fokker-planck and landau-lifshitz-bloch equations for ferromagnets. *Phys.Rev. B*, 55:3050–3057, 1997.

[10] D. A. Garanin and O. Chubykalo-Fesenko. Thermal fluctuations and longitudinal relaxation of single-domain magnetic particles at elevated temperatures. *Phys.Rev. B*, 70:212409, 2004.

[11] G. Grinstein and R. H. Koch. Coarse graining in micromagnetics. *Phys. Rev. Lett*, 90:207201, 2003.

[12] E. Callen H. B. Callen. The present status of the temperature dependence of magnetocrystalline anisotropy, and the z(z+1)/2 power law. *J. Phys. Chem. Solids*, 27:1271–1285, 1966.

[13] R. W. Chantrell D. Hinzke J. Barker, R. F. L. Evans and U. Nowak. Atomistic spin model simulation of magnetic reversal modes near the curie point. *Appl. Phys. Lett*, 97:192504, 2010.

[14] M. F. Toney J. A. Hedstrom J. U. Thiele, K. R. Coffey and A. J. Kellock. Temperature dependent magnetic properties of highly chemically ordered fe55xnixpt45l10 films. *J. Appl. Phys*, 91:6595, 2002.

[15] Landau and Lifshifz. *Electrodynamics of Continuous Media*. Pergamon Press, 1960.

[16] James H. Giusti Lei Wang, Shaoping Li and Juan Fernandez de Castro. Micromagnetic study of effect of media intergranular exchange interaction in perpendicular recording. *J. Apl. Phys*, 91:8381–8381, 2002.

[17] J. D. Livingston and C. P. Bean. Anisotropy of superparamagnetic particles as measured by torque and resonance. *J. Apl. Phys. Rev*, 30:318S–319S, 1959.

[18] T. W. McDaniel. Ultimate limits to thermally assisted magnetic recording. *J. Phys.: Condens*, 17:R315 – R332, 2005.

[19] U. Nowak R. W. Chantrell U. Atxitia N. Kazantseva, D. Hinzke and O. Chubykalo-Fesenko. Towards multiscale modeling of magnetic materials: Simulations of fept. *Phys. Rev. B*, 77:184428, 2008.

[20] L. Neel. *Selected Works of Louis Neel*. Gordon and Breach, New York, 1988.

[21] R. W. Chantrell O. Chubykalo-Fesenko, U. Nowak and D. Garanin. Dynamic approach for micromagnetics close to the curie temperature. *Phys. Rev. B*, 74, 2006.

[22] Ohashi and Y. Yasue. Newly developed inductive write head with electroplated conife film. *IEEE Trans. Magn*, 34:1462, 1998.

[23] J. Barker R. F. L. Evans and et al R. W. Chantrell. Constrained monte carlo method and calculation of the temperature dependence of magnetic anisotropy. *Phys. Rev. B*, 82:054415, 2010.

[24] Pu-Ling Lu S. H. Charap and Yanjun He. Thermal stability of recorded information at high densities. *IEEE TRANSACTIONS ON MAGNETICS*, 30:979–983, 1997.

[25] O. Kitakami T. Miyazaki Y. Shimada S. Okamoto, N. Kikuchi and K. Fukamichi. Chemical-order-dependent magnetic anisotropy and exchange stiffness constant of fept (001) epitaxial films. *Phys. Rev. B*, 66:024413, 2002.

[26] M.H.Kryder S.D.Granz. Granular $l1_o$ fept (001) thin films for heat assisted magnetic recording. *J.Magn.Magn.Mater*, 2010.

[27] M. P. Sharrock. Time-dependent magnetic phenomena and particle-size effects in recording media. *IEEE TRANSACTIONS ON MAGNETICS,*, 26:193–197, 1990.

[28] Y. Tanaka. Recording performance and system integration of perpendicular magnetic recording. *J.Magn.Magn.Mater*, 287:468–474, 2005.

[29] R. Wood. The feasibility of magnetic recording at 1 terabit per square inch. *IEEE TRANSACTIONS ON MAGNETICS*, 36:36, 2000.

[30] R. X. Gao Z. F. Chen T. S. Lai et al X. D. Liu, Z. Xu. Single laser pulse induced dynamic magnetization reversal mechanism of perpendicularly magnetized $l1_o$ fept films. *J. Appl. Phys*, 106:053907, 2009.